AL-MUSTANSIRIYAH JOURNAL OF SCIENCE

1978

CONTENT

PHOTODYNAMIC DEGRADATION OF SOME NUCLEIC ACIDS IN AQUEOUS SOLUTIONS

Saad K. Ismail*

ABSTRACT

The photodegradation of dGMP , dAMP, deoxyribose, and deoxyribose phosphate was investigated in aqueous solutions using eosin and methylene blue as sensitizers. The amount of ; released phosphate, destroyed ribose, base destroyed, and sensitizer desroyed were calculated. It has been found that the destruction of deoxyribose is one of the major effects of the sensitized destruction of nucleic acids.

INTRODUCTION

The photodynamic destruction of DNA and its constituent bases has been studied by a number of workers [1-4]. Attention has also been paid to the biological effects of the sensitized oxidation of DNA [5,6]. Simon and Van Vunakis [1,7] showed that one probable modification of Polynucleotides was a photosensitized destruction of guanine residue. They also concluded that methylene blue was one of the most efficient dyes for the selective destruction of guanine derivatives. However, it has been shown that (8) the efficiency of acridine orange, compared with methylene blue, in causing a photodynamic effect is much greater.

* Department of Physics, College of Science, Al-Mustansiriyah University, Baghdad, Iraq.

The conditions required to obtain a marked destruction with acridine orange are very severe compared with those adequate with methylene blue, and the reaction is very complex and leads undoubtedly to a mixture of several products all of which could not be identified [1,7]. They manage to identify four of them ; guanidine, urea, ribose, and ribosylurea. The points of attack on the guanine molecule were represented by the authors shown below:

R = Ribose

____ = Point of attack

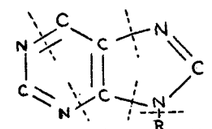

In this work an evidence is offered to show that deoxyribose is indeed attacked with either eosin or methylene blue as sensitizer. Also to show that eosin can bring about a selective photosensitized degradation of deoxyribose as well as guanosine.

EXPERIMENTAL

1. **Material** :

dGMP , dAMP , 2-deoxy-D-ribose, 2-deoxy-D-ribose phosphate, and tris buffer were of Sigma grade, used without any purification. Eosin (E) was of high purity grade from Hopkin and Williams. Methylene blue (MB) was of high purity grade from B.D.H. Diphenylamine was purified before use by two successive recrystallizations from ethanol. Isobutanol, ethanol, stannous chloride, sulfuric acid, acetic acid, KH_2PO_4 , and ammonium molybdate were all of Analar grade either from B.D.H. or Hopkin and Williams and used without any further purification. For aqueous solutions a triply distilled water was used.

2. Methods :

a- Inorganic phosphate estimation ;

Inorganic phosphate was measured by the method of Berenblum and Chain [9] as modified by Ennor and Stocken [10]. In this method 10 ml of the sample being irradiated were placed in a 50 ml separating funnel, followed by 1 ml of 10N sulfuric acid solution, 4 ml of distilled water and 5 ml of 5% ammonium molybdate solution. The separating funnel was then allowed to stand for 15 minutes to ensure completion of the reaction between phosphate and molybdic acid. 20 ml of isobutanol were then added and the whole mixture was vigourously shaken for varying intervals of time and the aqueous layer, after separation, was immediately run off. The alcohol layer was then shaken twice (10 seconds) with two successive volumes each of 10 ml of 1N H_2SO_4 , and then with 30 ml of 0.4% $SnCl_2$ solution which was prepared in 1N H_2SO_4. The alcohol layer containing the reduced phosphomolybdic acid was then made up to 25 ml with ethanol washings of the separating funnel and the sky-blue colour intensity measured at 700 nm using a Unicam SP 700 automatic double beam spectrophotometer against blank. A standard plot (O.D. versus concentration of known concentration of KH_2PO_4 was constructed using the above method.

b- Deoxyribose estimation ;

This was carried out by the diphenylamine method of Dische [11] and the optical density being measured at 595 nm on the Unicam SP 700. In this method the diphenylamine reagent was prepared by adding 2.75 ml of concentrated sulfuric acid to 100 ml of 1% of diphenyl-amine in glacial acetic acid. After mixing the sample being irradiated with the above reagent, the whole mixture was heated on a water bath for about three minutes, allowed to cool down with a running water, allowed to stand for

a few hours then measured against a blank solution at the specific wavelength.

c- Irradiation procedure ;

The nucleic acid components were dissolved at 2-10 x 10^{-4} M with sensitizer at 2 x 10^{-4} M. Either tris buffer PH 8.3 or triply distilled water PH 7 was used (see table for details). 80 ml of solution were placed in a water colled cell (with silica window) and irradiated by means of 1000 W Osram lamp. Aliquots were removed at intervals and their absorption spectra measured from 250 - 700 nm on a Unicam SP 700. From blank experiments with sensitizer and substrate alone, the U.V. spectrum of the substrate could be corrected for the change in the optical density of the sensitizer. (It is realised that absorbing products from both substrate and sensitizer will cause error in these measurements, but since we only wish to moniter the reaction in this way these are not corrected). After irradiation, in the methylene blue experiments, the solution was run over a column of IR 120 (Na^+ form) and eluted with NaCl solution to remove the sensitizer before analysis for phosphate and deoxyribose. In experiments with eosin the solutions were analysed without pre-treatment.

The cell and the glass vessels were cleaned before use with alcohol-nitric acid mixture and thoroughly rinsed, using several portions of distilled water, triply distilled water and dried in an oven at 50°C.

RESULTS AND DISCUSSION

From the table it can be seen that both eosin and methylene blue sensitise the photochemical degradation of guanine derivatives but not adenine as found previously by other workers [1 - 3]. This degradation is demonstrated in Figures 1 & 2 ; which shows the remaining concentration of the base plotted against the time of irradiation. Analysis for deoxy ribose destruction shows that

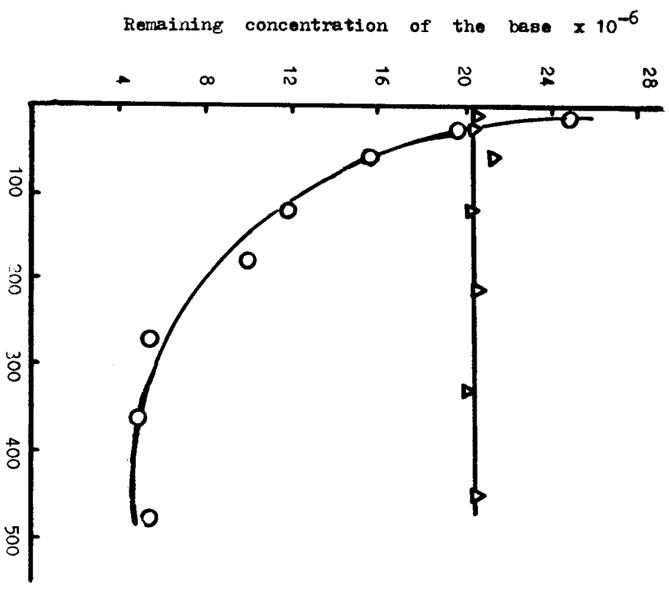

Fig. 1 Remaining concentration of the base vs time using (E).

Exper. No.	Irrad. Time (hrs.)	Solute used	Concen. Mx 10^5	Type of Sensit.	Concen. Mx 10^5	Phosphate Release Mx 10^5	Deoxyribose Mx 10^5	Base Destroyed Mx 10^5	Sensit. %	Destroyed	Tris
1	6	dGMP	66.7	E	13.3	0.22	8.8	54.7	95		Yes
2	6	dGMP	17.5	E	26.5	0.20	-	-	-		Yes
3	6	dGMP*	91.5	E	41.0	0.00	0.00	0.00	0.00		No
4	6	dGMP	83.0	M.B.	28.3	0.00	13.0	43.3	14.0		Yes.
5	6	dGMP	87.1	M.B.	24.4	0.10	-	-	-		No
6	12	dAMP	58.6	E	26.5	0.12	4.7	0.00	95		Yes
7	6	dAMP	84.0	M.B.	28.3	0.00	1.4	0.00	0.00		Yes
8	6	Deoxyribose	120.0	E	26.5	-	4.8	-	-		Yes
9	6	Deoxyribose 5-Phosphate	-	E	26.5	+	0.6	-	-		No

* Deoxygenated.

\+ Owing to the hydrolysis the amount of phosphate in the blank was too high to permit an accurate estimation.

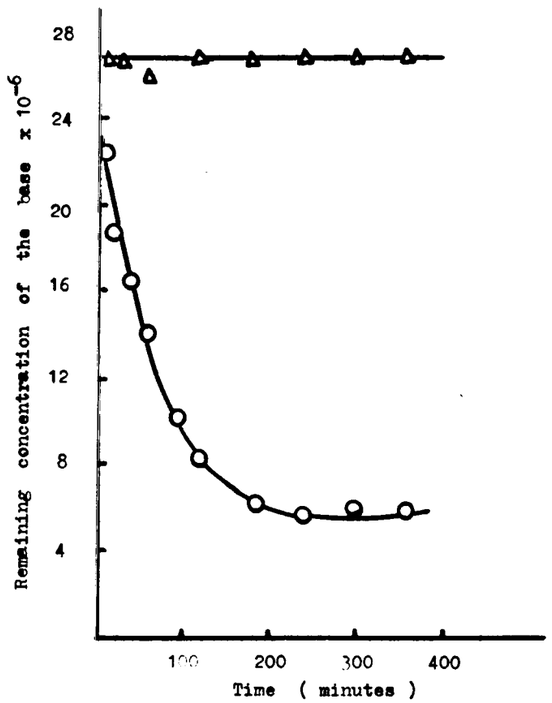

Fig. 2 Remaining concentration of the base vs time using (MB) .

this is a major reaction in the sensitized irradiation of deoxyribonucleotides with both methylene blue and eosin as sensitizers. In experiments concerning deoxyguanylic acid with methylene blue and eosin (Experiments 1, 2, 5) about 15% of the deoxyribose is destroyed for 50 - 80 % destruction of the guanine residue. With deoxyadenylic acid which show no effect on the base, deoxyribose is again destroyed (Experiments 6 & 7). Evacuated solutions of dGMP showed no change.

Phosphate released was also measured, and in these experiments only very small amounts of phosphate were released, indicating that most of the oxidation must take place on the 1' or 2' carbon of the sugar. One other effect was also noticed ; that in tris buffer solutions containing methylene blue as sensitizer no phosphate could be detected, whereas in water solutions some phosphate is released (Experiments 4 & 5). Deoxyribose itself is destroyed to some extent (Experiment 8) although with deoxyribose phosphate only a very small amount of deoxyribose is affected.

Overall therefore, it appears that destruction of deoxyribose is one of the major effects of the sensitized destruction of nucleic acid components and that effects on nucleic acids as such the loss of transforming ability, and a primer activity, may be in a large part due to deoxyribose destruction.

REFERENCES

1. M.I. Simon and H. Van Vunakis, J. Mol. Biol., 4, 488 (1962).
2. K.S. Sastry and M.P. Gordon, Biochim. Biophys. Acta. 129, 42 (1966).
3. J.S. Sussenbach and W. Berends, Biochim. Biophys., 95, 184 (1965).
4. D. Friefelder, P. F. Davison and E.P. Geiduschek, Biophys. J., 1, 389 (1961).
5. J.S. Bellin and G. Oster, Biochim. Biophys. Acta. 42, 533. (1960).
6. P. Chandra and A. Wacker, Z. Naturforsch, 21b, 663 (1966).
7. M.I. Simon and H. Van Vunakis, Arch. Biochem. Biophys., 105, 197 (1964).
8. K. Sivavama Sastry and M.P. Gordon, Biochim. Biophys. Acta, 129, 32 (1966).
9. I. Berenblum and E. Chain, Biochem. J., 32, 286, (1938).
10. A.H. Ennor and L.A. Stocken, Austr. J. of Exper, Biol. and Medicine, 28, 647 (1950).
11. Z. Dische, Mikrochemie, 4, 8 (1930).

DIELECTRON FORMATION IN THE γ - RADIOLYSIS OF SOME ALKALINE ICES

Saad K. Ismail *

INTRODUCTION

Although e_t^- and O^- are trapped in alkaline ices in approximately equivalent yields at low doses, this is not observed at high doses. The e_t^- dose yield curve levels off at about 2 M rads, independent of (OH^-), and the saturation yield is proportional to (OH^-). The most striking result is that at doses above 8M rads the e_t^- yield decreases until at 25 M rads it is about 50 % of its maximum value [1]. The O^- yield continues to increase over the same dose range and no new paramagnetic species are observed at high doses. Therefore, e_t^- must react above 8 M with a species other than O^- to form a diamagnetic species. An explanation for the dose saturation behaviour was suggested to the formation of dielectrons, $e_{2t}^=$, by the reaction shown below in competition with the trapping reaction in which T denotes a trap,

$$e^- + T \longrightarrow e_t^- \quad \ldots\ldots\ldots\ldots \quad (1)$$

$$e_t^- + e_t^- \longrightarrow e_{2t}^= \quad \ldots\ldots\ldots\ldots \quad (2)$$

In an $e_{2t}^=$ centre the second electron is probably bound much more weakly than the first electron. This is supported by the observation of the thermal dissociation reaction ;

$$e_{2t}^= \xrightarrow{135^\circ K} e_t^- \quad \ldots\ldots\ldots\ldots\ldots \quad (3)$$

* Department of Physics, College of Science, Al-Mustansiriyah University, Baghdad, Iraq.

Al-Mustansiriyah Journal of Science, Vol. 3 (1978).

Early work [2] indicated that optical bleaching of e_t^- led to a new, broad absorption in the near infrared.

$$e_t^- \xrightarrow{550\ nm} e_{2t}^= \quad \ldots\ldots\ldots\ldots\ldots \quad (4)$$

In recent work (1) a weak, broad band with a maximum near 900 nm in the near infrared has been assigned to $e_{2t}^=$. The band is very broad and difficult to study.

Keven has found that the reverse of reaction 4 induced by bleaching with 1000 nm light has been attempted with only irreproducible success, and stated that the weakness of the $e_{2t}^=$ band and the overlap of the e_t^- and $e_{2t}^=$ bands make this conversion experimentally difficult.

The model proposed for $e_{2t}^=$ is two electrons trapped in the same vacancy. This model is analogous to the F-centre in irradiated alkali halides [3]. The F-centre consists of two electrons trapped in the same halide ion vacancy, it is diamagnetic, and has broad optical absorption in the near infra-red. It can be thermally dissociated to yield F-centre which is analogous to e_t^-, and can be produced by optical bleaching of the F-centre.

EXPERIMENTAL

1) Materials:

Potassium hydroxide, Potassium Iodide are of B.D.H. Analar grade used without any further purification. Ethanol is Hopkin and Williams "spectrosol" grade bottled under nitrogen gas was used without purification. All aqueous solutions were made using triple distilled water.

2) Irradiation and dosimetry :

The irradiation source employed was Co^{60} γ-rays source. The dose-rate given in most experiments is located around 2.3×10^{17} ev ml^{-1} min^{-1}. The dose-rate at each position in the irradiation stand was determined chemically employing the Fricke dosimeter developed by Miller [4]. The dose-rate in the dosimetry solution was calculated using the expression,

$$D = \frac{O.D.}{\epsilon} \times \frac{1}{l} \times \frac{1}{G} \times 6.02 \times 10^{23} \times \frac{1}{t}$$

where D = dose-rate in ev ml^{-1} min^{-1}

ϵ = molar extinction coefficient of Fe^{3+} at 25°C
(Vis. 2.2×10^{3} M^{-1} cm^{-1}).

O.D = radiation induced optical density at 304 nm.

l = path length of silica cell in cm.

G = number of Fe^{3+} ions produced per 100 ev of energy absorbed (Vis. 15.5).

t = time of irradiation in minutes.

The dose-rate value was corrected for the natural radioactive decay of cobalt 60 ($T_{\frac{1}{2}}$ = 5.3 years).

Optical absorption measurements at 77°K :

Measurements of the optical absorption spectra of γ-irradiated alkaline glasses at 77°K were obtained by means of Unicam SP 800 spectrophotometer. The normal compartment of this instrument was replaced by a specially constructed variable temperature unit. Before irradiation, the optical absorption spectrum of the sample to be irradiated was measured at 83°K against a blank cell containing an identical glassy sample.

4) Variable temperature unit :

The RIIC variable temperature unit (- 190°C to 250°C / 83°K to 523°K) works on a Dewar principle utilizing a vacuum pressure of 50 microns Hg or 0.05 mm Hg. The unit consists of an outer Jacket has two demountable quartz windows. Each window holder is fitted with an electric heater to prevent condensation. Also the sample cell holder which is fitted directly to the base of the stainless steel refrigerant vessel. Facilities for vacuum pump connection and electrical leads are conveniently, arranged on the top plate of this vessel. The sample cell holder is fitted with two heaters which enables the raising of the temperature of the sample cell from - 190°C to 250°C.

The whole unit is connected to the vacuum pump, evacuated to a pressure of 0.05 mm Hg. The window heaters are switched on for 5 - 10 minutes and then the unit cooled down using liquid nitrogen. A steady temperature is reached in 15-20 minutes. The whole spectrophotometer is located in a dry box with dry nitrogen gas flowing continuously to avoid any moisture condensation. The same dry nitrogen gas is used to release the pressure inside the unit enabling the cells to be changed.

5) Sample preparation :

Sample vessels were constructed from 15 cm lengths of rectangular spectrosil radiation resistant fused silica tubing (internal dimensions 15 $\pm$ 0.5 mm x 5 $\pm$ 0.5 mm) supplied by Thermal Syndicate Limited. The cells were attached via silica to pyrex graded seals, to vacuum taps and B14 sockets. 2.5 ml were introduced into the vessels and the tap was greased with Apiezon-L high vacuum grease and the vessel attached to the vacuum line. The deaeration was carried out by means of several shaking-pump cycles at room temperature and by this method the solution could be thoroughly deaerated to a pressure of 10^{-4} mm Hg.

6) Photobleaching :

The photobleaching processes were done with visible light using a 1000 Watt tungsten lamp as a source. The samples were bleached in a pyrex dewar provided with silica windows placed vertically in front of the lamp for 3 - 5 minutes until the sample was colourless. Photobleaching was carried out using ethanol contained in silica cells as filter.

Infrared source (1 kw filament) was used for exposing the samples to infrared radiation after photobleaching the samples.

RESULTS AND DISCUSSION

Kevan has noticed that photobleaching the blue centres (trapped electrons) in 7 M alkaline glass at 585 nm gave rize to a new, very broad absorption in the infrared region extending between 800 - 1500 nm with its maximum at 900 nm. However he could not regain the blue colour at 585 nm by exposing the sample to an infrared source of wavelength 900 nm and he attributed this to experimental difficulties.

In this work (a) pure 7 M KOH glass and (b) 0.2 M Potassium iodide in 7 M KOH glass, were all given a dose of about 2 M rads at 77°K.

The samples were then photobleached with tungsten light, using water or ethanol filter to avoid effects of the infrared radiation, a colourless glass was obtained. This colourless glass gave a very weak and broad absorption above 850 nm (Fig. a) The above samples were then irradiated with an infrared light, leading to at dark blue colour absorbing at 580 nm (Fig. b). It was noticed also that the process of transformation from colourless to blue and from blue to colourless was reversible. If the concept of the dielectron is tenable, then the above transformation can be represented by :

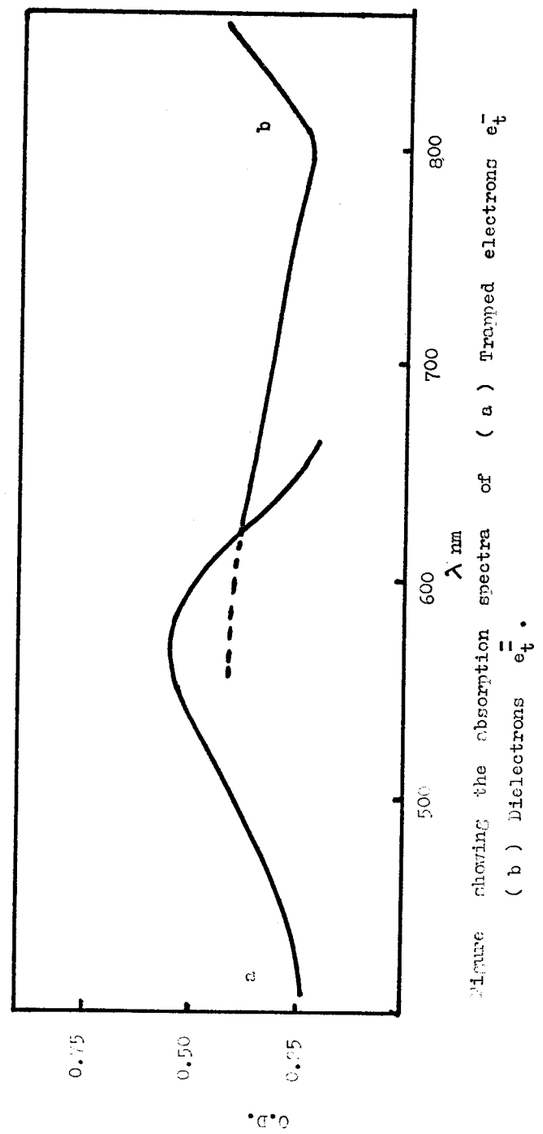

Figure showing the absorption spectra of (a) Trapped electrons e_t^- (b) Dielectron = e_t^-.

$$e^-_{t_1} + e^-_{t_2} \xrightarrow[+\ \text{filter}]{\text{visible light}} e^{=}_{2t} \quad \ldots\ldots\ldots \quad (5)$$

and

$$e^{=}_{2t} \xrightarrow[\text{source}]{\text{infrared}} e^-_{t_1} + e^-_{t_2} \quad \ldots\ldots\ldots \quad (6)$$

where t_1 and t_2 represent two different trapping sites. The above phenomena are explained according to two aspects in addition to the above dielectron formation. (a) The idea suggested by Buxton et al. [5] in which an electron photochemically ejected from a trap may not fall back into the same trap but also be retrapped elsewhere ; as shown below :

$$(e^-_t)_2 + h\nu \longrightarrow e^-_m \longrightarrow (e^-_t)_1 \quad \ldots\ldots\ldots \quad (7)$$

or it is possible that the electrons might be shuttled between shallower and deeper traps, and very few reach O^- and hence suffer total destruction :

$$\begin{array}{lll} e^-_t \text{ shallow} + h\nu\ (\text{IR}) \longrightarrow & & e^-_m \\ \uparrow & & \downarrow \\ e^-_t \longleftarrow & h\nu\ (\text{visible}) + e^-_t & (\text{deep}) \end{array} \quad \ldots\ldots\ldots \quad (8)$$

(b) The idea suggested by Gopinathan et al [6] in which they found an unstable species in photolyzed NaOH solution. The authors suggested the possibility for this species to ionize by light of wavelengths as long as 340 nm and produce e^-_{aq}, the hydrated electron. They attributed this species to a dissociable complex involving Na^+ and e^-_{aq} ; assuming its structure to be $Na^+.e^-$ and,

$$(Na^+.e^-)_{aq} + h\nu \longrightarrow Na^+_{aq} + e^-_{aq} \quad \ldots\ldots\ldots \quad (9)$$

The first two possibilities sounds more reasonable since in our experiments we are photolyzing with a visible light ranging from below 340 nm and upto 850 nm. By using the above range we were getting a colourless glass, and if the above last reaction or Gopinathan suggestion is true we should still get some blue

colour absorbing at 585 nm by the above transformation. Since the blue colour was regained by the effect of the infrared irradiation, we supported the two ideas presented by Kevan and Buxton.

REFERENCES

1. J.Zimbrick and L. Kevan, J. Am. Chem. Soc., 89, 2483 (1967).

2. M.J. Blandamer, L. Shields and M.C.R. Symons, J. Chem. Soc., 4352 (1965).

3. J.H. Schulman and W.D. Compton, Colour Centres in Solids. PP.107-112.

4. Miller and Wilkinson, Disc. Fara. Soc., 12, 50 (1952).

5. G.V. Buxton, F.S. Dainton, T.E. Lantz and F.P. Sargent, Trans. Farad. Soc., 66 (12), 2952-73 (1970).

6. C. Gopinathan, E.J. Hart and K.H. Schmidt, J. Phys. Chem., 74, 4169 - 71 (1970).

CLAY MINERALOGY AND GEOCHEMISTRY OF LAKE DEPOSITS FROM KHARGA AND DAKHLA OASES, EGYPT

M.E. Milmy, S.A. Hussein*, and N. Saad

ABSTRACT

The clay fractions of the lake deposits from Kharga and Dakhla Oases (Western Desert, Egypt) have been studied in detail from their mineralogical and geochemical points of view. The following minerals have been identified and described using X-ray diffraction analysis, infrared spectrometry and electron microscopy: Kaolinite, illite, montmorillonite, mixed layers, Calcite, dolomite and gypsum. Geochemically, the lake deposits are more enriched with average shale given by Degens [6] which is more illitic.

INTRODUCTION

Vast areas of lake deposits are known to occur in several localities of Kharga and Dakhla Oases (Western Desert, Egypt). These deposits were first reported and described by Beadnell [1] as lacustrine deposits. The name " lake deposits " was given by Awad et al [2], to the sand, silt and clay sediments of Pleistocene Recent age and deposited at the floor of both Kharga and Dakhla Oases. Gardner et al. [3] , divided these deposits into three groups: 1) loess-like or aeolian silt deposits. 2) well deposits

* Faculty of Science, Ain Shams University, Cairo, Egypt.
Now on deputation to Department of Applied Geology, College of Science, Al-Mustansiriyah University, Baghdad, Iraq.

Al-Mustansiriyah Journal of Science, Vol.3 (1978).

arrested by vegetation around past and present wells, 3) Pleistocene spring overflow deposits. Embabi [4] described these deposits geomorphologically as "Semi-playa" deposits.

More recently, Milmy et al. [5] , took over studies of these lake deposits from geological and sedimentological points of view, to determine their orgin and palaeonvironmental significance. According to Millmy et al. [5] , the lake deposits occur in the form of flat plains and hummocks oriented in a NNW-SSE direction. Texturally they were classified in the form of different varieties of sands and silts (e.g. sand, mud sand, silty sand, sand silt, ... etc.). The Carbonate percentage varies, between 3 % - 18 % in these deposits. Milmy et al [5] suggested that the lake deposits in Kharga and Dakhla Oases, were originated from the nearby formations, transported in a fresh environment and deposited in a shallow marginal environments of deposition (e.g. lakes, ponds, lagoons.... etc.).

The present study aims to present the results of the mineralogy, electron microscopy and geochemistry of the clay minerals existing in the lake deposits.

Location and Sampling

Kharga and Dakhla Oases are situated in the Southern Western Desert of Egypt, at about of 200 Km and 305 Km, respectively, west of the Nile (from Assiut), (Fig. 1). The analysed samples were collected from the following areas, which comprise the main outcrops of the lake deposits: Mahariqe, Bolaqe, Genah, Beris, El-Max and Kharga- Dakhla road (Kharga Oasis), El-Zayat and Mawhoob (Dakhla Oasis).

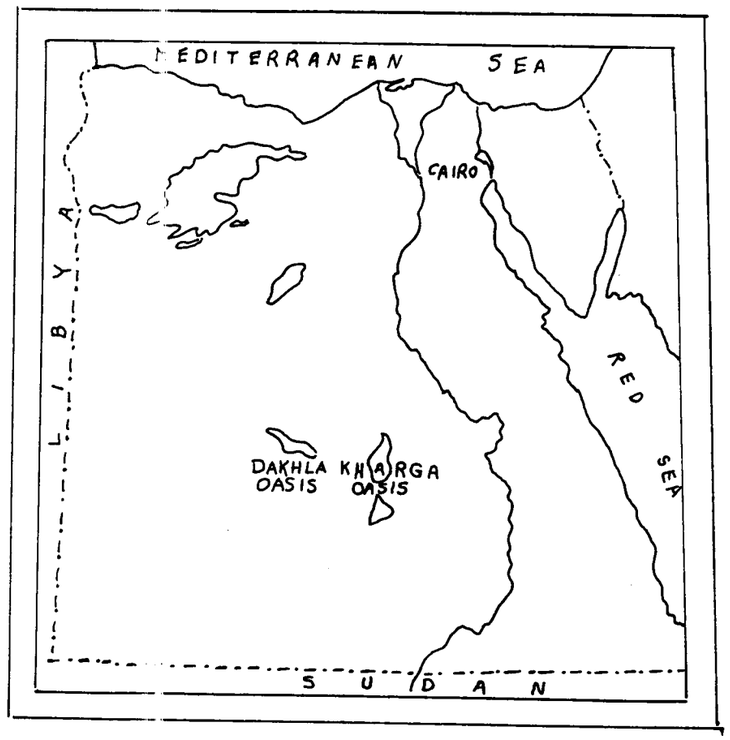

FIG(1) LOCATION MAP FOR KHARGA AND DAKHLA OASES

X-Ray analysis

Since the clay minerals existing in the lake deposits are of minute grain size and cannot be easily identified by means of the polarizing microscope, the powder X-ray diffraction technique is considered to be a suitable tool for their identification. To determine the clay and non-clay minerals present in the lake deposits, unoriented and oriented samples was analysed. In the first case, the original bulk sample was used, while in the second one, three oriented mounts for the clay fraction (< 2 u) was prepared and three diffraction patterns were run, i.e. Untreated, glycolated and heated at 550°C for two hours, Grim, [6,7] .

Seventeen samples from Kharga and Dakhla Oases were used in X-ray analysis. Table (1) illustrates location, description of these samples and the method used for analysis.

A- X-ray analysis of bulk samples

Six X-ray diffraction patterns of bulk samples of lake deposits are shown in Fig. (2). Their X-ray data revealed the presence of the following minerals:

1- Quartz: was found to the most ubiquitous non-clay mineral in the lake deposits. All samples were found to contain different percentages of quartz.

2- Kaolinite: was identified in all samples as the most representative clay mineral. The X-ray diffraction patterns of the untreated mounts of kaolinite show a series of basal reflections, the most intense of which are those at 7.15 A°. The

Table (1): Location, description of lake deposit samples and the method used for X-ray analysis

Sample No.	Location	X-ray method	d e s c r i p t i o n
1-	Mahariq (Kharga)	Untreated	Silty sand, compact, brownish, fine-grained, calcareous.
2-	" "	Oriented	Silty sand, compact, grey, fine-grained, calcareous.
3-	" "	Oriented	Silty sand, friable, brownish, fine-grained, calcareous.
4-	" "	Untreated	Silty sand, friable, brownish, fine grained calcareous.
5-	Bolaqe "	Untreated	Sand, friable, brownish, very fine-grained, calcareous.
6-	Beris "	Oriented	Silty sand, friable, brownish, medium-grained.
7-	" "	Oriented	Silty sand, friable, brownish, fine-grained.
8-	" "	Untreated	Silty sand with salt crystals and (carbonate), friable, brownish.
9-	" "	Oriented	Silty sand, friable, brownish, calcareous.
10-	El-Max "	Oriented	Silty sand, compact, brownish, calcareous.
11-	Kharga-Dakhla road.	Oriented	Silty sand, compact, brownish, calcareous.

Table (1) Cont'd.

Sample No.	Location	X-ray method	d e s c r i p t i o n
12-	Kharga-Dakhla road.	Untreated	Silty sand, compact, brownish, calcareous.
13-	Kharga-Dakhla road.	Untreated	Silty compact, brown, calcareous.
14-	Kharga-Dakhla road.	Oriented	Silty sand, compact, brown
15-	El-Zayat (Dakhla)	Oriented	Silty sand, compact, grey, calcareous, gypsum.
16-	Mawhoob "	Oriented	Sandy silt, slightly compact, very fine-grained, calcareous, gypsum.
17-	" "	Oriented	Silty sand, friable, brownish, calcareous, plant remains.

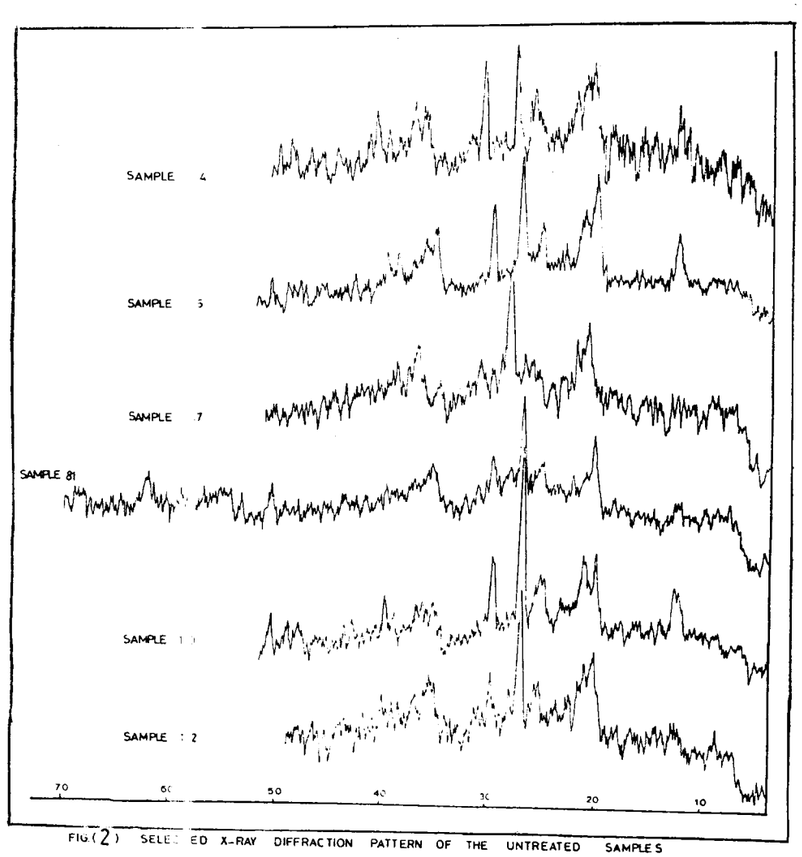

FIG.(2) SELECTED X-RAY DIFFRACTION PATTERN OF THE UNTREATED SAMPLES

number, intensity and sharpness of the diffraction peaks depend upon the degree of crystallization of kaolinite.

3- Illite: characterized by a series of strong, broad X-ray diffraction peaks at 4.52 A° , 4.29 A°. 3.42 A° and 3.36 A° that are unaffected by glycolation or heat treatment.

The X-ray diffraction patterns showed a reflection at about 10 A° which indicate the presence of illite or halloysite. But the presence of a basal reflection at 3.3 A° is caused only by the latice of illite.

4- Montmorillonite: It is a clay mineral in which the component layers are not tightly bounded by K^{+} ions (mica) or Mg^{+2} ions (vermiculite) but contains water molocules in a similar situation. When dried under ordinary room condition when it has Na^{+} , as the exchange ion, it has one molocular layer of water and a basal reflection at about 12.5 A°, when Ca^{+2} is the exchange ion has two molocular water layers and a basal reflection at about 14.15 A° Grim, [7] . Ca-montmorillonite is the type which is represented in the six samples of lake deposits under investigation.

5- Carbonate minerals: These are represented by calcite and dolomite. Calcite is identified in samples No. 3, 8, 12, 13, while dolomite is identified in samples No. 1, 5, 8.

B- X-ray analysis of oriented samples

The analytical data obtained from the eleven X-ray diffraction patterns of the oriented samples of lake deposits are shown in

Tables (2, 3, 4), while Figs. (3,4) shows the X-ray diffraction pattern of some selected samples. The following is a description of these patterns :

1- Untreated X-ray method: The X-ray diffraction patterns of the untreated samples (Figs. 3, 4) show the following characters :

a- The diffraction recordings of all samples are characterised by the presence of a relatively broad peak with a spacing in the range of 15.22 A° to 14.22 A° (see Table 2). This first- order basal reflection is present in most samples with a relatively moderate intensity and reaches its largest value in samples 6 and 9.

b- A sharp basal reflection appears in the X-ray diffraction patterns of samples 15 and 16 only at 7.55°A and 7.49° A.

c- A sharp basal reflection appears in the X-ray diffraction patterns of all samples at 7.18°A. This first-order peak is most intense in samples 6, 9, 11 and 14.

d- The X-ray diffraction patterns of all samples exhibit a basal reflection with a spacing at 3.56 A°. This second-order peak occurs with small intensity with the exception of samples 6, 9 and 11 where its peaks are instance.

e- Another peak in the range of 3.35 to 3.34 A° appears in the patterns of all the samples. This peak is of a relatively smaller intensity than the above one except samples 9 and 11 where this peak is the most intense peak.

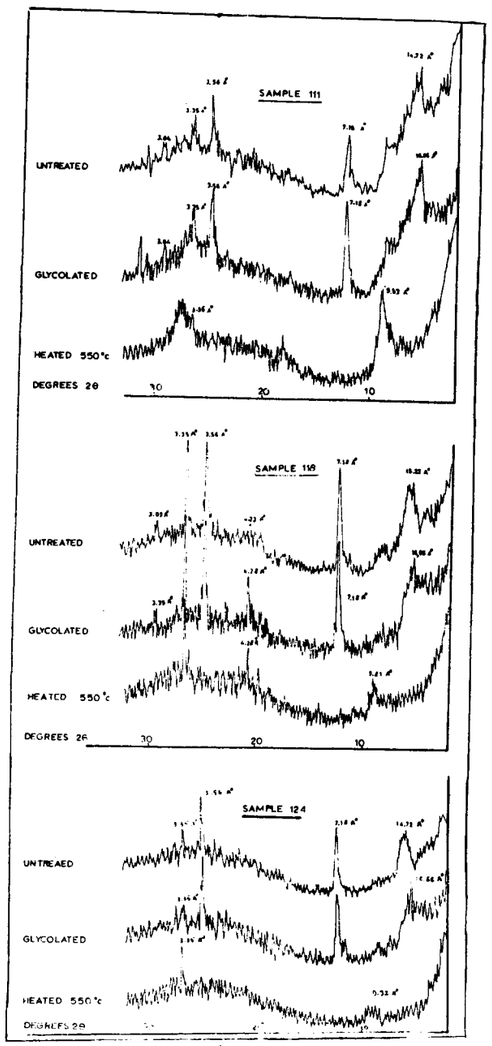

FIG(3)SELECTED X-RAY DIFFRACTION PATTERNS OF ORIENTED SAMPLES.

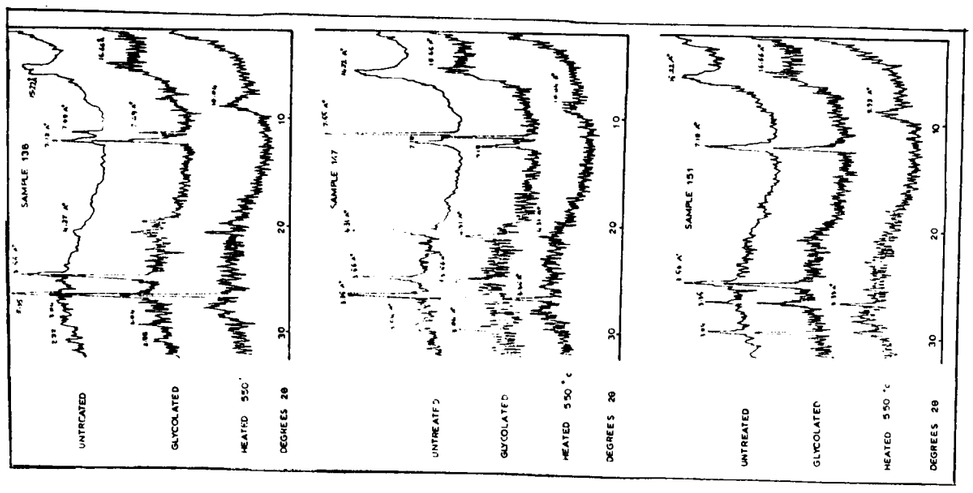

FIG (4) SELECTED X-RAY DIFFRACTION PATTERNS OF ORIENTED SAMPLES.

Table (2): X-ray diffraction data of the untreated clay samples

Sample 2		Sample 3		Sample 6		Sample 7		Sample 9		Sample 10		Sample 11		Sample 14		Sample 15		Sample 16		Sample 17	
dA°	I	dA°	I	dA°	I	dA°	I	dA°	I	dA°	I	dA°	I	dA°	I	dA°	I	dA°	I	dA°	I
14.72	30	15.22	33	15.22	40	14.96	100	14.72	39	14.72	100	15.22	33	14.72	40	15.22	57	14.22	40	15.22	55
---	--	---	--	---	--	---	---	---	--	---	---	---	--	---	--	7.49	70	7.55	100	---	--
7.18	36	7.18	73	7.18	66	7.18	67	7.18	41	7.18	91	7.18	89	7.18	100	7.18	70	7.18	25	7.18	100
---	--	---	--	---	--	---	---	4.27	24	---	--	4.23	22	---	---	---	--	4.31	62	---	---
3.56	26	3.56	76	3.56	100	3.56	71	3.56	54	3.56	96	3.56	78	3.56	73	3.56	77	3.56	48	3.56	91
3.35	91	3.35	100	3.35	77	3.35	83	3.35	100	3.35	61	3.35	100	3.35	47	3.34	100	3.35	62	3.35	52
3.02	100	3.04	70	---	--	---	--	3.04	13	3.04	36	3.03	22	---	--	3.04	100	3.04	22	3.04	25
2.88	47	2.90	45	---	--	---	--	---	--	---	--	---	--	---	--	2.88	20	---	--	---	--

f- A moderate intense peak appears in the range of 3.04 A° and 3.02 A° in all samples except samples 6, 7 and 14. Also another small peak appears in the range of 2.9 to 2.8 A° in samples 2,3 and 15. Samples 15 and 16 show a sharp peak at 7.49 and 7.55 A°. In samples 9,11 and 16 another peak is present at 4.27, 4.23 and 4.31 A° respectively.

2- Glycolated method: In the glycolated samples (Table 3) the X-ray diffraction patterns are almost identical with those of the corresponding untreated specimens (i.e. there is no remarkable shift in the position of the peaks), except for the first peak at 15.22 to 14.22 A°, which shifts to about 16.66 A°. Also there is no appreciable change in the relative intensities, e.g. the peak occurring at 3.35 A° in the untreated sample No.9 is the most intense one also the glycolated samples. The peaks appearing at 7.49 and 7.55 A° appears also in glycolated samples.

3- Heated method: Table (4) shows X-ray data of the heated samples. In the heated clay specimens, the X-ray diffractions show that the first peak in the range 14.22 - 15.22 A° (basal spacing) is shifted to about 10 A°. This is due to the removal of the absorbed interlayer water by heating to 550°C. The two basal reflections detected in the diffraction recordings of both the untreated and glycolated samples with spacings at about 7.18 A° and 3.56 A°, were completely destructed by heating. The peak at about 3.35 A° was unaffected. The peak

Table (3) : X-ray diffraction data of the glycolated samples

Sample 2		Sample 3		Sample 6		Sample 7		Sample 9		Sample 10		Sample 11		Sample 14		Sample 15		Sample 16		Sample 17	
dA°	I	dA°	I	dA°	I	dA°	I	dA°	I	dA°	I	dA°	I	dA°	I	dA°	I	dA°	I	dA°	I
16.66	100	16.66	65	16.66	90	16.66	80	16.66	50	16.66	50	16.66	30	16.66	60	16.66	40	16.66	60	16.66	64
—	—	—	—	—	—	—	—	—	—	—	—	—	—	—	—	7.49	44	7.55	95	—	—
7.18	50	7.18	78	7.18	90	7.18	100	7.18	56	7.18	100	7.18	100	7.18	90	7.18	75	7.18	55	7.18	90
—	—	—	—	—	—	—	—	4.27	30	—	—	4.23	40	—	—	—	—	4.31	67	—	—
3.56	80	3.56	100	3.56	100	3.56	88	3.56	63	3.56	87	3.56	95	3.56	100	3.56	98	3.56	80	3.56	100
3.55	80	3.55	94	3.35	94	3.53	85	3.35	100	3.35	42	3.35	95	3.35	30	3.34	100	3.34	100	3.35	65
3.02	50	3.04	30	—	—	—	—	3.04	17	3.04	30	3.03	26	—	—	3.04	30	3.04	55	3.04	85
2.88	30	2.90	30	—	—	—	—	—	—	—	—	—	—	—	—	2.88	17	—	—	—	—

at 3.04 A° disappeared upon heating. The small peak revealed by both the untreated and glycolated specimens of samples 2, 3 and 15 at about 2.88 A° disappeared upon heating. The peak revealed by both untreated and glycolated specimens at 7.49 and 7.55 A° of samples 15 and 16 disappeared also upon heating. On heating to 550°C the peak at about 4.27 A° showed a relative dearease in intensity.

Discussion of the results of X-ray diffraction analysis

A- Clay mineral

The above mentioned X-ray patterns reveal the presence of the following clay minerals:

1- **Kaolinite:**

The mineral was identified from the presence of a series of basal reflections, the most intense of which are those at about 7.1 A° and 3.56 A°. These two peaks were not affected by glycolation and disappeared on heating. The number, intensity and sharpness of the diffraction peaks depend primarily on the degree of crystallization of kaolinite. Kaolinite has been identified in all the studied samples. The disappearance of the two peaks 7.1 A° and 3.56 A° upon heating (due to the collapse of the clay lattice) is exhibited only by kaolinite at that temperature (550°C).

2- **Illite:**

It is characterized by a series of weak, broad, X-ray diffraction peaks at 10 A° (001), ~5 A° (002) and ~ 3.35 A° (003) which were not affected by glycolation or heat treatment.

Table (4) : X-ray diffraction data of the heated samples

Sample 2		Sample 3		Sample 6		Sample 7		Sample 9		Sample 10		Sample 11		Sample 14		Sample 15		Sample 16		Sample 17	
dA°	I	dA°	I	dA°	I	dA°	I	dA°	I	dA°	I	dA°	I	dA°	I	dA°	I	dA°	I	dA°	I
10.1	30	9.82	30	10.04	95	9.82	80	9.60	54	9.82	100	9.82	40	9.92	45	10.04	35	10.04	40	9.93	82
---	--	---	--	---	--	---	--	---	--	---	--	---	--	---	--	---	--	---	--	---	--
---	--	---	--	---	--	---	--	---	--	---	--	---	--	---	--	---	--	---	--	---	--
3.35	100	3.35	100	3.35	100	3.35	100	3.35	100	3.35	50	3.35	100	3.35	100	3.35	100	3.35	100	3.35	100
								4.27	--	---	---	4.23	52	---	--	4.31	33	---	--		

The peak which appears at 3.35 A° is the only one present in all samples of lake deposits whereas the other peaks were not all present.

3- Mixed-layer clay minerals:

The identification of mixed-layer clay was based mainly on the method adopted by Millot [8] .

The X-ray diffraction patterns of all samples revealed the presence of mixed-layer clays. The pattern of the untreated specimen is characterized by a broad basal reflection at about 14.22 A° which upon glycolation was shifted to about 16 A° , when heated to 550°C for two hours, this pattern collapsed to a spacing at 10 A°. According to Millot [8] , this behavior indicates a randomly interstratified Ca-montmorilloni e-illite clay. The spacing at about 14.22 A° in the pattern of untreated specimen is the average (001)/(001) spacing obtained from the 10 A° and 14 A° spacings characteristic of illite and Ca-montmorillonite respectively. The 16 A° spacing exhibited by the pattern of the glycolated specimen indicates that montomorillonite layers are abundant and this spacing is the result of the 10 A° / 17 A° combination. The peak reported in the tracing of the heated specimen at about 10 A° represents the comination of the 10 A° peak of illite and 9.8 A° peak of the heated Ca-montmorillonite.

B- Non-clay minerals

1- Carbonate: The carbonate minerals occur as calcite and dolomite. Calcite is represented by a moderately intense peak at

about 3.04 A° in all samples except samples 6,7 and 14.

Dolomite is represented by the peak at about 2.88 A° in samples 2, 3, and 15.

2- Gypsum: Is identified in only two samples 15, and 16 at 7.49 and 7.55 A° peak which disappeared on heating at 550°C.

3- Quartz: Is identified in all samples. It was revealed by the peak at 3.34 A° in the untreated, glycolated, and heated specimens.

Infrared spectrometry

It is possible to determine some of the vibration frequencies of atoms of a solid by using the absorption method in which the infrared radiation is passed through the sample. If the frequency of the radiation coincides with a vibration frequency, the solid absorbs some of all of the infrared radiation of frequency. The percentage of radiation which is absorbed by the samples is plotted against the incident wavelength (in frequency).

The infrared absorption spectra of the different clay minerals have been studied by several workers. Hunt et al [9] , and Keller et al [10,11] reported infrared spectra of many of the natural clay minerals in the range between 5000 cm^{-1} and 650 cm^{-1} Bellany [12] , extended the spectral range of study to 400 cm^{-1} .

The main groups in the lattice of clay minerals responsible for the infrared vibrations according to all workers are: the bonded (OH) group, the unbonded (OH) group, the (Si-O) group, the (O-H-Al) group, and the (Si-O-Al) group.

The infrared spectral analysis were carried out on the same seventeen samples which were examined by X-ray diffraction analysis. The samples were studied by infrared spectrometer (Unicam Sp. - 1200), using the procedure recommended by Keller et al. [11] . Table (5) shows the wave lengths of the identified bands in the analysed samples. Fig. (5) shows the infrared spectra of some selected samples.

These bands revealed the following characters :

1- A small absorption band (A) recorded in all samples, except samples 1, 11, with a vibration ranging from 470 - 475 cm^{-1}.

In most of the samples this band is resolved in to two or three minor bands (e.g. samples No. 17, 3, 14, 16). This band corresponds to the vibration of the (Si-O) group caused kaolonite at 470 cm^{-1}.

2- A very sharp and broad band (B) recorded in all samples in the range 520 - 540 cm^{-1}. This absorption band corresponds to the vibration of the (Si-O-Al) group, Pablo [13] .

In sample 4, this band represents the stretching vibration of this group caused by kaolinite at 540 cm^{-1}. In the spectra of all other samples it represents the vibration of the same group caused by illite at 520 cm^{-1}. Abu Zeid [14], recorded this band at 535 cm^{-1} .

3- A sharp band (C) recorded in the infrared spectral curves of all the samples in range 693 - 698 cm^{-1}. This absorption band represents the vibration of (Si-O) group shown by Kaolinite at 690 cm^{-1}.

Table (5): The infrared absorption spectra of the analysed samples

Band	Samples 1	2	3	4	5	6	7	8	9	10	11	12	13	14	15	16	17
A	—	470	470	470	470	470	470	470	470	472	470	—	470	475	470	470	440
B	525	530	520	540	523	520	520	530	520	523	520	530	525	523	530	520	523
C	695	695	695	695	695	695	695	695	695	695	695	698	695	695	695	595	695
D	780	775	778	778	778	778	778	778	780	780	778	780	775	780	775	775	780
E	798	799	798	795	798	798	798	795	798	798	798	800	798	798	795	798	798
F	875	875	875	875	880	875	875	875	875	875	875	875	875	885	875	875	875
G	912	915	910	910	915	912	912	912	910	912	912	912	910	910	915	910	915
H	1055	1050	1045	1050	1040	1055	1055	1050	1055	1055	1055	1055	1050	1045	1050	1050	1055
I	1440	1440	1440	1450	1420	1440	1440	1450	1440	1440	1440	1440	1440	1440	1440	1440	1440
J	1660	1660	1660	1660	1650	1660	1650	1660	1660	1660	1660	1660	1660	1660	1660	1660	1650
K	1700	1700	1700	1695	1700	1710	1700	1700	1700	1770	1770	1770	1770	1770	1770	1695	1770
K'	——	——	——	2000	——	——	——	——	——	——	——	——	——	2000	——	——	——
L	2360	2320	2210	2220	——	2220	2220	2210	——	2220	——	2210	2220	2220	2220	2220	2210
M	2510	2350	2360	2350	2360	2370	2360	2370	2370	2340	2360	2370	2380	2350	2340	2340	2340
N	3450	3450	3450	3450	3440	3440	3440	3450	3440	3440	3440	3430	3450	3440	3430	3450	3440
O	3620	3620	3620	3620	3620	3620	3620	3620	3620	3620	3620	3620	3620	3620	3620	3620	3620
P	3695	3695	3695	3650	3695	3700	3685	3695	3695	3695	3695	3700	3695	3695	3695	3695	3695

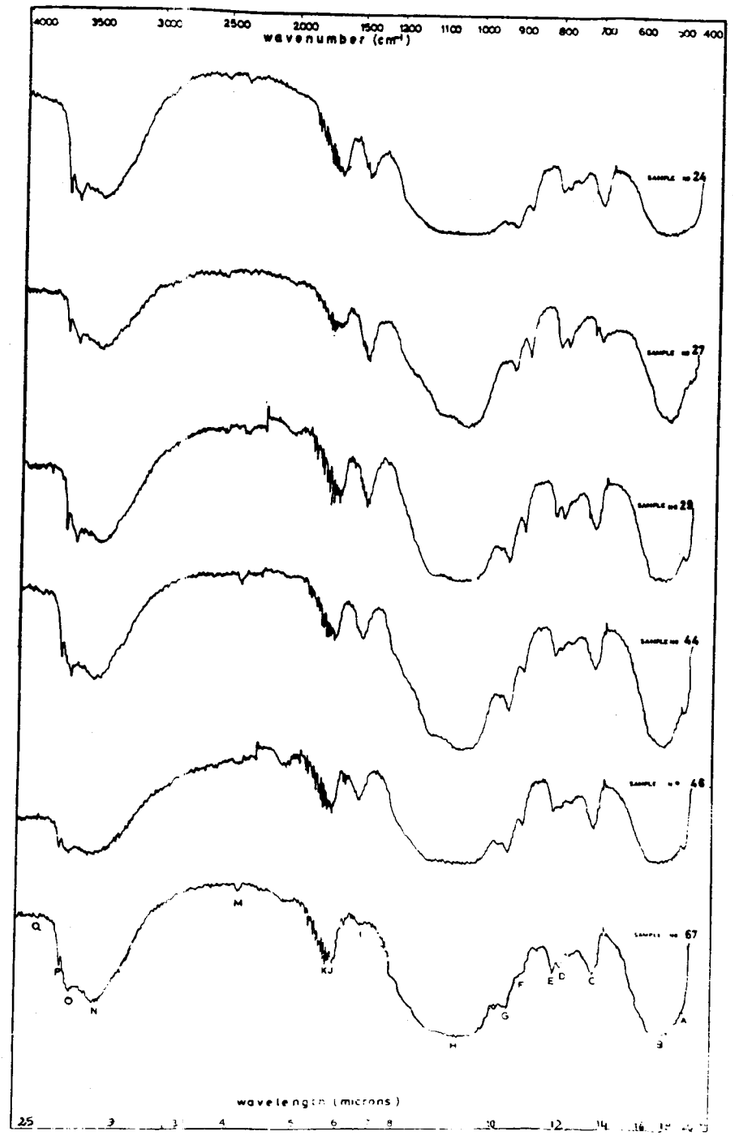

FIG(5) INFRARED SPECTRA OF SOME SELECTED SAMPLES.

4- A small absorption band (D) appeared in the spectra of all samples, in the range 775 - 780 cm^{-1}. This band corresponds to the vibration of quartz (Keller et al.) [10] .

5- A small absorption band (E) appeared in the infrared spectra of all samples in the range 795 - 798 cm^{-1}. This band represents the vibration of the (Si-O) group caused by kaolinite (according to Hunt et al. [9] , this group appeared at 793 cm^{-1}). Also Abu Zeid, [14] recorded this group in the range from 790 - 800 cm^{-1}.

6- A sharp absorption band (F) appears in all samples in the range 875 - 880 cm^{-1}. This band corresponds to the vibration of CO_3 group (dolomite), according to Keller et al [11] , who gave the spectra for dolomite at 878 cm^{-1} .

7- A sharp absorption band (G) in all the studied samples, but small in samples 1 and 11, appeared in the range 910 - 915 cm^{-1}. This band corresponds to the vibration of the (OH-Al) group. According to Hunt et al. [9] , this group is recorded at 909 cm^{-1} .

8- Very sharp and broad absorption band (H) appeared in all samples in the range 1040 - 1050 cm^{-1} characteristic to silicate minerals. This band is caused by illite at 1030 cm^{-1} , Abu Zeid, [14] .

9- A sharp band (I) appeared in all samples, except sample 124, in the range 1420 - 1440 cm^{-1}, represents the vibration of CO_3 group (calcite), according to Keller et al. [11], and Huang et al. [15] .

10- Two small and sharp bands appeared in all samples (J) at 1660 cm^{-1} and (K) in the range 1695-1710 cm^{-1} . These two bands represent the vibration of quartz (Keller et al [10] .

11- A small band (L) appeared in all samples, except samples 17, 5, 9, and 10, in the range of 2210-2230 cm^{-1} , represents the vibration of dolomite (Huang et al. [15] .

12- A small band (M) in all samples in the range of 2340-2380 cm^{-1}, except in sample, 1, it appeared at 2510 cm^{-1}. This band according to Huang et al [15] , represents the CO_3 group (Calcite).

13- A broad band (N) appeared in all samples in the range 3430-3450 cm^{-1} This band represents the vibration of bonded or absorbed OH). According to Van der Marel et al [16] , this band recorded at 2440 cm^{-1} .

14- A small band (O) at 3620 cm^{-1} appeared in all samples. This band represents the vibration of unbonded (OH) (Serratosa et al. [17] . It represents an overlap of the absorption bands caused by both illite and kaolinite.

15- A small band (P) at 3695 cm^{-1} appeared in all of samples. This band represents the vibration of unbonded (OH) group (Kaolinite) according to Ledoux et al [18] .

From the foregoing description of the infrared bands of the analysed samples and their interpretation and dentification, the authors arrive to the conclusion that the studied samples of lake deposit consist essentially of the main chemical groups, namely : OH, Si-O-Al, Si-O, CO_3 which represent

kaolinite, illite, quartz and carbonate minerals. These results are in agreement with those arrived at from X-ray diffraction analysis.

Electron microscopy

The development of the electron microscope has permitted the precise determination of the shape of the particles of the various clay minerals and its use has shed light on the range of particle size of the components of clay and on the degree of size variation of the clay particles according to duration of weathering and distance of transportation. The electron micrographs of the clay mineral particles were obtained using an Elmi D_2 Electron Microscope (Carl Zeiss Jena) with a resolving power ranging between 20 to 30 A^{o} .

Electron micrographs of the clay samples were obtained using the suspension method described by Kay [19] .

The study of different electron micrographs obtained, revealed certain morphological features for the clay particles which are described in the following: (See " Beutlpacher et al [20] .

a- The majority of the clay particles are present in the form of aggregates and spherulitic clusters represented in the electron micrographs as irregular patches of different shades.

b- In some micrographs, the single crystals display euhedral habit with a tendency to from six-sided flakes with prominent elongation in one direction. These crystals present a moderately well crystallized type of Kaolinite.

c- The clay minerals exhibit various shapes and forms, namely: (a) platy particles, (b) flakes with poorly developed hexagonal outlines in which the edges of the flakes are somewhat ragged and irregular, (c) lath-shaped and stick-like crystals, (d) nearly rounded outlines.

d- The remarkable variation in the grain size of the clay particles which was observed within each samples and between the different clay samples, in addition to the irregularity of some particles indicate that kaolinite crystals have undergone much mechanical work and abrasion during transportation.

e- A noticeable variation in thickness of the different clay particles is revealed from the differences in density of the different particles in electron micrographs since some particles are not opaque (dark toned) indicating a relatively large thickness, others are lighter indicating thinner particles, a third group is characterized by uniform thickness as indicated by the homogenity in density of the particles.

The following clay minerals and their morphological features were identified in the lake deposits samples (Plates 1 & 2):

1- Kaolonite:

Kaolinite occurs as moderately well-crystallized crystals which are represented by pseudohexagonal flake-shaped particles. Figs. (6,7). Sometimes the particles show a tendency to from aggregates with different shades indicating different thicknesses (Fig. 8).

Plate -1- electron micrographs of clay Particles

Fig. 6.

Fig. (7)

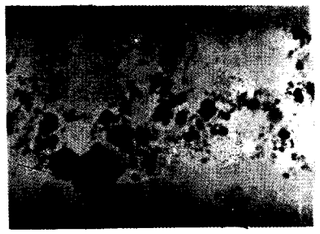

Fig.(8)

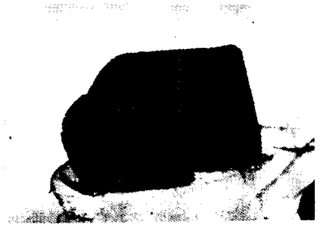

Fig.(9)

Fig.10

Fig. 11

Plate -2- electron micrographs of clay particles

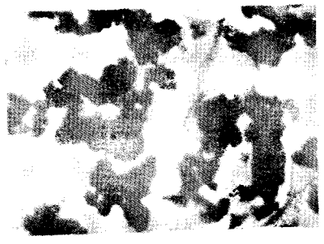

Fig. (12)

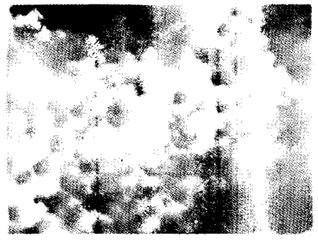

Fig. (13)

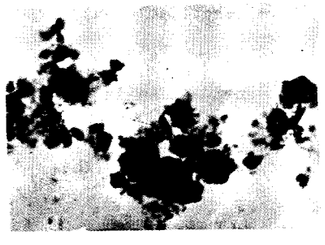

Fig. (14)

Fig. (15)

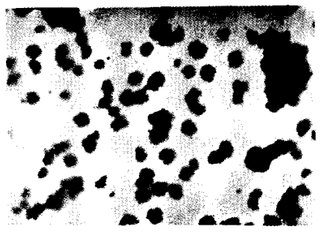

Fig. (16)

The well-crystallized, thick, well-formed and six-sided crystals are also represented. (Fig. 9).

Also some stick - like particles of Kaolinite occur (Fig. 10). Poorly crystallized kaolinite, on the other hand, occurs in the electron micrographs as smaller and thinner particles than those of the moderately well-crystallized kaolinite (Fig. 11).

2- Montmorillonite:

Montmorillonite is represented in the electron micrographs by irregular, more or less equidimensional, extremely thin flakes of different sizes (Figs. 12, 13). In some instances, the flake-shaped units are descrinable but frequently they are too small to be seen individually.

In some electron micrographs, montmorillonite is represented by irregular flake-shaped aggregates which appear to be stacking units without regular outlines (Fig. 14).

3- Illite:

Illite is represented in the electron micrographs by small, poorly defined, platy particles, occasionally with angular borders and commonly grouped in irregular aggregates without any distinct outlines (Fig. 15).

4- Mixed-layer clays:

The montmorillonite-illite mixed - layer clay is represented in the electron micrographs by spherulitic clusters and thin platy particles of undefined habits (Fig. 16). Adequate data for any generalization on the electron micrographs of mixed-layer clays are not available.

GEOCHEMISTRY OF LAKE DEPOSITS

Fourteen representative samples of lake deposits were selected for chemical analysis. The analysis were carried out for the fine (-200 mesh) bulk samples according to a modified scheme (El-Hinnawi) [21] , based essentially on the method of Shapiro and Brannock [22] . In this method, silica, alumina, iron, manganese, titanium and phosphorous were determined spectrophotometrically. Calcium, magnesium were determined titrametrically, while sodium and potassium were determined by flame photometry.

The results of the chemical analysis are given in Table (6). The following chemical characteristics of lake deposits are arrived at based on the results of the chemical analysis : -

Silica : (SiO_2)

Silica is present bound to alumina and other elements in the structure of clay minerals and in some cases, as free silica forming quartz grains. The percentage of silica varies between 87.97 % and 38.21 %. These values of SiO_2 depend on the following:

i- The amount of free quartz: the higher values of silica are mostly encountered in the highly sandy samples.

ii- The amount and type of clay minerals present: generally kaolinitic samples have higher silica than illitic/or montmorillonitic ones.

iii- The percentage of calcareous matter; it was observed that the highly calcareous samples, show little amounts of silica (e.g. samples No. 4,5).

Table (6) : Chemical analysis of lake deposit samples

Sample No.	1	2	3	4	5	6	7
SiO_2	57.78	55.24	62.28	38.21	39.79	78.97	69.73
Al_2O_3	11.55	11.84	9.38	14.93	10.98	2.42	5.67
Fe_2O_3	4.46	5.89	5.56	6.55	7.50	1.52	2.71
MgO	2.09	2.99	3.38	3.71	6.32	0.86	1.09
CaO	5.73	7.46	6.19	11.32	7.83	3.73	3.36
NaO	0.57	0.78	0.40	0.39	0.40	0.38	0.89
K_2O	0.82	0.96	0.87	0.87	1.77	0.34	0.48
Pe_2O_5 ---	0.03	0.02	0.19	0.39	0.13	0.21	0.18
TiO_2	0.73	0.77	0.75	0.87	0.67	0.22	0.40
MnO	0.02	0.07	0.07	0.06	0.62	0.03	0.03
SO_3 ---	0.33	0.53	0.75	1.23	0.99	0.07	0.10
Cl^-	0.07	0.22	0.10	0.18	0.23	0.41	0.95
L.O.I.	15.75	13.15	10.07	20.86	22.72	3.79	14.24
Total	99.93	99.92	99.99	100.07	99.98	99.95	99.83

Table (6) Con'd.

Sample No.	8	9	10	11	14	15	16
SiO_2	67.71	67.20	71.25	58.19	58.04	52.95	52.26
Al_2O_3	7.06	5.87	5.26	10.44	14.01	11.72	14.58
Fe_2O_3	4.08	2.75	3.08	4.65	5.61	1.05	7.83
MgO	1.40	1.01	0.86	2.14	2.23	2.90	1.57
CaO	4.26	4.58	4.36	7.99	3.73	4.59	5.20
NaO	0.53	0.73	0.32	0.40	0.46	0.72	0.92
K_2O	0.67	0.67	0.83	0.82	0.92	0.96	0.96
Pe_2O_5	0.52	0.18	0.19	0.17	0.18	0.17	0.23
TiO_2	0.[illegible]	0.45	0.42	0.80	1.05	0.87	0.98
MnO	0.03	0.06	0.04	0.06	0.06	0.07	0.05
SO_3	0.19	0.14	0.07	0.48	0.67	0.57	0.89
Cl^-	0.[illegible]	0.41	0.22	0.31	0.37	0.64	0.09
L.O.I.	12.[illegible]	15.01	13.04	12.83	12.02	21.67	14.45
Total	99.[illegible]	99.06	99.54	99.28	99.55	99.87	100.01

Alumina : (Al_2O_3)

The percentage of alumina varies between 14.93 % and 2.42 %. Alumina forms a considerable part of the clay minerals present. Kaolinitic samples have higher percentages of alumina than montmorillenitic and/or illitic ones e.g. sample No. 16 which mainly consists of kaolinite, (from X-ray diffraction analysis) has a higher percentage of Al_2O_3 (14.58 %). While sample No.6 which consists of montmorillonite has a low value (2.42 %).

On the other hand low values of almina are observed in the highly calcareous and/or sandy samples.

Iron : (Fe_2O_3)

The iron present in lake deposits occurs mainly in the iron III state. It is present either in the structure of the clay minerals and/or as independent strainings of hematite, or goethite. The percentage of iron III varies between 7.50 % and 1.04 %.

Manganese : (MnO_2)

It was detected in all samples but in low percentages. It varies between 0.02 % and 0.62 %. The higher percentage occurs in Genah area. It is mostly present as colloidal manganese hydroxides and/or absorbed on the clay particles. According to Goldschmidt [23] , the ionic potential of divalent manganese is low, therefore vulnerable to leaching. In hydrolysate sediments, manganese content depends very much on conditions of sedimentation. Under reducing conditions, manganese is selectively removed from the hydrolysate material, while under oxidizing conditions a selective manganese fixation takes place. It has

been found that the MnO content increases in finer colloidal fractions relative to other size fractions. Its abundance is, however, appreciably affected by post depositional conditions.

Calcium and Magnesium : (CaO, MgO)

The percentage of calcium and magnesium in the lake deposits varies between 11.32 % and 1.73 %, for calcium and 6.32 % and 0.86 % for magnesium. Most of calcium and magnesium in the lake deposits is present mainly as carbonates (calcite and dolomite) deposited simultaneously with the lake deposits.

Sodium and Potassium : (Na_2O, K_2O)

Sodium and potassium in the lake deposits occurs in two distinct forms, the first as water soluble salts, and the second as constituents in the clay mineral structure. In the second case, it is well known that potassium and sodium may occur in montmorillonite and the montmorillonite-illite mixed layer clay minerals.

Sodium and potassium are present in all areas and their higher values can be explained by the fact that illite and mixed layer montmorillonite and illite constitute a considerable part in the clay fraction in these areas.

Titanium : (TiO_2)

Titanium is present in the analysed samples in minor amounts. Its percentage varies between 0.22 % and 1.05 % in all the samples. Goldschmidt [23] , suggested that only small amounts of titanium are chemically or physically bounded to the clay minerals, but the titanium of hydrolysates is probably present as very finely crystalline TiO (or TiO_2 - hydrate) deposited along with

the tiny flakes of the clay minerals. A high titanium content in clays may be related to the amount of trioctahedral illite, and decomposition of biotite (from the parent rock) is a likely titanium source.

Phosphorus : (P_2O_5)

The percentage of P_2O_5 varies between 0.02 % and 0.55 % in all samples of the lake deposits.

Ignition loss :

It is a measure of the organic matter content, chemically combined water and, in calcareous samples, the CO_2 driven off from carbonates. Its percentage varies between 3.79 % and 22.72 %. The remarkably higher values of the ignition loss is attributed to the fact that it is mainly calcareous and rich in organic matter (Plant remains).

Conclusions regarding the geochemistry of lake deposits:

The following conclusions are arrived at from the above mentioned characters of the lake deposits in the studied area :

1- These deposits consist essentially of SiO_2, Al_2O_3 , calcareous, and organic materials. The silica is present as free quartz or as Si-O groups within clay structures (as detected from X-ray and infrared analysis). Alumina occurs essentially in the form of clay minerals (Kaolinite, illite, montmorillonite). The calcareous materials (CaO, MgO) occur in the form of calcite and dolomite. The organic

materials (ignition loss) is present in the form of organic matter plant remains).

2- The sandy lake deposits are generally poor in calcareous materials, and the opposite is true for clayey deposits.

3- Degens [24] , gave the relationship between K_2O + Na_2O + Cao, FeO + Fe_2O_3 + MgO and Al_2O_3 in a ternary diagram. Fig. (17) shows this relation from which it appears that lake deposits are more enriched with the average shale given by Degens [24] , which is more illitic than Kaolinitic and montmorillenitic.

CONCLUSIONS

The clay fractions of the lake deposits was studied in detail to identify their mineralogical composition. X-ray diffraction analysis of bulk samples and oriented samples (untreated, glycolated and heated samples) made possible for the identification of the following minerals: Kaolinite, illite, montmorillonite, mixed layers, calcite, dolomite and gypsum.

The infrared spectrometry revealed the presence of the main chemical groups in the clay fraction of the lake deposits samples, namely : OH, Si-O-Al, Si-O and CO_3. These groups represent kaolinite, illite, Quartz and Carbonate minerals.

Study of morphological features of the minerals, using the electron microscope showed that kaolinite is found as moderately well-crystallized pseudohexagonal flake-shaped particles, six-

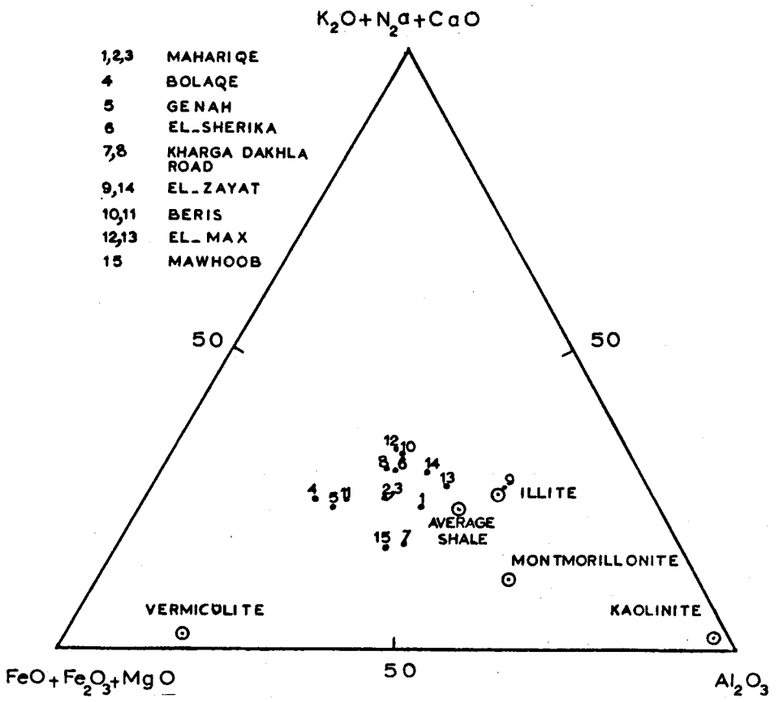

FIG.(17) PLOT OF LAKE DEPOSITS IN TERNARY DIAGRAM

sided, stick-like and aggregates with different shades. Montmorillonite is represented by irregular, more or less equidimensional thin flakes as well as by irregular flake-shaped aggregates. Illite is represented by small poorly defined, platy particles, occasionally with angular borders and commonly grouped in irregular aggregates without any distinct outlines. Some montmorillonite-illite mixed layer is represented in the electron micrograph by spherulitic clusters and thin platy particles of undefined habits.

Chemical analysis of the lake deposits shows that they consist essentially of SiO_2 , Al_2O_3 , calcareous and organic materials. The silica is present as quartz and as a Si-O group within clay structures (as detected from X-ray and infrared analysis). Alumina occurs essentially in the form of clay minerals (kaolinite, illite, montmorillonite). The calcareous materials (CaO, MgO) occur in the form of calcite and dolomite. The organic matter is mainly due to plant remains present in the lake deposits. The sandy lake deposits are generally poor in calcareous materials and the opposite is true in the case of the clayey deposits.

The geochemical relationships, indicate that the lake deposits are more enriched with the average shale of Degens [24] which contains more illite than kaolinite and montmorillonite.

REFERENCES

1. H.J.L. Beadnell. An Egyptian Oasis, an account of the Oasis of Kharga of the Libyan Desert. Murray, London. (1909).
2. G.H. Awad, and M.G. Ghobrial. Zonal stratigraphy of the Kharga Oasis. Geol. Surv. and Min. Res. Dept. Cairo (1965).
3. Gardner and Caton, Thompson. The prehistoric geography of Kharga Oasis. Geograph. Jour., 80, pp. 369 - 406 (1932).
4. N.S. Embabi. The semi-play deposits of Kharga depression, Western Desert, Egypt. Bull. Soc. Geogr. Egypt. T. XLI - XLII, pp. 73 - 87, (1972).
5. M.E. Hilmy, S.A. Hussein, and N. Saad. Geological and sedimentological investigations of the lake deposits from Kharga and Dakhla Oases. Western Desert, Egypt. El-Mustansiriyah Journal of Science. (In Press),(1978).
6. R.E. Grim. Some application of clay mineralogy. Amer. Min., 45, 3 - 4, pp. 259 - 270 (1961).
7. R.E. Grim. Clay mineralogy. McGraw-Hill Book Co., New York (1968).
8. M. Millot. Geology of clays. Springer - verlag, New York (1970).
9. J.M. Hunt, M.P. Wisherd and L.W.B. Bonham. Infrared absorption spectra of minerals and other inorganic compounds. Anal. Chem., pp. 1478 - 1497 (1950).

10. W.D. Keller, and E.E. Pickett. Absorption of infrared radiation by powdered silicate minerals. Amer Min. pp. 853 - 868 (1949).

11. W.D. Keller and E.E. Pickett. The absorption of infrared radiation by clay minerals. Amer. Jour. SCi., 24, pp. 264 - 273 (1950).

12. L.J. Bellamy. The infrared spectra of complex molecules. London. Methuen and Co. Ltd. New York, John Wiley and Sons Inc. (1956).

13. D.L. Pablo. A disordered kaolonite for Conception De Buenos Aner. Jahisco, Mexico, 13th Nat. Conf. on clay and clay minerals (1964).

14. M.M. Abu Zeid. Contribution to the minsralogy and geochemistry of variegated and Dakhla shales, E.A.R. Ph.D. Thesis, Ain Shams Univ., Cairo (1974).

15. C.K. Huang, and P.F. Kerr. Infrared absorption of carbonate minerals. Amer. Min., pp. 311 (1960).

16. H.W. Van der Marel, and J.H.L. Zwiess. OH stretching bonds of the Kaolin minerals, Silicates. Ind. Jour., 24, pp. 359 - 368 (1958).

17. J.M. Serratosa, and W.F. Brodley. Infrared absorption of OH bonds in micas. Nature, 181, 211 (1958).

18. R,L. Ledoux, and J.L. White. Infrared studies of the hydroxyl group in intercalated Kaolinite complexes. Clay and clay minerals, 13th Nat. Conf., 289 - 315 (1964).

19. D.H. Kay. Techniques for electron microscopy. Blackwell SCi. Publ. Oxford. (1967).

20. V. Beutlpacher and V.D. Mayel. Atlas of electron microscopy of Clay Minerals. Springer ver-lag. New York (1968).

21. E.E. El-Hinnawi. Rapid analysis of rock analysis.Int. Rep. Earth SCi. Lab., N.R.C., Cairo (1971).

22. L. Shapiro, and W. Brannock. Rapid analysis of silicates, carbonate and phosphate rocks. Bull. Geol. Surv., U.S.A. 1144-7 (1962).

23. V.M. Goldschmidt. Geochemistry. Oxford. Clarendon Press. (1954).

24. E.T. Degens. Geochemistry of Sediments. Prentice-Hall, New Jersey (1965).

GEOLOGICAL AND SEDIMENTOLOGICAL INVESTIGATIONS OF THE LAKE DEPOSITS FROM KHARGA AND DAHKLA OASES, WESTERN DESERT, EGYPT.

M.E. Hilmy, S.A. Hussein* and N. Saad

ABSTRACT

The Pleistocene-Recent deposits of Kharga and Dakhla Oases (Western Desert, Egypt) comprise wide areas of typical lake deposits. These deposits were studied in detail to determine their origin and palaeoenvironmental significance. They occur in the form of flat plains and hummocks oriented in a NW-SSE direction, and consist mainly of different varieties of sands and silts. It is suggested that these deposits were originated from the nearby formations, transported in a fresh environment and deposited in a shallow marginal environments of deposition.

INTRODUCTION

One of the most important problems facing the world today is the over-increasing pressure of population, on a limited area of cultivated lands. Therefore much attention has been recently paid to solve this problem. The most important and largest project of the EGDDO (Egyptian General Desert Development Organization) is the New Valley project. This project relies on the underground water potentiates and making use of the soil and clay

* Faculty of Science, Ain Shamus University, Cairo, Egypt.
Now on deputation to the Department of Applied Geology, College of Science, Al-Mustansiriyah University, Baghdad, Iraq.

Al-Mustansiriyah Journal of Science, Vol. 3 (1978).

deposits available in the western Desert, Egypt (about 750,000 square kilometers in area). Kharga and Dakhla Oases Constitute the essential and major area of the new valley project.

Previous workers [1 - 17] on the Kharga and Dakhla Oases, were mainly concerned with their geology and stratigraphy.

More recently, several authors [18 - 21] took over studies of the mineralogy of some formations encountered in both Oases.

In the above literature, no information can be found about the lake deposits in Kharga and Dakhla Oases. These deposits cover a wide area in both Oases and consist of silty deposits which can be conducted on a wide scale for agricultural expansion.

The present study deals with geology and petrology of the lake deposits encountered in Kharga and Dakhla Oases. Eight locations were chosen for this study, where best outcrops of these deposits were met. These are Mahariqe, Geneh, Bolaqe, Beris, El-Max, Kharga-Dakhla Road, El-Zayat and Mawhoob. The origin of these lake deposits and their environmental of deposition were also discussed.

LOCATION

Kharga Oasis is situated in the Southern Western Desert of Egypt, at about 200 km west of Nile (from Assiut). Its length is oriented in a north-south direction. It is located between latitudes 24° 32 & 26° 05' North and longitudes 30° 25' & 30° 50' East, Fig. (1). The elevation of Kharga Oasis ranges from 4 to 98 meters and in few cases it reaches up to 136 meters above sea level.

Dakhla Oasis is located in the South Western Desert, at about 305 km South 50° West of Assiut. It forms a depression lying at about 120 km

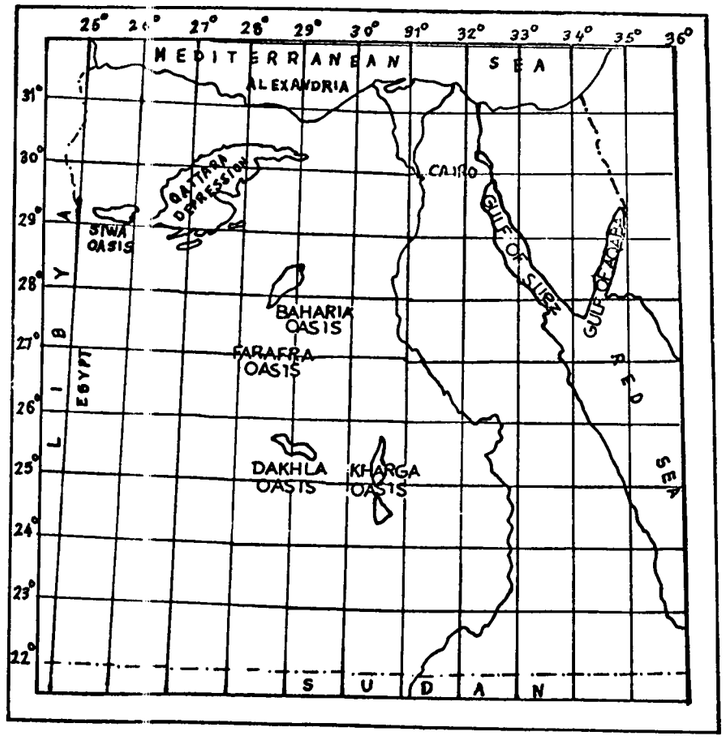

FIG(1) LOCATION MAP FOR KHARGA AND DAKHLA OASES

West of Kharga Oasis. The Oasis is elongated in a north-west, south-east direction. It is located in the south part of the western Desert and extends from latitude 25° 15' North to 26° 00' North and from longitude 28° 30' East to 29° 47' East, Fig. (1).

STRATIGRAPHIC POSITION OF LAKE DEPOSITS

Kharga and Dakhla Oases are occupied by sedimentary rocks belonging to Quaternary and Pre-Tertiary Eras. However, small hillocks of granite are exposed in the southern part of Kharga Oasis, and their age has been considered as Pre-Carboniferous [22] .

The general succession of the stratigraphic sequence of Kharga and Dakhla Oases, compiled by the authors from different sources in the literature, can be summarized in Table (1) from top to base.

Table (1) shows that the lake deposits in Kharga and Dakhla Oases, belong to Quaternary deposits. Lake deposits consist mainly of more or less isolated patches of soft friables alternating bands of shales and sandy clays. They contain some plant remains, stone impliments, and frequently rich in crystalline gypsum flakes. The thickness of these lake deposits varies between few meters to more than 15 meters.

GEOLOGY OF LAKE DEPOSITS

The name "lake deposits" was given by Awad et al. [17] , to the sand, silt and clay sediments deposited at the floor of both Kharga and Dakhla Oases. These deposits were first reported and described by Beadnell [5] as lacustrine deposits. Gardner et al. [7] , divided these deposits into three groups:

Table (1) stratigraphic sequence of Kharga and Dakhla Oases

Kharga Oasis	Dakhla Oasis	Type and thickness	Age
Aeolian deposits	Aeolian deposits	Sand-dunes	Recent
Salt deposits	Salt deposits	Salt-marches	Recent
Lake deposits	Lake deposits	Sands and silts	Pleistocene Recent
Gravel Terraces	-----	Gravels of flint and limestone.	" "
Caliche	-----	Caliche salts	" "
Travertine	-----	Spring deposits	" "
Thebes formation	Thebes formation	Limestone (23-146 m)	Lower Eocene
Esna shale	Esna shale	Shale (20 - 130 m)	Upper Paleocene
Trawan chalk	Tarawan chalk	Chalk, limestone (3-45 m).	Paleocene
Dakhla shale	Dkhla shale	Shale, mudstone, limestone (+ 150 m)	Paleocene-cretaceous
Phosphate formation	Phosphate formation	Phosphate, shale, limestone, (0.1 - 6 m).	Cretaceous
Nubia formation	Nubia formation	Sandstone, shale (+ 100 m).	Pre-cretaceous
Granite	-----	Granite	Pre-carboniferous

1- Loess like or Aeolian silt deposits.

2- Well deposits arrested by vegetation around past and present wells.

3- Pleistocene spring overflow deposits.

Embabi [23] described these deposits geomorphologically as Semi-playa deposits.

Lake deposits occur in several localities in Kharga and Dakhla Oases. They are generally situated in the low-lying areas of the two depressions, because the Nubian sandstone is the older strata present in the depression, lake deposits are generally observed in the nearby localities and the contact between them can be easily recorded.

The following areas comprise the main outcrops of these deposits:

Mahariqe, Bolaqe, Genah, Beris plain, El-Max and Kharga-Dakhla road (Kharga Oasis), Zayat plain and Mawhoob (Dakhla Oasis).

In the field, lake deposits exhibit a well-marked stratification (Fig.2). The lamination and bedding planes are mostly horizontal, but some inclined planes were observed (Fig. 3). Different surfaces of unconformity are detected within these deposits (Fig. 4) indicating the breaking in the sequence of deposition.

The most common structures observed within these deposits are graded-bedding, cross-bedding (Fig.5), and color-banding. Several joints (Fig.6) and small - scale faults occur separating and cutting these deposits (Fig. 7).

Lake deposits are lacking of fossils except for some plant remains which are common in these deposits (Figs. 8,9).

In the field lake deposits exhibit the following morphological features:

Fig. (2) Stratification in lake deposits

Fig. (3) Inclined beds in lake deposits.

Fig. (4) Local unconformity within the hummocks.

Fig, (5) Cross-bedding within the lake deposits

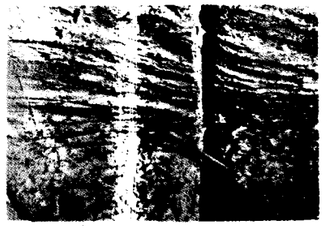

Fig. (6) Vertical joints in the lake deposits

Fig. (7) Minor displacement in lake deposits.

1- Flat plains :

These plains are the most common and extensive forms developed by lake deposits. They are nearly flat with small variations in levels and slopes and with thicknesses varying between few centimeters to 2 m. Some of the plains seem to be cracked by vertical jointing. The most important plains are the Sherika plain (part of Kharga Village), Beris plain (in the Southern part of the depression) and Zayat plain in the mid-way between Kharga and Dakhla depression.

2- Hummocks :

These are small longitudinal ridges occurring in groups oriented in a NNW-SSE direction (Fig. 10). They were observed and described in most areas where these deposits were found (in the flat plains). The hummock is a small conical hill, having a length varying between 3.0 to 30 meters, a width between 0.5 and 2 meters, and a height between 0.5 and 5 meters above the adjacent plains. In general, the fronts of the hummocks are broader and higher than the snouts. They have steep sides which exhibit wind scouring, vertical faces with slipped backs at the front. The body of the hummocks is full of plant remains in contact with the adjacent plains. The hummocks from the side view show a triangular shape (Fig. 11). The body of the hummocks has also an orthogonal system of joints which run along their longitudinal axes and across them.

The deposits have a prevailing brown tint color which changes in some localities to yellowish or greyish, depending on the ratio between sand, silt and clay in the deposits.

Some of the horizons show some sort of stratification, such as thin horizontal beds, or cross-bedding. This stratification is a good evidence of slow and shallow water action at the time of deposition. Between the

Fig. (8) Plant remains and Columnar structure in lake deposits due to extensive weathering

Fig. (9) Plant remains within the lake deposits

Fig. (10) General view of the hummocks.

Fig. (11) Side view of a hummock.

Fig. (12) Gypsum crystals within lake deposits.

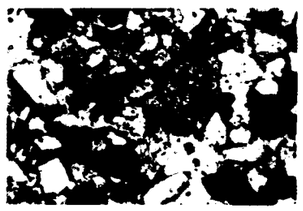

Fig. (17) Photomicrograph of sandy silt, notice the presence of glauconite pellets. Crossed Nicols X 26

zone which forms the base of the hummocks and the underlying zone which forms the adjacent plains, local unconformities were observed e.g. in the sherica plain and the southern part of the Beris plain. This is an indication that these deposits were laid down during different pluvial periods which were separated by dry periods during which the deposits were dried up and exposed to wind action.

Due to the friability of these deposits they are well acted upon by weathering processes (wind and rain) and they show columnar structures (Fig. 8). The main trend of the hummocks is due to these actions and indicate the main direction of these wind (NNW-SSE).

Within the lake deposits there are several salt beds which occur as fine white materials between the deposits. Also, few scattered gypsum crystals and gypsum veinlets are observed within these deposits (Fig.12).

SAMPLING

One hundred and fifty three samples of lake deposits were collected by the authors. These samples represent the different varieties of lake deposits. Table (2), represents the location (Fig.13) and number of samples collected.

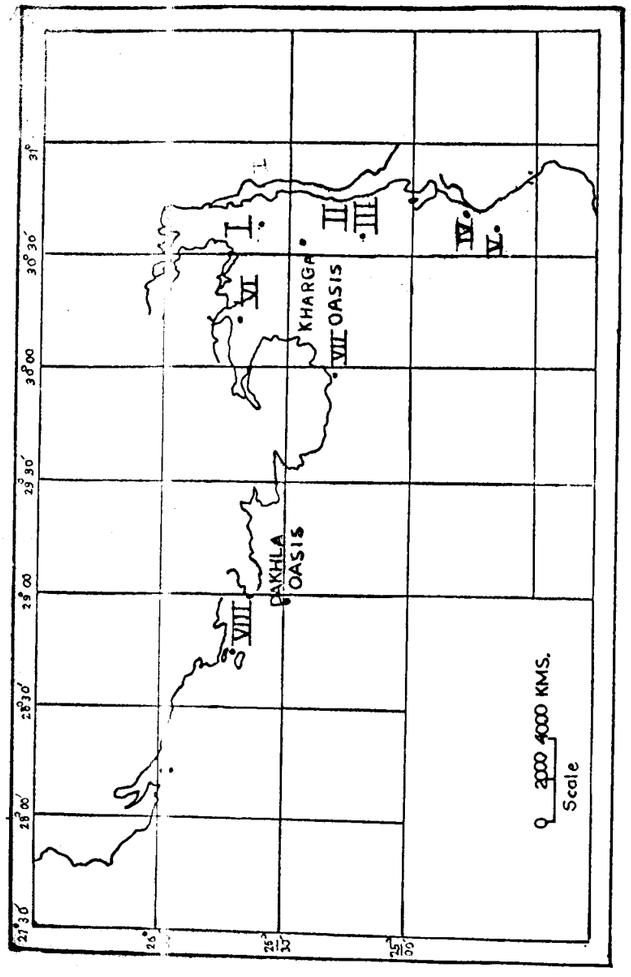

FIG(3) MAP SHOWING LOCATION OF THE STUDIED SAMPLES.

Table (2) : Location and number of samples studied

Location		No. of Samples Collected	Serial Numbers of Samples
I-	Mahariqe	47	1-47
II-	Genah	2	1-2
III-	Bolaqe	19	52-71
IV-	Beris	36	72-108
V-	El-Max	7	109-115
VI-	Kharga-Dakhla road	9	116-124
VII-	El-Zayat	13	125-138
VIII-	Mawhoob	14	139-153

PETROLOGY OF LAKE DEPOSITS

The petrographic characters of the lake deposits are treated under the following headings :

1- Granulometric analysis.
2- Textural classification.
3- Carbonate - silt - sand relationship.
4- Thin section study.
5- Heavy mineral analysis.

1- Granulometric analysis :

Two techniques were used for the determination of the particle size distribution in the lake deposits. These are :

(1) the settling velocity technique for the clay and silt fraction (the pipette method after "Kilmer and Alexander" 1947), and

(2) the sieving technique for the sand - size fraction using a set of sieves of different mesh diameters.

Table (3) shows the sand and silt ratios in the studied lake deposit samples.

In the present work the statistical grain size parameters of Folk and Ward [24] were applied. Table (4) shows the average calculated grain size parameters of the analysed samples of each locality. The average mean size values "Mz" range between 5.5 ϕ to 1.33 ϕ , which means that these deposits have grain sizes ranging from medium silt to medium silt. The average inclusive graphic standard deviation values " σ I" range from 1.81 ϕ to 0.40 ϕ , which range between moderately to well-sorted except for some few samples which are poorly sorted. The average inclusive graphic skewness "SKI"

Table (3) : Sand and silt ratios in lake deposit samples

Sample No.	sand %	silt %	sample No.	sand %	silt %	sample No.	sand %	silt %
1	23.75	76.25	44	44.75	55.25	84	56.99	43.01
2	24.65	75.35	45	44.58	55.42	85	51.90	48.10
3	33.61	66.39	46	28.76	71.24	86	55.21	44.79
4	15.24	84.76	47	15.95	84.05	87	55.76	44.24
5	10.78	89.22	52	93.33	6.67	88	51.03	48.97
6	40.51	59.49	53	91.57	8.43	89	50.59	49.41
11	33.37	66.63	54	89.19	10.81	90	52.97	47.03
13	38.35	62.65	55	93.70	6.30	91	50.33	49.67
14	39.29	60.71	56	86.15	13.85	92	63.04	36.96
15	41.64	58.36	58	93.05	6.95	93	51.29	48.71
21	37.01	62.99	59	73.54	26.46	94	47.19	52.81
22	30.59	69.41	60	51.51	48.49	95	67.48	32.52
23	30.71	69.29	61	30.02	69.98	96	56.29	43.71
24	25.68	74.32	62	48.35	51.95	97	61.31	38.69
25	32.66	67.34	63	58.43	41.57	98	42.12	57.88
26	30.05	69.95	64	75.03	24.97	99	48.06	51.94
27	40.56	59.44	65	51.95	48.05	100	43.69	56.31
28	31.81	68.19	66	35.46	64.54	101	31.56	68.44
29	36.03	63.97	68	67.06	32.94	102	43.29	56.71
31	42.45	57.55	69	69.72	30.28	103	59.91	40.09
32	43.73	56.27	70	66.03	33.97	104	35.39	64.61
33	40.30	59.70	71	77.02	22.89	105	49.43	50.57
34	36.67	63.33	74	33.38	66.72	106	52.94	47.06
35	20.16	79.84	75	55.34	44.66	111	35.01	64.99

Table (3): Cont'd.

Sample No.	sand %	silt %	Sample No.	sand %	silt %	Sample No.	sand %	silt %
36	45.30	5..70	76	51.22	48.78	115	51.95	48.05
37	12.02	87.02	77	59.87	40.13	108	30.19	69.81
38	23.75	7..25	78	63.16	36.84	109	57.94	42.06
39	38.19	6..81	79	76.27	23.73	110	52.83	47.17
40	38.44	6..56	80	54.88	45.12	112	42.26	57.74
41	42.93	5..07	81	42.77	58.23	113	37.63	62.37
42	32.22	6..78	82	29.52	70.48	114	47.79	52.21
43	40.34	5..66	83	54.26	45.74	116	19.21	80.79
117	36.12	6..88	128	6.76	93.24	142	22.17	77.83
118	35.02	6..98	129	13.37	86.63	143	41.81	58.19
119	35.22	6..78	131	22.66	77.34	144	35.24	64.76
121	45.87	5..13	134	35.39	64.61	145	30.61	69.39
122	21.38	7 .62	135	36.00	64.00	146	19.77	80.23
123	31.49	6..51	136	24.03	75.97	147	12.24	87.76
124	16.74	8 .26	137	32.48	67.52	149	20.21	79.79
125	11.38	8..62	138	28.10	71.90	151	43.46	56.54
126	20.00	80.00	140	32.87	67.13	152	36.54	63.46
127	5.72	9 .28	141	41.38	58.62	153	43.29	56.71

Table (4) : Average calculated grain size parameters of lake deposit samples

Location	MZ		GI		SKI		KG	
	sand	silt	sand	silt	sand	silt	sand	silt
Mehariqe	2.32	5.20	1.81	0.45	-0.09	0.07	0.87	0.95
Genah	---	5.50	---	0.40	0.00	0.01	0.90	1.10
Bolaqe	1.33	---	0.75	---	-0.01	0.11	1.09	0.90
Beris	3.01	---	0.78	---	-0.07	0.07	0.67	1.33
El-Max	2.90	---	1.25	---	0.01	0.02	1.00	1.10
Kharga-Dakhla road	4.02	5.30	0.54	0.42	-0.02	0.08	0.90	1.10
El-Zayat	2.65	5.22	0.40	0.54	0.01	0.05	1.00	1.10
Mawhoob	3.65	5.30	1.40	0.50	-0.04	0.04	0.92	0.94

Table (5): Average function values of Sahu

Locality	Y_1	Y_2	Y_3	Y_4
Mahariqe	-14.5217	117.1569	-0.7303	8.928
Bolaqe	-3. 4700	102.02353	-5.0450	7.2347
Beris	-4. 9660	94.7353	-3.5129	7.2109
El-Max	-3. 0986	123.6914	-10.6175	7.063
Kharga-Dakhla road	-14.888	117.0350	-0.6175	9.190
El-Zayat	-14.9440	116.7475	-0.5783	9.1425
Mawhoob	-14.9910	118.9067	-0.5325	9.3738

values, range between - 0.01 to 0.11 which indicate that the sediments are nearly symmetrical in character. The average graphic Kurtosis (KG) values range between 0.67 and 1.33, this indicate that lake deposits range from platy - to leptokurtic character. In the same time, the discriminent functions of Sahu [25] were calculated (Table 5).

From the average values in Table (5), and according to Sahu [25] functions, it appears that the lake deposits were deposited in a shallow marginal environment of deposition (e.g. lakes, ponds, lagoons,... etc), with a significant role of turbidity currents. In some stage of deposition, aeolian processes prevailed, sediments were carried and deposited in these shallow environments giving rise to small scale deltiac - like deposits.

The authors proceeded further, by constructing "C M" pattern of Passega [6] to establish the relationship between texture of sediment and proces of deposition. The " C M " diagram is shown in Fig. (14). It is concluded that the lake deposits samples are scattered in the region of median diameter larger than 125 microns, in an area parallel to C = M line. The coarsest grained sediments are more frequently at Bolaqe and Beris, while the finest grained sediments are more frequently at Mahariqe, El-Max, Kharga - Dakhla road, El-Zayat and Mawhoob.

From ' Passega regions " plotted on the "CM" diagram it appears that the studied sediments were generally deposited from uniform suspension and with a clear effect of turbidity currents.

2- Textural classification of lake deposits :

In this work the nomenclature scheme for textural classification of fine-grained sediments adopted by Pettijohn [27] , are used to classify the analysed samples. The mechanical analysis data were used in this

study. According to their mechanical composition the sand and silt ratios are given in Table (3). Fig. (15) illustrates the relationships between clay, sand and silt for the studied samples according to the classifications given by Pettijohn [27] .

According to the symmetrical scheme of Pettijohn [27] Mahariqe samples are classified as silt and sandy silt, Bolaqe as sand and silty sand, Beris samples are classified as silty sand, and sandy silt, at El-Max the samples are sandy silt and silty sand, Kharga-Dakhla road, El-Zayat and Mawhoob samples are sandy silt and silt, while Genah samples are silt.

3- Carbonate - silt - sand relationship ;

The percentage of carbonates was determined using HCl (1:10) for leaching them and the carbonate loss was then calculated. Table (6) shows carbonate percentage in each sample.Fig. (16) represents ternary diagrams showing carbonate-silt-sand relationships.

From Fig. (16), it is clearly observed that Mahariqe lake deposits are rich in carbonates (8.6 - 18.08 %), also in Kharga - Dakhla road the percentage of carbonate may reach up to 14.9 %, in the other localities, carbonate percentage varies between 3.9 and 8.3 %. From Fig. (16), one can conclude also that Kharga- Dakhla road, El-Zayat, Geneh, Mawhoob and Mahariqe deposits are more silty while Bolaqe, Beris and El-Max lake deposits are more or less sandy, a conclusion which is in harmony with that obtained from the textural classifications of these deposits.

4- Thin section study :

According to the above-mentioned textural characters of lake deposits, these deposits consist mainly of different varieties of sand and silt

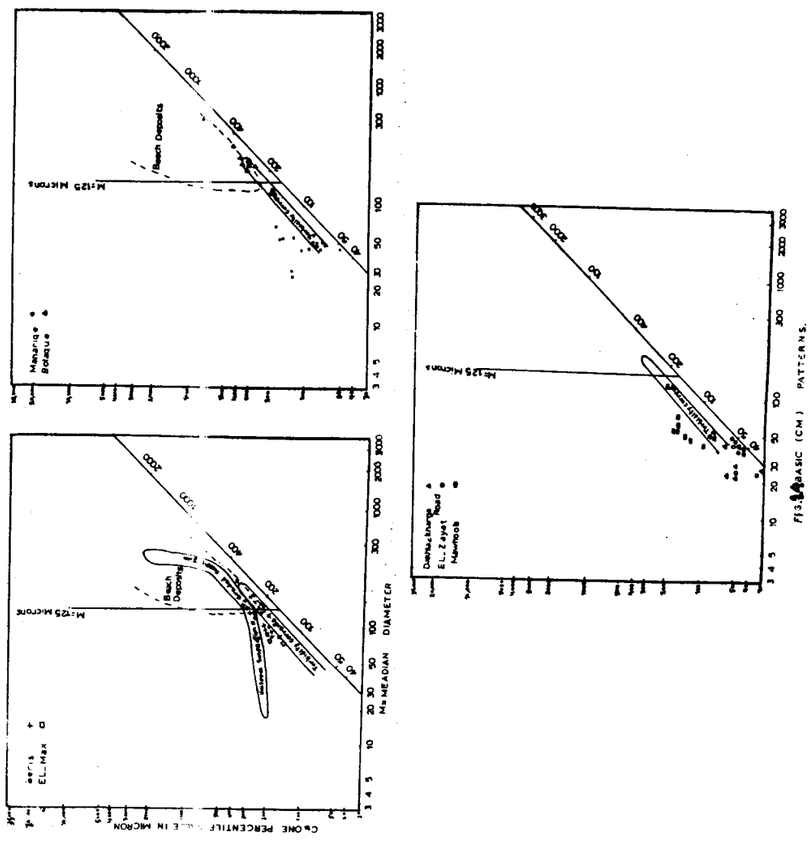

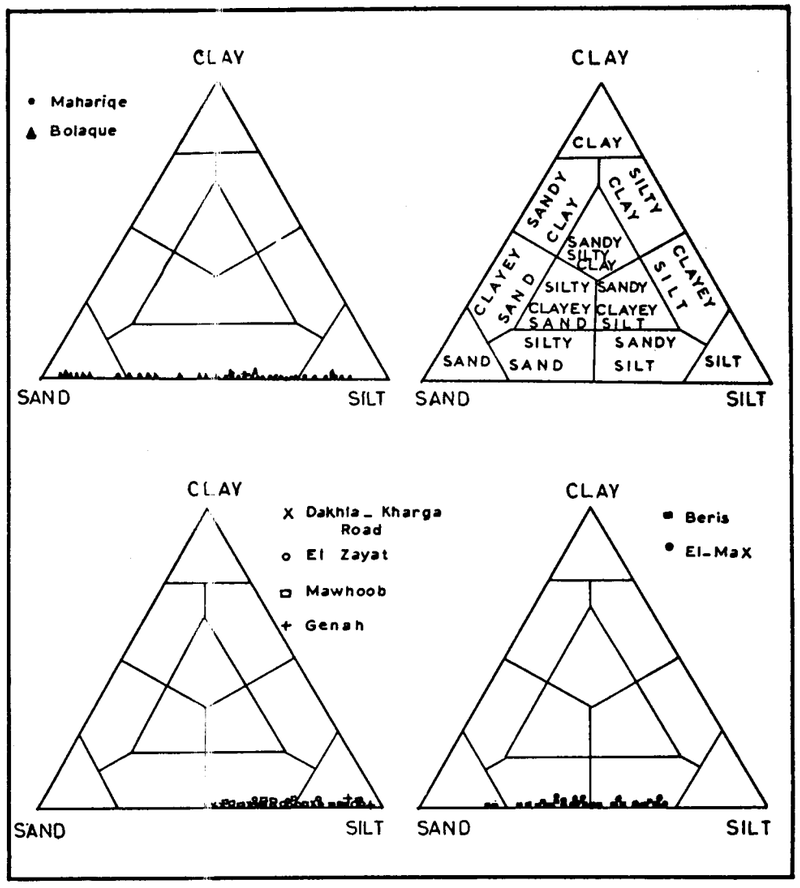

FIG.(15) TERNARY DIAGRAMS SHOWING MECHANICAL COMPOSITION OF THE ANALYSED SAMPLES (symmetrical scheme; after Pettijohn et al., 1973)

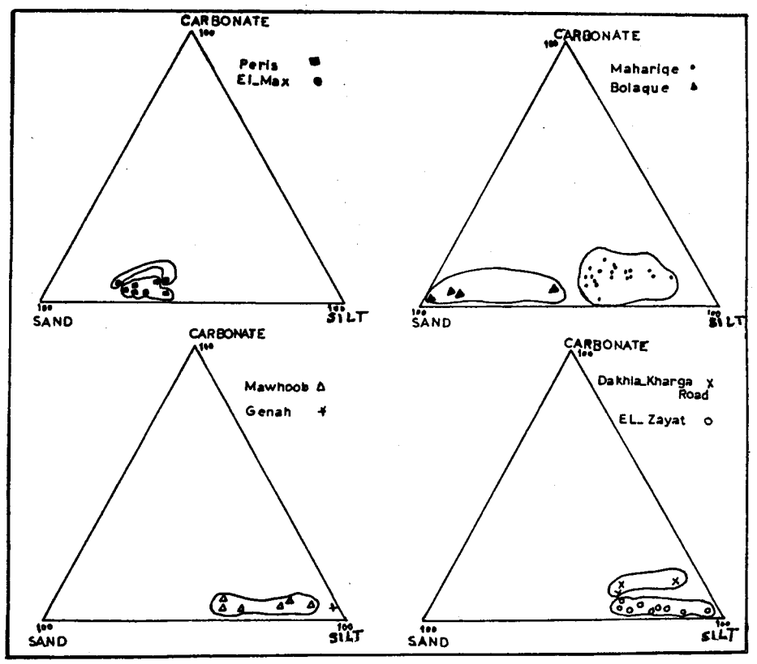

FIG.(16) RELATION BETWEEN CARBONATE, SILT AND SAND PERCENTAGES.

Table (5) : Carbonate percentage of lake deposits samples

Sample No.	Carbonate %	Sample No.	Carbonate %	Sample No.	Carbonate %
5	10.2	43	3.52	119	10.40
8	8.8	44	10.7	124	14.9
12	14.5	45	8.64	126	3.52
13	10.7	47	11.36	127	1.76
14	18.0	54	3.9	129	2.56
15	10.0	61	7.5	130	4
22	12	64	6	134	7.04
23	10.4	66	5.28	135	4.16
24	8.32	70	4	136	3.36
25	10.3	76	6.4	138	5.44
27	14.2	78	6	141	4.96
28	12.96	82	4.2	142	5.44
29	15.04	94	4.6	143	7.84
31	9.12	107	5.1	144	4.80
33	9.12	108	8.3	147	5.92
34	10.40	109	6.2	149	7.84
38	13.12	111	7.9		
39	10.24	115	7.6	Genah 2	5.28
41	13.92	118	13.1		

deposits. About "50" thin sections of sand and silt samples were made and studied petrographically. These thin sections were prepared from representative samples of lake deposits from different localities in Kharga and Dakhla Oases.

Petrographic Description of Sandstones (Figs. 17 - 23)

a- **Mineralogical composition :**

Quartz is the most common mineral found in sandstones of lake deposits, it ranges between 20 % to 80 % of the total mineral composition. The size of quarts ranges between coarse and fine grains. Most of the quartz grains are single ones showing straight to slightly undulose extinction except in Mawhoob and Bolaqe where the grains are single and composite. Accessories are found in addition to quartz and clay minerals e.g. calcite, which constitutes about 10 %, minor amounts of feldspars and rounded pellets of glauconite.

b- **Cementing materials :**

Cement commonly exceeds 5 % of the rock. There are different types of cementing materials in the sandstones of lake deposits. The most common is the hydrated iron oxides and argillaceous materials. Carbonate minerals (calcite and/or dolomite) have been observed in the sandstones (in Mahariqe). They fill the interspaces between the quartz grains.

c- **Texture of sandstone :**

In thin section sandstone minerals exhibit different textural characters. Sandstones are moderately sorted, ranging from subrounded and angular fine grains.

Medium grains are also found in some areas but not common as fine grains. The sandstone generally exhibits heterogeneous fabric without any

indication of grain arrangement. According to the textural classification of Folk 28 , these sandstones are considered immature to submature sediments.

Petrographic description of silts

a- Mineral composition :

Silt samples consist mainly of very fine - grained silty minerals, which are difficult to be identified under the polarising microscope. The clay minerals are grey, steel black or opaque in color. Dissiminated in these argillaceous materials, there are some quartz grains, carbonates (calcite, dolomite), iron oxides, glauconite and some other accessory minerals (e.g. zircon, tourmaline, staurolite).

b- Texture of silts :

In thin section the silt is mainly very fine-grained under high magnification, the grains seem to be rounded. Embedded in this silty material, several minerals are observed e.g. quartz, feldspars and carbonates. Different forms of reworked fossils are observed, they are rounded and poorly preserved. These silts are rich in plant remains.

5- Heavy mineral analysis :

The authors proceeded further by separating the heavy and light minerals from some samples using bromoform as a separating medium (sp.gr. 2. 85). Fractions with grain size between 0.20 and 0.63 mm were used in this study, since the bulk of the heavy minerals tend to concentrate within these size limits (Table 7). From this table it can be observed that the percentage of heavy minerals increases with decreasing grain size.

Fig. (18) Photomicrogtaph of sandy silt enriched in opaque minerals (dark),p.p.L. X26

Fig. (19) Photomicrograph of sandy calcareous silt, notice the presence of very fine and rounded carbonates, crossed Nicols, x26 .

Fig. (20) Photomicrograph of sandy silt, showing quartz,feldspar, microcline and carbonate grains embedded in silty matrix, crossed Nicols, X 26.

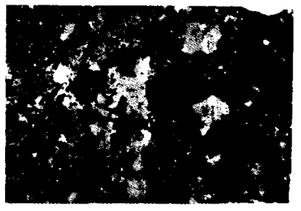

Fig.(21) Photomicrograph of calcareous patch within silt crossed Nicols, X 26.

Fig. (22) Photomicrograph of Calcareous silt with some reworked foraminferal tests, Crossed Nicols, X 26.

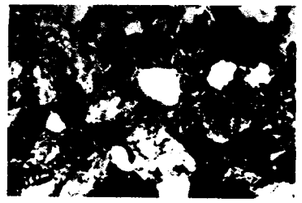

Fig. (23) Photomicrograph of sandy Calcareous silt,with some Composite Quartz grains, Crossed Nicols, X 26.

Table (7) : Percentages of heavy minerals separated from different fractions

Locality	0.25-0.17 mm	0.17-0.125 mm	0.125-0.063 mm
Mahsriqe	1.07	1.24	3.32
Bolaqe	0.409	0.90	3.67
Beris	0.22	0.75	3.18
El-Wax	1.02	1.41	3.74
Kharga-Dakhla road	3.89	3.24	3.38
El-Zayat	3.21	3.15	3.50
Mawhoob	0.84	0.86	6.42

Mineralogy of heavy fractions :

The heavy minerals encountered in lake deposits consist mainly of opaque minerals, zircon, tourmaline, staurolite and rutile. Garnet, biotite, glauconite and monazite are present in subordinate amounts. The percentage distribution of the main heavy mineral constituents was determined by counting under the microscope. The results are given in Table (8). The following is a description of the most common heavy minerals :

Opaque minerals :

These constitute the major part of the heavy minerals. They are mainly represented by iron oxides, iron-titanium oxides and hydrated iron oxides (hematite, ilmenite, limonite). They occur as subangular to rounded grains.

Non-opaque minerals :

The non-opaques were identified by means of the polarizing microscope. The following is a description of the minerals:

1- Zircon:

It is one of the most common heavy minerals encountered in lake deposits. Generally it is present in the form of euhedral prismatic grains with irregular terminals. Subhedral and subrounded grains are also common. Zircon is generally colorless with different amounts of inclusions.

2- Staurolite :

It occurs in the form of subhedral to anhedral grains mostly sub-angular to angular. It varies in color from yellow to brownish. The dark color varieties show different contents of inclusions.

3- Tourmaline :

It occurs in all samples in significant amounts. Its form varies

Table (8): Distribution of heavy minerals in lake deposits

Mineral	Mabarige	Bolaqe	Beria	El-Max	Kimarga Dakhla road	El-Qayat	Mawhoob
Opaques	93.20	85.20	80.90	79.20	78.64	82.00	82.1
Zircon	3.3	8.26	10.55	11.00	10.2	7.7	9.8
Tourmaline	1.3	1.66	2.90	2.5	3.4	2.65	2.9
Staurolite	1.5	2.5	3.40	3.8	2.2	2.85	3.00
Rutile	0.5	0.61	0.73	1.1	0.33	0.90	0.2
Monazite	0.6	0.84	0.44	0.3	0.65	—	0.9
Garnet	0.26	0.23	0.47	0.5	0.33	0.30	0.4
Biotite	[illegible]	[illegible]	[illegible]	[illegible]	[illegible]	[illegible]	[illegible]
Epidote	0.01	0.01	---	---	---	---	---
Glauconite	0.2	0.26	0.3	0.7	1.2	0.8	0.1

between elongated prismatic and oval. Rounded grains are common. Its color is pale green, yellow , grey, and dark brown with strong pleochrism.

4- Rutile :

It is one of the common minerals in the non-opaque heavy mineral fractions of the lake deposits. It is characterized by rod and knee-shaped forms with rounded termination. It exhibits three distinct yellow, red and brown colors.

5- Garnet :

It occurs in less amounts in some samples. It is characterized by granular triangle forms, colorless and isotropic.

Mineralogy of light fraction :

The light fraction of the lake deposits was examined microscopically. It was found that quartz forms up to 99 % of the light fraction while feldspars form about 1 %. Quartz occurs as colorless to turbid grains. The majority of the grains are of the simple type (monocrystalline) and show parallel extinction. Composite grains with slightly undulose extinction are rare.

Feldspars are present in angular forms (microcline, orthoclase). Microcline is represented by colorless grains and shows the common cross-hatching twinning between corssed nicols.

Origin of lake deposits and their environment of deposition :

Based on their field occurrence and pertrographic properties, lake deposits are though to have their main constituents derived from the nearby formations.

Lake deposits consist mainly of different varieties of sand and silt deposits (e.g. sand, mud sand, silty saad, sandy silt,... etc). The sands

increase and concentrate at the centre of depression of Kharga, while silts increase northward and westward. This is well illustrated in Fig. (24) which shows the isolines of sand/shale ratio in the studied area.

From this figure, it can be concluded also that these deposits originated essentially from the nearby formations. The sands in lake deposits increase near the sandstone formations (e.g. Nubian sandstone). Also the lake deposits become more clayey near the different formations rich in silt and shale deposits (e.g. Dakhla shale). The two arrows in Fig. (24) show that the silt increase in the north and west directions, these directions are mainly toward the escarp of the depression where best outcrops of the shale and clay formation are observed. On the other hand the sand increases in opposite directions to these arrows (i.e. toward the centre of the depression). It must be noted that, the Nubian sandstone formation outcrops in low-lying areas of the depression, which lies at the centre of the area.

The carbonate content increases in same manner as silt content (Fig.25). This is also attributed to the occurrence of limestone formations in these directions (e.g. Tarawan chalk, Thebes formation ... etc). The decrease of carbonate ratio in lake deposits is mainly observed at the centre of the depression which is accompanied by an increase of sand content.

The different varieties of heavy and light mineral assemblages encountered in lake deposits, are very closely similar to those determined in the Nubian sandstone formation [19]. The individual minerals have in general, the same characteristics.

The granulometric analysis, discrimenent functions of Sahu, and "CM" Pattern, indicate that lake deposits were mainly deposited in a shallow marginal environment of deposition (e.g. lakes, ponds, lagoons...etc). Such an environment

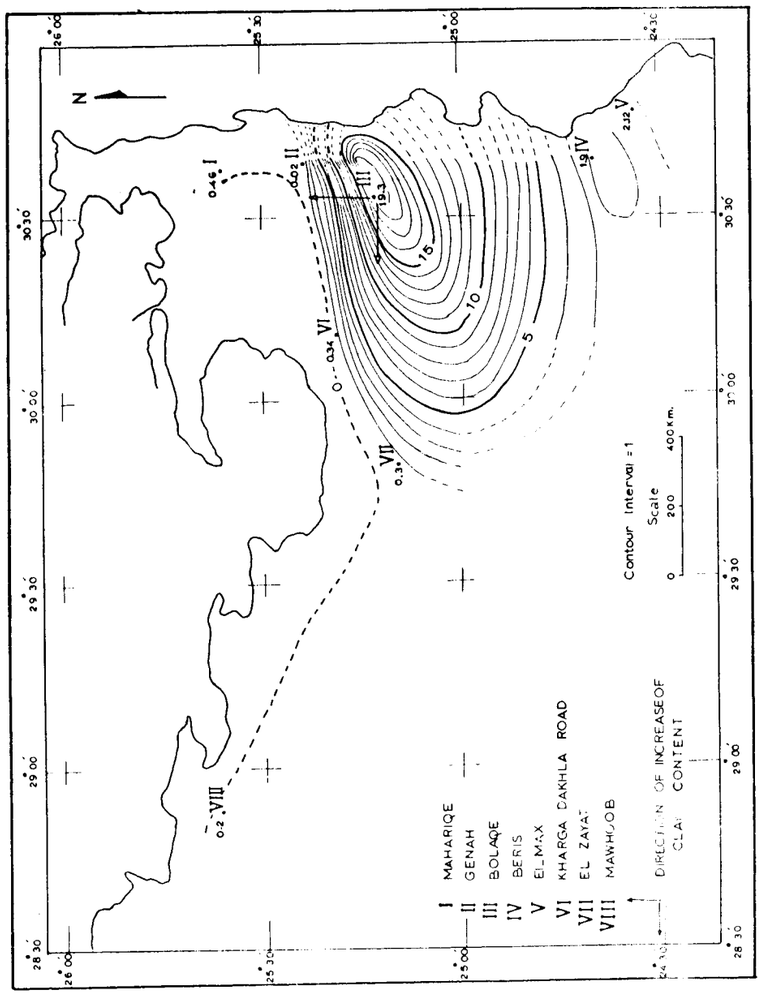

FIG.(24) ISOLINES OF THE SAND / SHALE RATIO OF LAKE DEPOSITS, KHARGA - DAKHLA CASES.

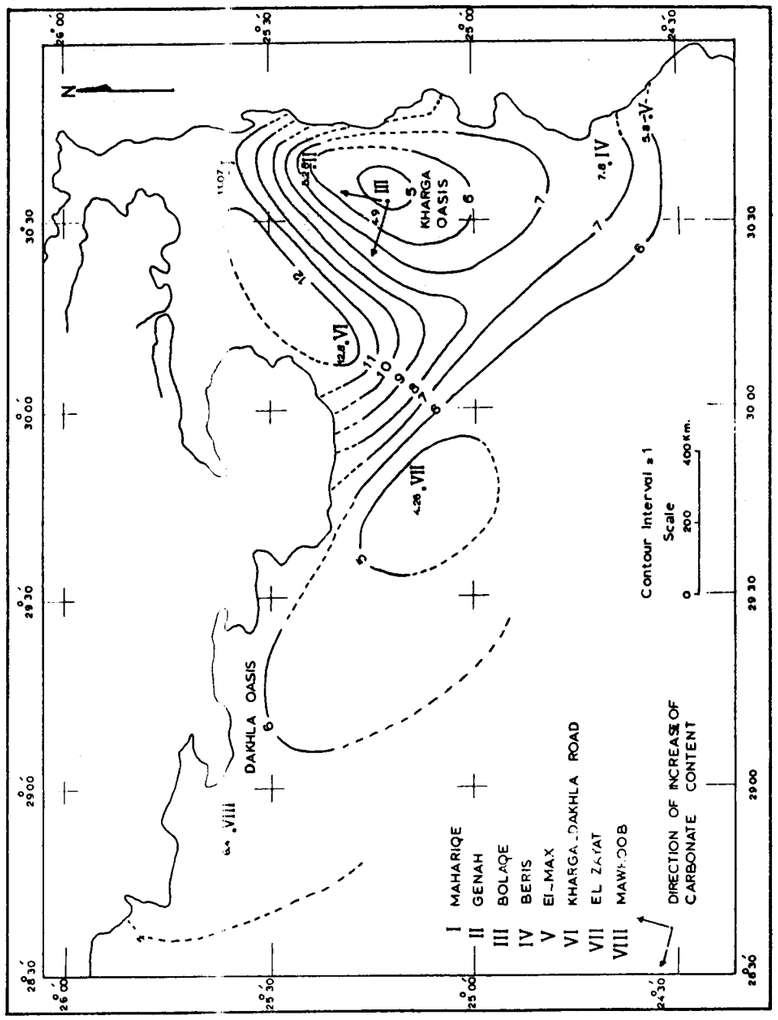

FIG. 25 ISOLINES OF CARBONATE CONTENT IN LAKE DEPOSITS , KHARGA - DAKHLA OASES.

lies mainly in the low sites within the depression. The sediments were transported in a fresh water medium (as indicated from plant remains). In the dry seasons, aeolian processes prevailed. A small - scale deltaic environment appears in the sites of deposition. Turbidity currents were important during processes of deposition, and the finer materials were generally deposited from a uniform suspension.

CONCLUSIONS

The present work deals with the geology and petrology of the lake deposits (pleistocene-recent) in both Kharga and Dakhla Oases. Eight locations were chosen for this study, these are: Mahariqe, Genah, Bolaqe, Beris, El-Max (Kharga Oasis), Kharga Dakhla road, El-Zayat and Mawhoob (Dakhla Oasis).

Field observations show that lake deposits are generally situated in the low-lying areas and show a well-marked stratification. Different sedimentary structures are observed within these deposite (e.g. graded-bedding, cross-bedding, color banding, small-scale faulting and unconformity). These deposits lack fossils except for some plant remains which are common in them.

Lake deposite exhibit two main morphological forms: The first one, which is the most common and extensive form, is called " flat plains ". The second, is in the form of small longitudinal ridges occurring in groups oriented in a NNW-SSE direction. These forms are called " hummocks ".

Grain size analysis of lake deposits reveals that these deposits range in size between medium sand and silt. They are well to moderately-sorted, nearly symmetrical skewed and range from platykurtic to leptokurtic characters. Discriminent functions of Sahu show that they were deposited in a shallow marginal environments of deposition (e.g. lakes, ponds, lagoons ... etc), with a significant role of turbidity currents. At some stages of deposition, aeolian processes prevailed and the sediments were carried and deposited in these shallow

environments giv ng rise to a small scale deltaic - like deposits. The aeolian processes prevai ed in dry seasons. The "CM" pattern of Passega indicates that the finer materi ls deposited from uniform suspension and with a clear effect of turbidity cur ents.

Petrologi al studies indicate that these deposits consist mainly of different variet es of sands and silts (e.g. silt, sand, silty sand, sandy silt ... etc.). The sands increase and concentrate at the centre of depression, while silts increase northward and westward. The carbonate content increases in the same manner as the silt content. The different varieties of heavy and light mineral assemblage encountered in the lake deposits are very closely similar to those identified in the Nubian sandstone formation and the individual minerals have the same characteristics. Based on their petrological characters the lake deposits are thought to have been transported and deposited in a fresh - water environment (as indicated from plant remains) and originated from the nearby formations. These deposits became more sandy near the Nubian sandstone formation (at the centre) and more clayey and calcareous near the calcareous and the clayey formations (northward and westward).

REFERENCES

1. A.K. Zittel : Beitraga Zur Geologie and Paleantologis der Libyschen Wusto Und der Angrenzendern Gebiete Von Aegypten. Paleantographica, Vol. 30 (1), pp. 1-112 (1883).

2. H.G. Lyons ,: On the stratigraphy and physiography of the Libyan Desert of Egypt. Q.J.G.S., London. Vol.50, pp. 531-456 (1894).

3. J. Ball : Kharga Oasis, its topography and geology. Egypt. Surv. Dept., Cairo (1901).

4. H.J.L. Beadnell : Dakhla Oasis, its topography and geology, Egypt. Surv. Dept., Cairo (1901).

5. H.J.L. Beadnell : An Egyptian Oasis, an account of the Oasis of Kharga of the Libyan Desert. Murroy, London (1909).

6. Quaas : Beitrag sur Kenntins der fauna der obersten Kre: debildungen inder Libyschen wusts. Paleantograshica, Vol. g.30. pp. 153 - 134 (1902).

7. Gardner and T. Caton. : The pre-historic geography of Kharga Oasis. Geograph. Jour. Vol. 80. pp. 369-406 (1932).

8. M.Y. Hassan. : The occurrence of Nummulites Deserti de la Harp in Kharga Oasis and the age of Lower Libya in Southern Egypt. Bull. Inst. Des. Egypt. Vol. 3(2). pp. 114-122 (1953).

9. M.Y. Hassan, : The place of zittel's overwegischichten in the Upper Senonian stratigraphy with a note on the orovincial affinities of its fauna (type area Kharga Oasis). Bull. Inst. Des. Egypt. Vol. 28. pp. 77 - 84 (1956).

10. El-Nakkady : Biostratigraphy of Umm El Ghanayem section, Egypt. Micropaleantology, Vol. 51 pp. 453 - 472 (1959).

11. N. El-Gezeiry : On the geology of Kharga Oasis, El-Kharga area. Internal report, Geol. Surv. and Min. Res. Dept. Cairo.(1960).

12. Z. Zagorac I. Rimac, K.Febic and S. Kovacevis : Report on gravimetrical and geological surveys, Kharga and Dakhla Oases. Report by " Heophiziko " Zagrob, Yogoslavia to Gen. Res. Dev., Cairo (1961).

13. R. Said : Tectonic framework of Egypt and its influence on the distribution of foraminefra. Bull. Am. Ass. Pet. Geol., Vol.45,2, pp. 198 - 219 (1961).

14. R. Said : The Geology of Egypt. El-Sevier pub. Co., Amsterdam (1962).

15. M.H. Hermina : Geology of the north western approaches of Kharga. Gen. Surv. and Min. Res. Dept. Cairo. (1967).

16. G.H. Awad, : The application of statistical methods to zonation of the Upper Cretaceous Fauna of Egypt. Annual meeting of Egypt. Geol. Society (1964).

17. G.H. Awad and M.G. Ghorrial : Zonal stratigraphy of the Kharga Oasis. Geol. Surv. and Min. Res. Dept. Cairo (1966).

18. S.A. Hussein : Studies on the mineralization in wadi El-Gedid area. Ph.D. Thesis. Ain Shams Univ., Cairo (1971).

19. S.A. Hussein : White sand occurrence in Wadi El-Gedid area. Bull. Fac. Sci., Ain Shams Univ., In Press (1974).

20. M.E. Hilmy, S.A. Hussein, E. El-Hinnawi, and A. Osman. : Sedimentology and paleocurrent study of Nubia Sandstone in Kharga Oasis. Bull. Coll. Sci., Baghdad, Univ. Vol. 17, No.2, pp. 425-452 (1976).

21. M.E. Hilmy, S.A. Hussein and A. Osman : Petrology and mineralogy of shale intercalations within the Nubia sandstone from Kharga Oasis, Egypt.
Jour. Geol. Soc. of Iraq, In Press (1976).

22. M.A. Ezzat : Preliminary report on the hydrology of the new valley. W. Desert, with special emphasis on Kharga Oasis. Egypt. Gen. Des. Org. Cairo (1962).

23. N.S. Embabi : The semi-playa deposits of Kharga depression, Western Desert, Egypt. Bull. Soc. Geogr. Egypt. XLI , XLII, pp. 73 - 87 (1972).

24. R.L. Folk, and W.C. Ward : Brazoa River bar : A study in the significance of grain size parameters. J. Sed. Pet., Vol. 27. pp. 3 - 27 (1957).

25. B.K. Sahu : Depositional mechanism from the size analysis of clastic sediments. Jour. Spd. Pet. Vol. 34. pp. 73 (1964).

26. R. Passega : Texture as a characteristic of deposition. Bull. Am. Assoc. Petrol. Geol. Vol. 41. pp. 1942 (1957).

27. E.J. Pettijohn, : Sands and sandstone. Springer - verlag, New York, (1973).

28. R.L. Folk : Petrology of sedimentary rocks, Hemphills, Austin, Texas (1968).

MINERALOGY AND CHEMISTRY OF SALT AND ALUM DEPOSITS FROM KHARGA AND DAKHLA OASES WESTERN DESERT, EGYPT

S. A. HUSSEIN*

A B S T R A C T

Surface salt occurrences are known to occur in several parts in the floor of both Kharga and Dakhla Oases (Western Desert, Egypt). Among these salt occurrences alum deposits are recorded. A number of representative samples of these deposits were studied by X-ray diffraction analysis, infrared spectroscopy and were chemically analysed in order to reveal their exact composition. Beside halite, sodium and potash alums have been found. The mode of occurrence and origin of these salts are also discussed.

I N T R O D U C T I O N

Surface salt occurrences of encrustations are known to occur in several parts on the floor of both Kharga and Dakhla Oases. Although Beadnell[1,2] recorded the presence of alum in some localities in Kharga Oasis, no detailed work has, hitherto, been carried out to reveal the exact nature of these salts. The present paper gives the results of mineralogical and chemical analyses carried out on a number of representative samples collected from Kharga and Dakhla Oases (from Boulaq, Kharga-Peris, Massara, Teneida and Mut).

* Geology Department, Ain Shams University, Cairo, Egypt. Now on deputation to Department of Applied Geology, College of Science, Al-Mustansiriyah University, Baghdad, Iraq.

Al-Mustansiriyah Journal of Science, Vol. 3 (1978).

In these localities, the salt marches and encrustations occur in the shallow depressions and are generally mixed with sand and clay. However, the upper layers of the salt are almost white and pure. The thickness of the salt deposits vary generally from few centimeters to about two metres, particulary near the centre of the depressions (Lakes). Here the salt is almost pure and well-crystalline.

The alum occurs in several localities in Kharga Oasis, e.g. El-Maharique, Bellaida, Gebel Taref, Beris and in the hills west of Qasr Lebekha. In Dakhla Oasis, alum occurs as encrustations surrounding water wells near Mut and Qalamun.

Mineralogy of salt and alum encrustations:

The salt deposits occur generally as earthy masses, sometimes with clear and well-developed crystals of halite in some cases, (Plate-1). Admixtures of clay and sand give light greyish colour to the salt. The alum occurs mainly in the form of white to white greyish concretions with different forms and sizes, (Plate-1).

X-ray diffraction analyses of some salt samples reveal the presence of halite and quartz admixture (Table 1); some samples show the presence of clay minerals (particularly kaolinate and illite) Fig. (1). On the other hand, samples of alum have been found to consist mainly of halite, quartz, potash-alum and sodium-alum (Tables 2 and 3), Fig. (2).

Table (1) : X-ray powder diffraction data of salt sample

Sample data		Halite(1)		Quartz(2)	
d Å	I/I_o	d Å	I/I_o	d Å	I/I_o
4.35	13			4.26	35
3.34	97			3.34	100
2.83	100	2.82	100		
2.47	4			2.46	12
2.29	4			2.28	12
2.14	4			2.13	9
2.00	89	1.99	55		
1.82	7			1.82	17
1.71	4	1.70	2		
1.68	3			1.67	7
1.63	18	1.63	15		

1. ASTM card No. 5-0628.

2. ASTM card No. 5-0490.

PLATE

Fig. (a): Photograph of earthy salts from the surface of the lake with much impurities.

Fig. (b): Photograph of white clear crystalline salts.

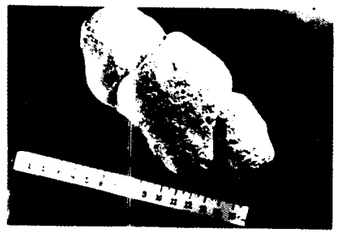

Fig. (c): Photograph of an alum concretion.

Fig. (d): Photograph of different forms and shapes of alum concretions.

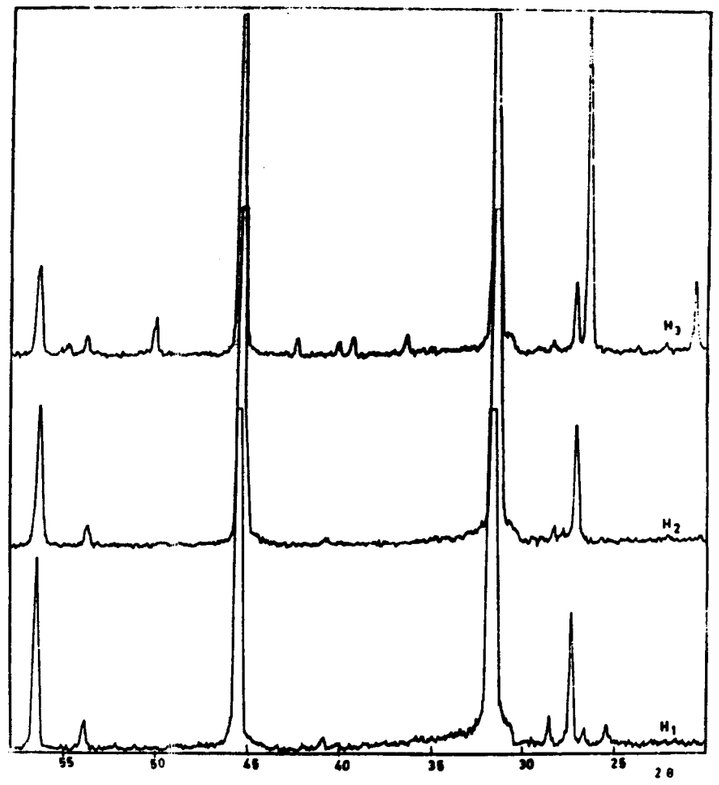

Fig.(1) X-ray diffraction patterns of salt samples H_1, H_2 & H_3.

Table (2) : X-ray powder diffraction data of alum sample

Sample data		Halite(1)		Quartz(2)		Na-Alum(3)	
d Å	I/I_o	d Å	I/I_o	d Å	I/I_o	d Å	I/I_o
4.26	11			4.26	25	4.23	100
3.96	12					3.98	40
3.68	7					3.65	50
3.35	68			3.34	100		
2.81	100	2.82	100			2.90	6
2.44	10					2.47	8
2.30	7					2.32	6
2.14	5			2.13	9	2.19	4
1.99	49	1.99	55	1.98	6	2.04	2
1.82	14			1.82	17	1.82	2
1.70	4	1.70	2			1.69	2
1.67	5			1.67	7		
1.63	12	1.63	15			1.62	4
1.54	11			1.59	13	1.50	2
1.41	11	1.41	6				
1.38	10			1.38	11		
1.26	15	1.26	11				
1.20	4			1.20	4		
1.15	10	1.15	7				

1. A.S.T.M. card No. 5-0628.
2. A.S.T.M. card No. 5-0490.
3. A.S.T.M. card No. 1-0397.

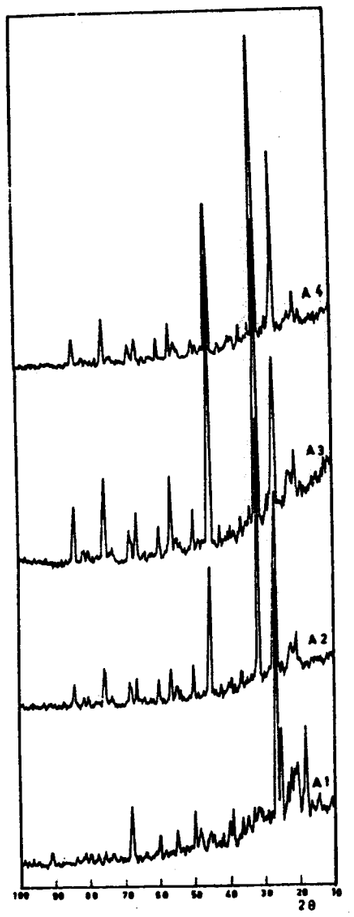

Fig.(2) X-ray diffraction patterns of alum samples: A_1, A_2, A_3&A_4.

Table (3) : X-ray powder diffraction data of alum sample

Sample date		Halite(1)		Quartz(2)		Na-Alum(3)	
d Å	I/I_o	d Å	I/I_o	d Å	I/I_o	d Å	I/I_o
4.27	17			4.26	25	4.29	100
4.11	11					4.03	40
3.38	46			3.34	100	3.24	40
3.12	7					3.03	16
2.81	100	2.82	100			2.85	10
2.70	6					2.71	6
2.48	7			2.46	12	2.45	6
2.36	4					2.33	8
2.30	4			2.28	12	2.25	4
2.01	86	1.99	55	1.98	6	2.02	8
1.83	12			1.82	17		
1.68	3	1.70	2	1.67	7		
1.64	22	1.63	5	1.66	3		
1.55	9			1.54	13		
1.42	15	1.41	6	1038	11		
1.27	25	1.26	11				
1.20	4			1.20	5		
1.15	17	1.15	7				

1. A.S.T.M. card No. 5-0628.
2. A.S.T.M. card No. 5-0590.
3. A.S.T.M. card No. 1-0384.

Infrared spectral analysis of selected samples of salt and alum were carried out using a UNICAM sp. 1200 infrared spectrophotometer in the range between 4000 cm^{-1} and 400 $cm.^{-1}$ The sample was mulled in a reference chemical compound, e.g. Nujol (a heavy medicinal mineral oil) which was used by Miller and Wilkins [ ] in their excellent study of the spectra of inorganic chemicals. The "background" of Nujol absorption is subtracted from the mineral graph to obtain the absorption characteristics of the mineral.

The infrared spectra of salt samples (Fig. 3) show the presence of quartz and absorbed water. The quartz spectra occur at the following wave lengths: 4.25 u, 8-10 u, 12.50 u, 12.85 u and 14.90 u. While the water bands occur at : 6.20 u, 4.20 u and 2.70 - 3.00 u.

The infrared spectra of alum (Fig. 4) show also the presence of quartz and water spectra beside the sulphate spectra at 8.50 - 9.10 u, 14.90 u and 15.50 u. No carbonate, phosphate or borate spectra have been detected.

<u>Chemistry of salt and alum samples</u>:

Six samples of salt from Kharga and Dakhla Oases were chemically analysed; the results are given in Table (4). These analyses show that water insoluble residue (W.I.R.) which consists mainly of admixed sand grains and clays, varies according to the sample collected. Samples near the margin of the salt marches contain high percentages of such admixtures. On the other hand, samples from the inner parts of the lakes consist of nearly pure salt.

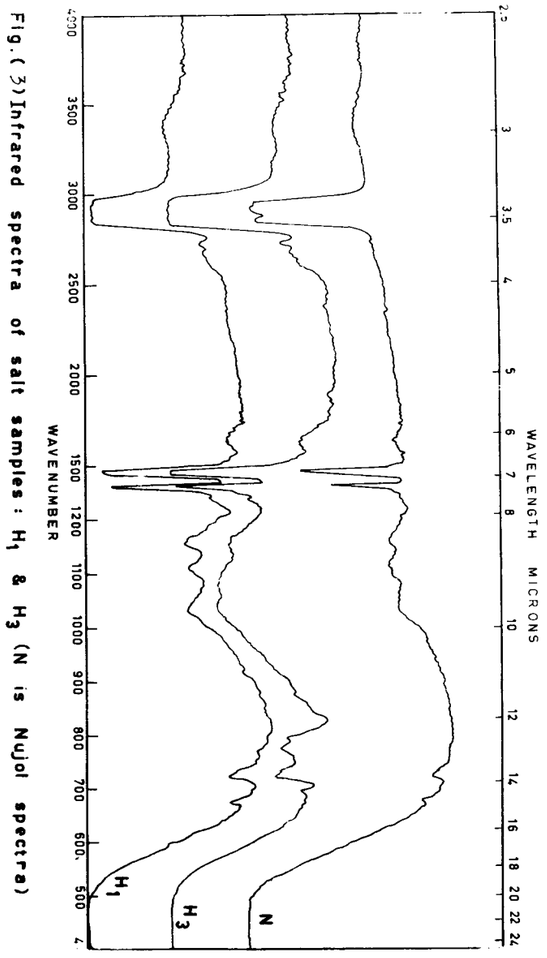

Fig.(3)Infrared spectra of salt samples : H_1 & H_3 (N is Nujol spectra)

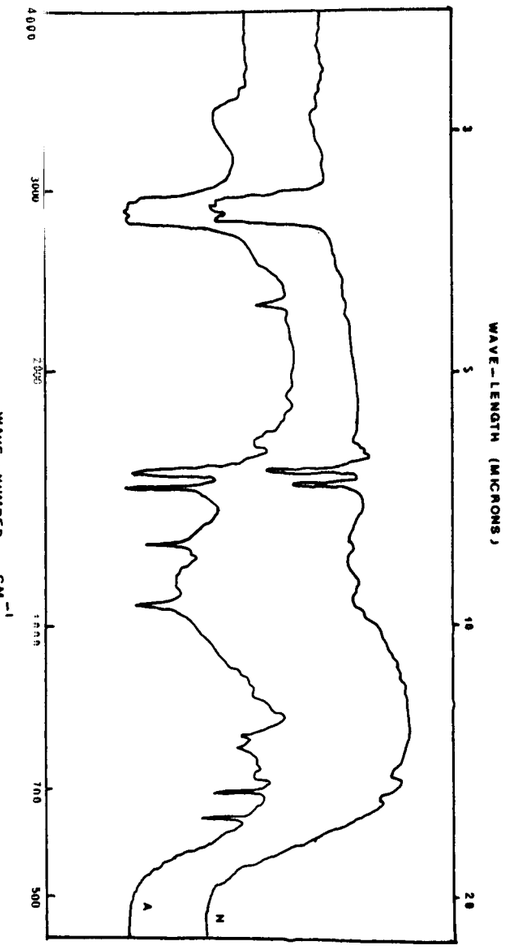

Fig.(4) Infrared spectra of alum sample "A" (N is Nujol spectra)

Table (4) : Chemical analyses of salts from Kharga and Dakhla Oases

	1	2	3	4	5	6
Na	29.78	27.01	24.36	24.72	35.01	29.16
K	0.72	1.62	0.52	2.38	2.72	5.10
Mg	1.00	0.80	0.50	0.50	1.18	1.92
Ca	1.57	nil	1.00	1.00	0.10	1.68
Cl	48.70	55.20	40.62	34.32	57.00	53.62
SO_4	2.90	2.56	nil	2.76	2.54	3.88
W.I.R.	15.86	2.20	31.36	25.52	0.92	4.28
Total	100.53	99.39	99.36	100.20	99.47	99.64

All the samples (water soluble portion) consist mainly of sodium chloride with minor amounts of potassium and magnesium chlorides and sulphates.

Furthermore, three samples of alum were chemically analysed (Table 5), and it appears that the samples contain also a higher percentage of clays. The calculated potash-alum in the samples varies from 32-72% (as calculated from the K-salt.

Organic of salt and alum encrustations:

Field observations beside mineralogical and chemical investigations reveal that the salt and alum encrustations were formed by leaching the salts by the circulating ground waters and then deposited in the suitable depressions on the floor of Kharga and Dakhla Oases by normal evaporation. A direct proof of this is the presence of salt-alum encrustations around some water wells in the Dakhla Oasis. As a matter of fact, most of the shale members overlying the Nubian sandstone contain abundant salt alum stringers. By digging a pit in such shales it has been noticed that after few days or weeks the pit will be filled with salt-alum encrustations and/or concretions. This can be explained by the fact that both sodium chloride and potash-sodium alum are highly soluble, the humidity within the pit expecially at night (the temperature falls down to below 10°C) plays major rule in dissolving such salts which move toward the pit by osmosis (creaping phenomena). It is interesting to note that such mechanism of collecting alum, on a very small scale has long been by the inhabitants in Kharga and Dakhla Oases.

Table (5) : Chemical analyses of alum samples

	1	2	3
Na	18.00	21.50	26.26
K	4.90	2.72	6.12
Mg	1.00	1.08	1.20
Ca	1.21	1.62	1.70
Cl	30.32	42.00	18.68
SO_4	22.02	12.72	18.68
Al_2O_3	6.00	3.20	7.30
W.I.R.	15.54	14.02	10.40
Total	98.99	98.86	98.18
K-alum	60.00	32.50	72.00

C O N C L U S I O N

Surface salt and alum occurrences are known to occur in several parts in the floor of both Kharga and Dakhla Oases. X-ray diffraction analyses of the salt reveal the presence of halite and quartz and clay admixtures. The alum consists mainly of halite, quartz, potash-alum and sodium-alum The infrared spectra of salt show the presence of quartz and absorbed water, while the spectra of alum show also the presence of quartz and water beside sulphate spectra. The salt consists chemically of sodium chloride with minor amounts of potassium and magnesium chlorides and sulphates. The alum consists from 32-72% potash-alum, beside sodium chloride and water insoluble materials. As to genesis of the salt and alum deposits, it was proved that they were leached from the everlying shale members and deposited in the suitable depressions on the floor of Kharga and Dakhla Oases.

R E F E R E N C E S

1) H.J.L., Beadnell, Dakhla Oasis, its topography and geology; Egypt. Surv. Dept., Cairo, U.A.R. (1901).

2) H.J.L., Beadnell, An Egyptian Oasis; An account of the Oasis of Kharga in Libyan Desert: Murray London. (1908).

3) F.A. Miller, C.H., and Wilkins, Infrared Spectra and Characteristic Frequencies of inorganic ions; Anal. Chem., Vol. 24, pp. 1253 - 1994. (1952).

SEISMIC FIELD TEST APPLICATION FOR CIVIL ENGINEERING

M. Mashkour*

ABSTRACT

The evolution of construction techniques in the field of large civil engineering works makes more and more imperative to gain a deeper knowledge of the geo-mechanical characteristics of the rock mass in which the structures are founded or framed.

Amongest the geo-mechanical properties of foundation rock, the young's Modulus of Elasticity (E) now can be obtained from the relationship deriving from the theory of elasticity by which (E) is tied to square of (Vp) compressional wave velocity. However, in the majority of cases, seismic method yields value of (E) much higher than the value of (E) derived by the classical static test. Hence the object of this paper is to present a comprehensive studies into the factors causing the differences between them, evaluating the seismic field surveys for Civil Engineering, and finally finding a relationship between (Vp) and (E) for insitu different types of rocks.

* Department of Applied Geology, College of Science, Al-Mustansiriyah University, Baghdad, Iraq.

Al-Mustansiriyah Journal of Science, Vol. 3 (1978).

INTRODUCTION

The mechanical properties of insitu rocks depend on the essential character of the rock constituents as determined either by a. Petrological origin ; b. The intersities together with alternation due to the water action ; and c. The variable discontinuities in the rock mass, such as bedding, lamination, foliation, schistocity, jointing and faulting. When the last two factors which generally cause a reduction in the mechanical properties (strength and the Modulus of Elasticity) of the rock mass are absent, they are expected to behave in a similar manner to samples collected from the same rock mass as tested in the laboratory. Since it is impossible to have elastically uniform rock media, then tests on core samples will supply data on their mechanical properties which usually give values that may probably as high as 100% above the insitu test results Portland (1953)[1]. Therefore the numerical expression of the rock mass properties by field tests could be more useful when applied to engineering problems that are related to errection of large projects founded on rock mass or built as underground objects.

Amongest the mechanical parameters that can be adopted as a factor in the evaluation of the geomechanical properties of the rock mass is the Young's Modulus of Elasticity (E). This parameter can be defined (in case of compression) as the proportionality constant between the stress (σ) applied on a body and the resulted strain(ϵ). The greater the value of (E) for a solid the less will be the deformation resulting from a given compressive stress.

There are two field methods for testing (E), namely static and dynamic. In the first, loading of the rock during an experiment changes very slowly with time. Static tests usually are conducted by instruments such as

hydraulic jack and testing chambers. The measured value is called static modulus of elasticit ($E_{sta.}$).

The dynamic method is that which, on the basis of causing impact on the ground enables gauging of the velocity of the elastic waves that transmit through the body of the rock mass. The seismic body velocities are usually measured by techniques as direct measurement through adjacent closely spaced bore-holes, and the seismic refraction method. The measured value is called seismic modulus of elasticity (E seis). In the majority of cases (E seis) is considerably higher than the (E sta). The difference between these two values has interested many research people for several years.

The main objectives of the work are : 1. Correlation between the (E seis) and (E sta) insitu rocks, 2. Evaluating the seismic method for determination (E seis), and 3. Finding a relationship between the (Vp) and (E) for different types of insitu rock masses.

2. CORRELATION BETWEEN (E SEIS) AND (E STA) OF INSITU ROCK MASS

Theoretically seismic and static methods should give the same value of (E) for homogeneous and elastic material. However the seismic method usually yield values higher than those arrived at statically by various percentages depending on the rock quality of the insitu media; Murphy and Holt (1966)[3], Obert and Duvall (1966)[5]; M. Bramlette (1966)[4]. The large discrepancies recorded between E sta. and E seis. of rocks explained by a lack of homogeneity, isotropy or perfect elasticity. As linearity is concerned, Iida (19[illegible])[2] showed that dynamic and static determination of (E) for bars of homogeneous isotropic material, like common materials, are found to agree within one or two percent.

The stress strain behaviour of rocks is non-linear. The nature of non-linearity can be classified into two groups, extrinsic non-linearity when a rock mass involving many discontinuities so that its response in bulk to loading is non-linear and intrinsic non-linearity when a specimen of rock (contains minute cracks) is tested in the laboratory where it often display a non-linear stress-strain curve.

In the field, the rock mass that response to loading will exhibit both extrinsic and intrinsic non-linearity. Hence the non-linearity can be rightly attributed to the influence of variable discontinuities into rock mass and to the micro cracks and pores in the rock Walsh (1965 a)[6]. The cracks and pores in the rock affect both determined E sta. and E seis. Under the static loading, the load is usually so high to cause the re-adjustment and closing of the cracks and pores which consequently results in sliding of cracks faces along each other that will eventually cause an energy dissipation, Walsh (1965 b)[7]. Seismically determined (E) of rocks however is entirely free from the effect of the cracks and pores since the maximum alternating stresses arising from seismic tests is too low to permit the slow readjustment and deformation of rock fabrics which usually have a role of application several orders of magnitudes higher than the statically determined modules. Generally known that elasticity modules of rock is a highly sensistive indicator of minute differences in the material. The smallest changes in petrographic constitution, density, structure, humidity content and state of conservation are clearly revealed. Also in compact rock samples, E-value commonly is a function of pressure. In several cases it was found that for a greater number of rock samples of similar external appearance taken from a limited area of a quarry, the value of (E) showed variations from the mean in excess of 10 %, Link (1964)[8]. These dispersions increase with the size of the rock samples. Tests on a granite specimen, for instance, resulted in an (E)

value of about 3.5×10^5 Kg/cm^2 measured over a length of 15 cm but of 8.0×10^5 Kg/cm^2 for a 1 cm length, Philips (1948)[9]. Deviation of such extent made the civil and mining engineers to relay on field test of rock mechanical properties rather than on test of small samples.

The possibility of direct application of seismic method is sometimes not too optimistic, since the method gives always higher values than those derived by static loading. Hence one must shed some light on the causes affecting the differences between E seis. and E sta. measured in the field.

1. E seis. determind in the field for that part of the insitu rock traversed by the elastic waves. The insitu E. sta. is measured by a static loading tests over an area which is but a fraction of the area of the seismic wave path. It is therefore incorrect to attempt to correlate those two values. In view of the great differences between the two areas of influence, one would actually be correlating different regions of the rock. For instance insitu static loading by flat jack is to be conducted on the immediate periphery of the tunnel or foundation (The zone which is usually affected by many fractures and cracks present originally in the rock mass or induced due to the process of blasting and excavation). Therefore, one may expect that the E sta. will be much less than the E seis. obtained from the (Vp) comming from solid part of the rock mass a way from the excavation.

2. Field static loading usually takes several days, a possibility of inducing cracks in the immediate vicinity of the loading causes stronger deformation that result in lower values of E sta.

3. Higher E seis. may also be due rock humidity and water in the cracks. E sta. under monoxial pressure is lower for humid than for dry rocks, Hughes and Cross (1951)[10]. When rock tests are performed in exploration

galleries of shafts, the surrounding rocks will always be extensively unwatered by the gallery. E seis of a large rock mass, particularly at the bottom of a valley will, in most cases be influenced by water - saturated fractures.

3. EVALUATION OF THE SEISMIC METHOD FOR E SEIS DETERMINATION

During the last two decades, seismic method for determining the elastic properties of rock has found increasing application in the field of rock engineering, particularly in connection with dam foundations, tunnel construction and mining projects. Generally, the method has been advantageously employed to the design of the engineering structures especially when they are supplemented by other types of field and laboratory tests Onadera (1963)[11]. The widspread use of this method is explained by the following facts :-

1- In engineering practice when high rates test data are to be applied to problems of rapid loading, such as drilling, crusning and blasting, seismic determination of (E) can be valuable tests.

2- In seismic method, the measurements are made at a pertinent location in the field and hence seismic pulse is affected to a certain extent by the number and character of the existing discontinuities. Moreover costs involved are low and that the method permits a rapid determination of (E) for strata of greater extent. Thus by this method, zones of different properties can be separated relatively quickly in a hetrogeneous rock complex.

In the case of large dams, for instance, separated zones of defined elastic properties expressed by E seis can be obtained along the profile and at the required depth. In the case of tunnels and shafts, these

zones are established along their Lay-out, Hedstrom and Kollert (1949)[12]. Field measured E sta. is time consuming and expensive, and therefore limited to a small number of sites. Moreover, the choice of the testing area is frequently restricted by various considerations. Besides, extending the validity of the values found for small areas to other zones of the dam foundation is often problematic, the more so as the values are likely to show a wide dispersion.

3- As the field seismic velocity, is not only influenced by the number and type of discontinuities in the path of the pulse, it is also influenced considerably by the properties of the intact rock. The effects of the discontinuities in the rock mass can be estimated by comparing the field seismic velocity with the laboratory sonic velocity of an intact core obtained from the same rock mass, and the ratio E seis/E sonic is called soundness of rocks in situ. The highest the ratio the less fractured, jointed the rocks in situ, i.e. the soundest the rocks in the field. Onadera[11] produced a soundness classification table of rocks in situ. Such classification helps to facilitate communications among civil engineers, design engineers and contractors.

4- The seismic technique while it is used for determination of E seis in a foundation rock mass can provide an assessment of the geological and engineering condition of the sites such as :-

i- It gives good result when employed for location zones of loosened structures in connection with the deriving of tunnels, determining the effectiveness of grout injections, and investigating large areas at dam sites with the aim of detecting irregularities in the rock formations of the valley and the flanks.

ii- Shallow structural feature can be mapped such as faults which may be disappear under overburden or under the waters of a lake, shear zones, contact zones, buried structural features, such as old limestone sink holes may be delineated by the method.

iii- The strike and dip of geological formations may be determined.

iv- Determination of lateral and vertical substratum homogeneity.

v- Depth of water table.

vi- Prediction of grout take.

4- DISCUSSION OF THE VARIOUS PARAMETERS CONSTITUTE THE EQUATION OF (Vp).

A rock medium (in spite of its crackings, diaclases and lack of homogeneity) can as a whole be considered relatively elastic in its mechanical behaviour. In the field of seismic refraction work, several types of propagating waves are generated on impaction the ground. The most importance of the propagating waves are, the compressional and shear wave velocities (Vp) and (Vs) respectively. The percentages amount of (Vs) to be generated in a particular impact is different according to the volume and way of impact. The (Vp) mode has the highest velocity and is the mode normally detected in refraction seismic surveying. Since the (Vs) travel slowly and unless their amplitude is relatively large, they are up to be confussed with (Vp). Furthermore, impact senses usually produced a prolonged vibration so that a succession of arriving waves will merge with one another instead of remaining distinct. Therefore the opportunity to measure the (Vs) velocity in the field often produces difficulties.

The mathematical theory of elasticity furnishes the following general expressions for the (Vp) and (Vs) velocities, Dobrine (1960)[13].

$$E = \frac{\rho (Vp)^2 \ (1+\sigma) \ (1-2\sigma)}{(1-\sigma)} \qquad (1)$$

$$E = 2\rho (Vs)^2 \ (1-\sigma) \qquad (2)$$

$$\sigma = \frac{1 - 2\left(\frac{Vs}{Vp}\right)^2}{2 - 2\left(\frac{Vs}{Vp}\right)^2} \qquad (3)$$

Where σ , ρ , and E are the poisson's ratio, density and Young's Modulus of Elasticity of the material respectively. When E seis of the insitu rock is to be determined by the equation (1), the three parameters (σ) , (ρ), and (Vp) must be investigated. Each of these parameters has a relative effect on the resultant value of elasticity modulus. For the purpose of evaluating the relative effect of each of these elements, it is convenient to represent equation (1) in the following manner : -

$$E_{seis} = F\left[f\left(\frac{p.n}{g}\right), \ (\sigma), \ (Vp)^2\right] \qquad (4)$$

Thus E seis is a function of : -

i- Density of the rock (ρ) :-

This can be measured either in laboratory on core samples or in the field. The volume weight of the rock is a function of petrology (p) and porosity (n) ; (g) is the acceleration, and $\left(\frac{p.n}{g}\right)$ is the mass of the rock. Rocks of different petrology with smaller weight have, as a rule, a smaller p-velocity, whereas rocks of the same petrology show an increase of velocity with decrease in porosity, and, consequently with increase in volume weight. To illustrate the effect of density on the calculated E seis. The curve in Fig.1. was generated. This curve was produced by assuming constant Vp = 12500 ft/see and poisson's ratio (σ) =

0.25 in the formula No.1, but the value of rock density was varied from 1.5 to 3.5 gm/cm^3 by an increment of 0.5 gm/cm^3 each time. The calculated E seis. was then plotted versus each chosen value of density. The curve shows that higher values of density raise the curve upwards.

Usually the volume weight of rock (p,n), gauged insitu is always smaller than the volume weight tested on samples of the same rock. Kedo et al in Onadera[11] showed by intense field tests of densities at several dam sites by means of gamma ray logging in holes drilled in the rock media, that although the density varied with the depth, the values of the density of the insitu rock mass were usually 10 - 15 % smaller than the values of densities measured in the laboratory on core samples. The average of this range is taken in the calculation (section 5).

ii- Poisson's ratio of the rock (σm) : -

This ratio can be calculated by static loading on core samples or in the field on the basis of measurements of both Vp - and Vs - velocities using equation (3). As was pointed out at the beginning of this section, it is hard to carry out the correct following up of phases of Vs-waves in seismic records. Therefore, it will be more appropriate to assume a value of Poisson's ratio, provided that it will not affect seriously the calculation of (E). This assumption serve to minimize both time and cost. In engineering practice, where silicate rocks are usually encountered. Poisson's ratio of which varies over a narrow range (0.15 - 0.3) for hard rocks. This is small to the theoretical possible variation of the value from -1 to 0.5. Hence, for compact rocks, the value of Poisson's ratio in the formula of (Vp) may in fair approximation be taken equal to 0.27. To justify this approximation, the curve in fig. 2 was plotted. It was produced by assuming constant Vp = 12 500 ft/sec and rock density (ρ= 2.5 gm/cm^3 in the formula No.1, but the value of poisson's ratio (σ) was varied from

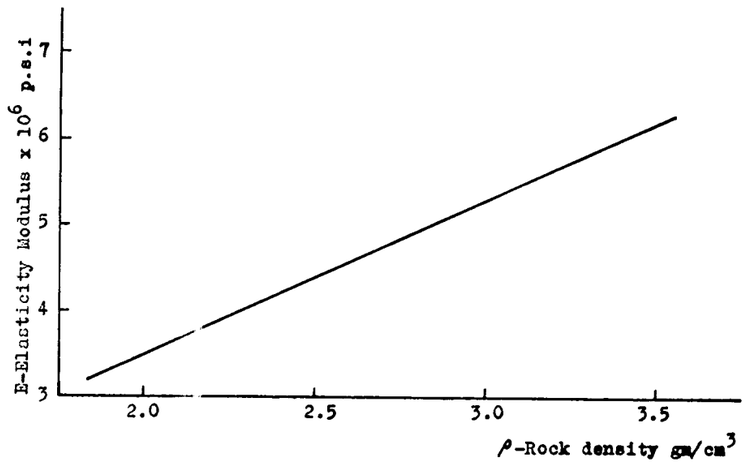

Fig. 1. Illustration of the effect of density on the calculated (E) for VP=12,500 ft/sec. and σ = 0.25.

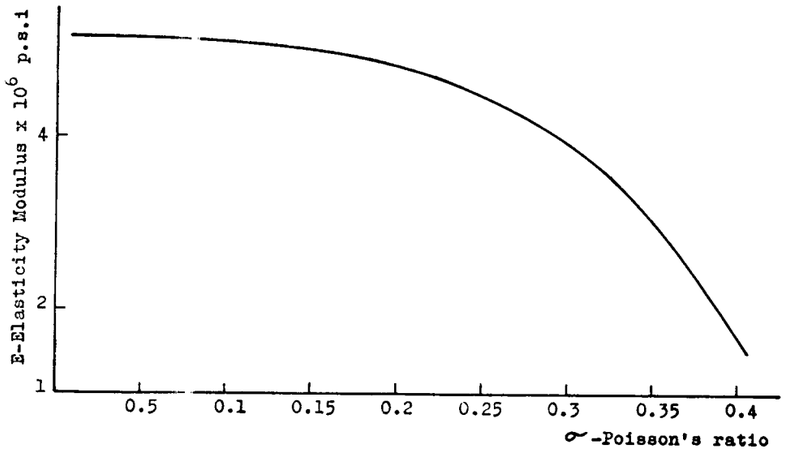

Fig. 2. Illustration of the effect of Poisson's ratio on the calculated (E) for VP = 12,500 ft/sec. and ρ = 2.5 gm/cm^3.

0.05 to 0.40, by an increment of 0.05 - each time. The calculated E seis. was then plotted versus each chosen value of poisson's ratio. The figure shows that values of poisson's ratio less than 0.27 shift the curve upwards and greater values shift it downwards. The slope of the curve is always small for the part of poisson's ratio range between 0.1 and 0.27. Hence an error in assuming a value for the poisson's ratio in this range will have very little effect on the actual and correct calculation of E seis. of rocks. Whereas the sharp downwards increasing in the slope of the curve for values of Poisson's ration above 0.3 indicate that serious errors will be introduced if a ratio is chossen above this limit. For example, if a value of σ = 0.3 was assumed for a type of rock, while in fact σ = 0.35, then the estimation of (E) would be 30 % larger which conceivably leads to serious consequences. Therefore for rocks having inferior elastic properties it is important to measure the insitu Poisson's ratio seismically. This can be achieved without difficulty, since the accuracy of detecting the (Vp) and (Vs) wave velocities is higher in rocks having larger values of Poisson's ratio contrary to harder rocks. Figure (3) by Evison (1956)[14] illustrate this fact.

iii- Compressional wave velocity (Vp) : -

This is determined on the basis of the first arrivals of seismic records. The relative effect of the parameter (Vp) on the calculation of E seis. can be deduced from the equation (4), since the value of (E) involves function of (σ) and (ρ) but of an appropriate velocity squared. Hence a little change in the velocity will cause considerable changes in the calculation of E seis. To illustrate this effect, the curve Fig. 4 was plotted. This was produced by keeping Poisson's ratio (σ) and rock density (P) at 0.25 and 2.5 gm/cm^3 respectively constant in the formula No.1, but the valve of VP - velocity was varied from 7500 ft/sec to

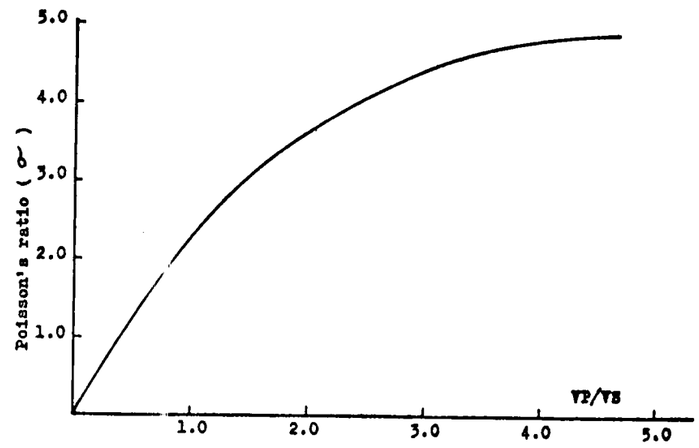

Fig. 3. Theoretical variation of Poisson's ratio with ratio of seismic wave velocities (After Evison (1956)[14]).

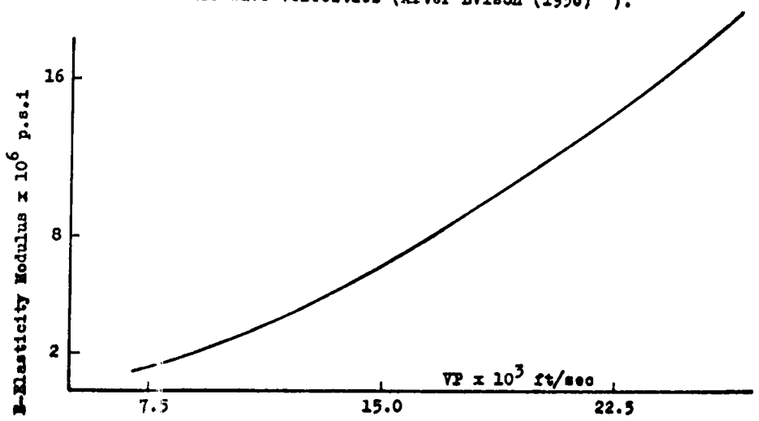

Fig. 4. Illustration of the effect of compressional wave velocity on the calculated (E) for σ = 0.25 and ρ = 2.5 gm/cm^3.

30,000 ft/sec, by an increment of 1000 ft/sec each time. The calculated E seis. was then plotted versus each chosen value of velocity. Therefore in the field of seismic tests, a correct measurement and interpretation of the received Vp-velocity is of great importance if accurate calculation of E seis is required.

Generally, the Vp-velocity is affected by many environmental factors some of these factors increase the velocity, others tend to decrease it. In both cases field determination of E seis. will ultimately affected, the common variable factors likely to occur within the earth engineering work are presented as follows :-

1- Effect water saturation: Vp-velocities always increases with the saturation. Laboratory studies on the effect of saturation on the velocity measurements was studied by Hughes and Jones (1951)[15]. In their experiments, the velocity started to drop after it reached 90% of the complete saturation. In order to study the function of saturation variation on the velocity, consider the schematic pattern of sandstone grains as closed packed sphered for four degrees of saturation as shown in Fig.5, after Hughes and Kelly (1952)[16]. In these packing of spheres, the interstitial water is shown in black, and the interstitial air is white. In looking at dry, unstressed rock, we find that the grains are in loose contact, in this case, we expect low signal, but if a small amount of water is added and it wets the rock, it will be pulled into the small cracks and will serve to increase the area of contact effectively at atmospheric pressure. Usually a very small quantity of water results in signals, so when more water is added, the effect would be expected to be small.

The model by Hughes and Kelly[16] given above explains the general variation of velocity curve with the variation of the saturation degrees.

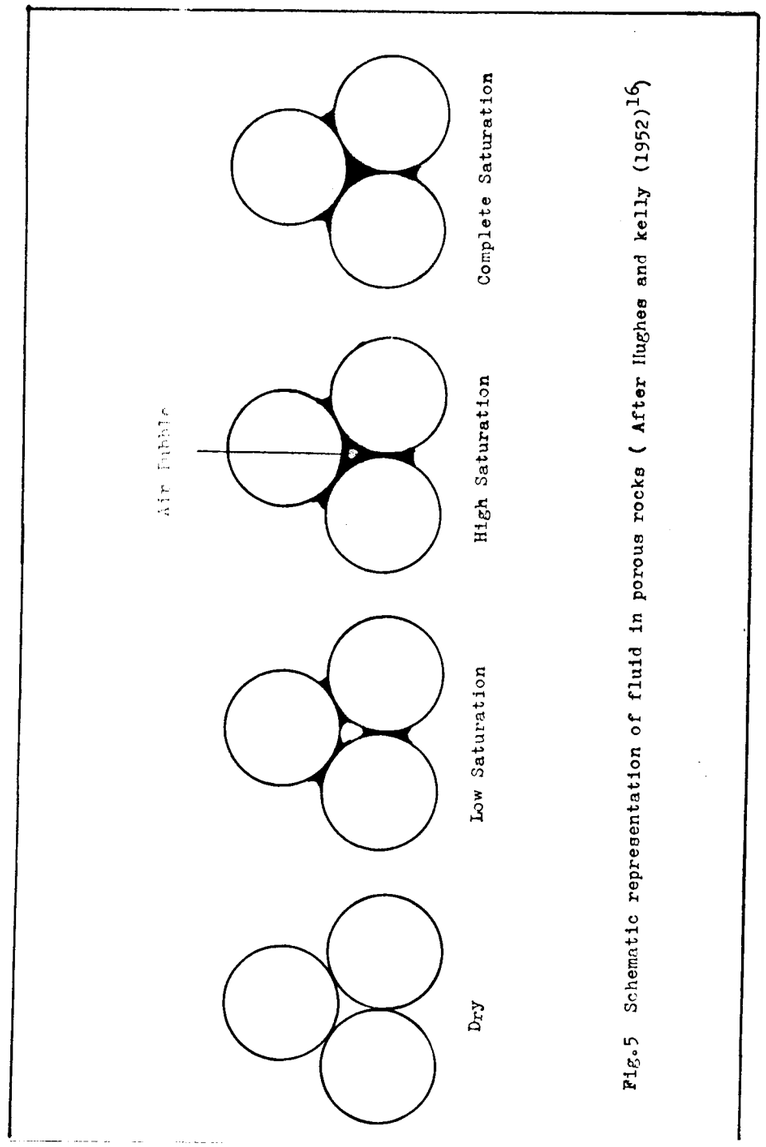

Fig.5 Schematic representation of fluid in porous rocks (After Hughes and kelly (1952)[16]

measured velocities in dry state, except for the material having very low compressibility. To explain this fact, one may refer to the conclusion by Hughes and Cross (1951)[17], that in dry sample, the pulse is travelling alternatively through rock and air, while in water saturated rocks, the pulse is travelling alternatively through rock and water. Because water has much higher velocity than air, then the initial velocity in water saturated rock would be higher than in dry rock.

Nur and Simmon (1969)[18] have noticed that the Vp-velocity increase greatly when measured below the water table, while the S- shear wave velocity remained essentially unaffected. Therefore the use of Vp-velocity are calculating E seis. is discouraged for the case of low quality rock masses (vp = 10,000 ft/sec) below the water table. Water (Vp = 5,000 ft/sec) couples the seismic energy across joint openings, coupling much shorter travel paths than would be possible in the same rock mass above the water table. Thus, Young's modulus calculated from observed compressional (Vp) would be much too large. In this case, the measurment of shear wave velocities is much more valuable because they will remain unaffected for heavilly jointed rock masses below the water table, Ambraseys and Hendron (1968)[19] suggested that Young's modulus may be more appropriately determined from equation of shear wave velocity.

Effect of rock anisotropy : Insitu rock masses are anisotropic in nature, Therefore they exhibit directional properties. The common cases of anisotropy, likely to occur in rock masses, are bedding and various kinds of fractures. Measurements of (Vp) along the bedding is always higher than those measured perpendicular to the bedding, Wantland (1963)[20]. The orientation of the velocity measurements relative to the anistropy present in the rock mass is of considerable significance; Knill (1968)[21], showed

that marked anisotropy in granite foundation due to stress relief joints, contributing to an extreme variation of 50 % in the measured velocities, whereas anisotropy due to slightly cleaved argillaceous rocks contributed to a variation in the velocity not more than 16 %.

3- Effect of High-velocity zone: Presence of a zone or a layer of high velocity material along the seismic line will provide a path through which the arriving waves will travel. This will not be a representative or an average velocity for the rock mass as a whole Wantland[20]. For example, a limestone bed in a shale sequence or a silicified fault zone in an altered granite mass may give misleading results if adequate care is not taken in interpretation of seismic results.

4- Effect of confining pressure : Generally Vp-wave velocity increase, where measured in specimen subjected either to uniaxial or confined pressure. This is because in unstressed samples, the rock grains are in loose contact, but as the pressure is increased, the loose grains are brought into contact and reduce the porosity. Thus making the rock a better a coustic medium, Gregory (1966)[22]. The rate of velocity increases in dry porous rock under confined pressure is less than that for saturated samples Wyllie et al (1958)[23].

Insitu, the overburden and the adjacent rock serves as confining pressure on any part of the rock in place. Hence logically, when cores brought up from certain depth of " insitu " rock mass, the coring operation causes the samples to be almost instantenously decompressed from overburden pressure to the atmospheric pressure. Hence the mechanicsl and physical properties of the rock will change to a certain extent that the Vp-velocity measured through them would not be the same, had measurements were taken in the same type of rock at the particular depth where they come from. Thus for

a correlation between " insitu " and laboratory measurements of Vp-velocities, we are faced with the task of restoring the samples to their original state of stress in order to make meaningful measurements. The nature of the three dimensional stress field to which rocks under different circumstances are subjected, is a point to argue. The horizontal stresses in a rock can be as much as two or three times the normal overburden pressure. The intensity of horizontal stresses may also be varied in different orthogonal direction. If the aim is to investigate the effect of confining pressure on the Vp-velocities in close simulation to " insitu " condition of stress, the conventional triaxial testing is the best available method, since results can be reproduced to a wide range of circumstances. Finally the reader may refer to the extensive result by Birch (1961)[24], on the effect of confining pressures on the Vp-wave velocities in different types of rock samples.

5 - RESULTS AND CONCLUSIONS

Utilizing the fact of the great dependibility of (E) on the (VP) which has just pointed out in section 4, a relationship between these two parameters is plotted in Fig.6, and the derived formula is :

$$E_{seis.} = 0.0201\ VP^2 - 0.0052\ VP - 0.0182 \text{ lb/sq. in} - (5).$$

In plotting the relationship of Fig. 6, the following consideration are taken :

1- Large number of (VP) measurements done in different insitu types of sedimentary, metamorphic and igneous rocks are used, some of 95 values were collected from different literatures, mainly from Bransilav[4], Headstrom and Kollert[12], Oliphon (1950)[25], Hasslstrom (1969)[26], Molotova and Vassilev (1960)[27], Linhan (1962)[28], Flavio (1966)[29], and Hobson and Hunter (1969)[30].

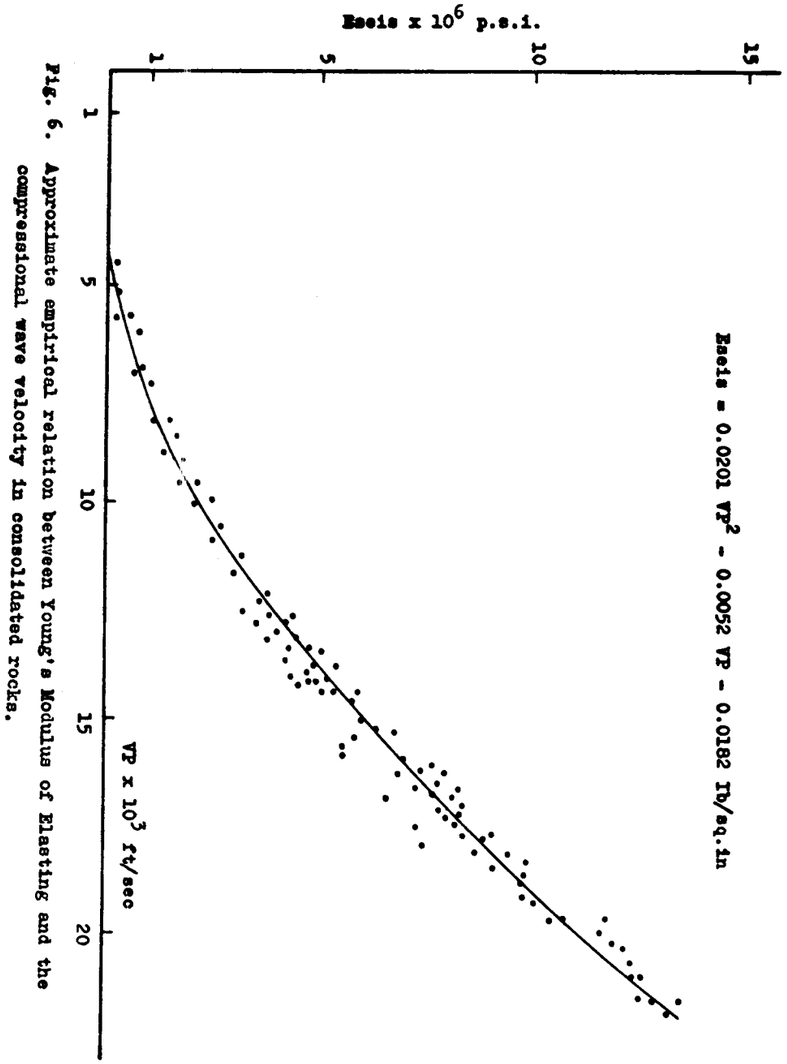

Fig. 6. Approximate empirical relation between Young's Modulus of Elasting and the compressional wave velocity in consolidated rocks.

2- The density was taken separately for each type of rock as an average of a considerable number of measurements on core samples taken mainly from Daly et al (1966)[31], and Smithson (1971)[32]. Laboratory average density for each type of rocks was reduced by 12.5 % to obtain the field rock density (see Section 4 - i), and

3- The value of Poisson's ratio was taken equal to 0.27 (see Section 4-ii).

The relation of equation (6) does not represent the first of its kind. A similar relation was plotted by Brown and Robertshaw (1953)[33], which was later replotted in logarithmic scale by Hawkins (1969)[34] and the derived formula is :

$$E = Vp^{2.34} \times 10^{-3} \quad lb/Sq.in. \qquad (6)$$

However equation (6) has definite advantages over the relationship of equation (6) for the fact that Brown and Robertshaw[33], used the results given by Reich given in [33] were originally based on erroneous assumptions for the reasons that the majority of the 70 calculated modulii of elasticity used in the plot were not computed directly from the Vp-velocities, but the values of (E) were determined statically and the velocities were calculated assuming Poisson's ratio to be equal to 0.27 and appropriate density.

Two examples of application are given in the table below to compare the values of E seis. obtained by equations (5) and (6) with the field E sta. The table shows that field E sta in solid foundation compare better with the E seis calculated by equation (5) than from Equation (6). This is representing an improvement in the direction of the closing the gap between the values of (E) arrives at the two methods, and then make the civil engineers to safely relay on seismic method for testing this parameter. In the case where the site is fractured and faulted, E seis. is much higher than E sta. This is quite justified, since a site has an inferior elastic properties has a Poisson's ratio greater than

0.27 (the value which assumed in the relation of equations 5 and 6). Therefore when these equations were used in the calculation, an error was introduced which had remarkably caused the over-estimation of the calculated E seis. For illustration see Fig. (2). Therefore in condition like this the value of Poisson's ratio must be measured seismically.

Example of Application

Rock name	ρ x 10^3 kg / m^3	E.seis.x 10^6 psi(equ.5)	E seis.x 10^6 psi(eqa. 6)	E sta x 10^6 psi	Site condition
Granodiorite	3.9 *	1.58	1.74	1.33 +	Solid
Andesite	9.9 *	1.96	2.24	0.25 +	cracked and faulted

* measured by Kudo et al in Candera [11].

6 - CONCLUSION

An approximate empirical relation between Young's Modulus and the compressional wave velocity in consolidated rocks is derived. Upon measuring the Vp- velocity in the rock media, E seis, can be obtained directly without reference to the values of the Poisson's ratio and rock density. However for correct computation of E seis. in sites having inferior elastic properties, the value of Poisson's ratio should be measured insitu seismically.

REFERENCES

1. D.F. Portland, : Determination of the modulus of elasticity of rocks for pressure tunnels and shafts: Bulletin Geological Society of America, Vol. 64. Dec. P. 1425 (1953).

2. V.J. Murphy, and R.J. Holt : Seismic velocities and elastic modulii measurements : Proceedings of the first congress of the International Society of Rock Mechanics, Vol. I, Lisbon, P. 711 - 712 (1966).

3. K. Drosed, and B. Louma : The correlation of modulii of elasticity determined by microseismic measurements and static loading : Proceedings of the first congress of the International Society of Rock Mechanics, Vol. 1, Lisbon, P. 291 - 293 (1966).

4. K. Branislav : Correlation between static and dynamic investigation of rock mass insitu : Proceedings of the First Congress of the International Society of Rock Mechanics, Lisbon, P. 565 - 570 (1966).

5. J.A. Ide : Comparison of statically and dynamically determined Young's Modulus of Rocks: Proceedings of the National Academy of Sciences, Vol. 22, P. 81 - 92 (1936).

6. J.B. Walsh : The effect of cracks on the compressibility of rock : Journal of Geophysical Research, Vol. 70, No.2, P. 381 - 389 (1965 a).

7. J.B. Walsh : The effect of cracks in rocks on Poisson's ratio: Journal of Geophysical Research, Vol. 70. No. 20, P. 5249-5254 (1965 b).

8. H. Link : Evaluation of elasticity modulii of dam foundation rock determined seismically in comparison to those arrived at statically: 8th International Congress on large dams, Edinburgh, P.833-849 (1964).

9. D.W. Philips : Tectonics of mining : Sheffield mining magazine, P. 47 (1948).

10. D.S. Hughes and J.H. Cross : Elastic wave velocities at high pressure and temperature : Geophysics, Vol. XVI , P. 577 - 593 (1951).

11. T.T. Onadera : Dynamic investigation of foundation rocks insitu : Proceedings of the 5th Symposium on Rock Mechanics at the Univeraity of Minnesota, Pergamon, New York, P. 517 - 533 (1963).

12. H. Hedstrom and R. Kollert : Seismic soundings of shallow depths : Tellus, Vol. 1, No.4, P. 24 - 36 (1949).

13. M.B. Dobrine : Introduction to Geophysical Prospecting, 2nd Edition, International Student. Tokyo (1960).

14. F.F. Evison : The seismic determination of Young's Modulus of Elasticity and Poisson's ratio for rocks insitu : Geotechnique, Sept. P. 118 - 123 (1956).

15. D.S. Hughes, and H.J. Jones : Elastic wave velocities in sedimentary rock: Transaction of the American geophysical union. Vol. 32, P. 173 - 178 (1951).

16. D.S. Hughes, and J.L. Kelly : Variation of elastic wave velocity with saturation in sandstone : Geophysics, Vol. 17 , P. 739 - 752 (1952).

17. D.S. Hughes, and J.H. Cross : Elastic wave velocities at high pressure and temperature : Geophysics, Vol. XVI, P. 577 - 593.

18. A.Nur, and G. Simmons : The effect of saturation on velocity in low porosity rocks : Earth and Planetary Science letters, Vol. 7. P. 183 - 193 (1969).

19. N.N. Ambraseys, and A.J. Hendrom : Dynamic behaviour of rock masses : Rock mechanics in Engineering practice edited by Stagg and Zienkiewics, P. 203 - 236 (1968).

20. D. Wantland : Geophysical measurements of rock properties insitu, state of stress in the earth crust, editor William R. Judd, California, P. 145 - 159 (1963).

21. J.L. Knill Application of seismic methods in prediction of grout take : Journal of British geotech. (1968).

22. A.R. Gregor : Shear wave measurements of sedimentary rocks under compression : Rock mechanics, Ed. C. Fairhurst, Publ. Pergamon Press, London. (1966).

23. M.R.J. Wyllie, A.R. Gregory, and G.H. Gardner : An experimental investigation of factors affecting elastic wave velocities in porous media : Geophysics, Vol. 23. P. 160 - 179 (1958).

24. F. Birch, 1961 :

a- The velocity of compressional waves in rocks to 10 kilobars, Part I. P. 1066 - 1092.

b. The velocity of compressional waves in rocks to 10 Kilobars, Part II. P. 1093 - 2022.

c. Journal of Geophysical Research, Vol. 66, No.7.

25. C.W. Oliphan : Comparison of field and laboratory measurements of seismic velocities in sedimentary rocks : Bulletin of the geological society of America, Vol. 61, P. 759 - 788 (1950).

26. B. Hasslstrom : Water prospecting and rock investigation by the seismic refraction method : Geoexploration, Vol. 17, P. 113 - 132. (1969).

27. L.V. Molotova, and Yu.I. Vassilev : Velocity ratio of Longitudinal and transverse waves in rocks : Akad. Nauk. USSR. Izv. SER, Geofiz, No. 7, P. 731 - 743 (English translation) (1960).

28. D.S.J. Linhan, and V.J. Murphy : Engineering Seismology applications in metropolitan areas : Geophysics, Vol. XXVII, No.2, P. 213 - 220 (1962).

29. P.A. Flavio : Application of seismic field test in some rock media: Proceedings of the first International Congress of Rock Mechanics Society, Vol. 1, Lisbon, P. 3 - 6 (1966).

30. G.D. Hobson , and J.A. Hunter : Insitu determination of elastic constants in overburden using a hammer seismograph: Geoexploration, Vol. 7, P. 107 - 111 (1969).

31. R.A. Daly, G. Edward, and Sydrey : Handbook of physical constants : The geological society of American Memoir, Vol. 97. P. 19 - 26 (1966).

32. B. Simpthson Scott. : Density of metamorphic rocks : Geophysics, Vol. 36, No.4, P. 490 - 694 (1971).

33. P.D. Brown, and J. Robertshaw : The insitu measurements of Young's Modulus of Elasticity for rock by a dynamic method : Geotechnique, Sept. P. 283 - 286 (1953).

34. L.V. Hawkins : Seismic refraction surveys for Civil Engineering : Geophysical Memorandum, No.2, 11P (1969).

THE PROBLEM OF CRACK OF ARBITRARY SHAPE UNDER ARBITRARY LOADING

S.M. Sharfuddin*

ABSTRACT

The problem of crack of arbitrary shape subject to arbitrary loading has been investigated. The displacement field is represented by single-layer and double-layer potential of second kind. The equation for crack opening displacement has been established. Crack opening displacement under pressure has been analysed.

INTRODUCTION

General methods of solving crack problems in Two-dimensional Elasticity Theory has been developed by Inglish [1] , Westergaard [10] , Sneddon [3, 5, 14, 20] , Cottrel [13] , Barenblatt [2] , Sanders [4] , Sharfuddin [6, 8] and others. Problems of system of cracks have also been tackled by Koiter [9] , Sharfuddin [7] , and others. Methods used by most of the authors are Fourier Transforms, Integral Equations (sometimes dual) or Hilbert's technique as presented by Muskhelishvili [11, 12] .

* Institute for Advancement of Science and Technology Teaching, GPO Box. 809, Dacca - 2 , Bangladesh. Now on deputation to Department of Mathemathics, College of Science, Al-Mustan-siriyah University, Bagdad, Iraq.

Al-Mustansiriyah Journal of Science, Vol.3 (1978)

In Three-dimension the problem of a plane crack under pressure acting on its face has been analysed by the well known Boussinesq-Papkovich representation. The displacement field $u_i(x)$ is generally represented by means of Newtonian Potential, the density of which is equal to the crack opening displacement (Buckner [19]). There are other representation of the displacement field in the elastic body as functions of crack opening displacement viz the elastic potentials introduced by Kudpradze [15] . Kossecka [16] made use of this single layer potential and double-layer potential of the first kind and found an equation of crack opening displacement.

Here in this paper we consider the general loading for a plane crack of arbitrary shape. Our representation of displacement field gives a set of three integral equations for the crack displacement discontinuities. This method has some advantage for purpose of numerical analysis because integral equations extend over the crack surface only. Hence a Three-dimensional problem has been reduced to a Two-dimensional one.

2- Basic Equations and Tensors

Let x_i be the Cartesian co-ordinates of a point X, (i = 1,2,3) and e^i be base vectors. The displacement field u(x) is given by

$$\overset{*}{\Delta} u = \mu \Delta u + (\lambda + \mu) \text{ grad div } u = - f \qquad (2.1)$$

in domain Ω . λ , μ are La'me constants, f is the body force and Ω is finite range three-dimensional space filled with elastic material. When $\mu = 1$, $\lambda = -1$ we get $\overset{*}{\Delta} = \Delta$ (Laplace operator).

The generalised stress vector operator $P^{(n)}$ on an area element normal to unit vector n is

$$P^{(n)} \hat{u} = (\alpha + \mu) \frac{\partial \hat{u}}{\partial n} + \beta \hat{n} . \text{ div } \hat{u} + \alpha (\hat{n} \times \text{curl } \hat{u}) \qquad (2.2)$$

α, β are real numbers, where

$$\alpha + \beta = \lambda + \mu \qquad (2.3)$$

Betti's third formula on reciprocal relation can be written as (Kudpradze [15]) :

$$\int_{\Omega} (\hat{u} \cdot \Delta^* \hat{v} - \hat{v} \cdot \Delta^* \hat{u}) d\nu = \int_{d\Omega} (\hat{u} \cdot P^{(n)} \hat{v} - \hat{v} \cdot P^{(n)} \hat{u}) ds, \qquad (2.4)$$

where $d\Omega$ is the boundary.

When $\alpha = \mu$, $\beta = \lambda$ we get physical stress vector operator $T^{(n)}$ given by

$$T^{(n)} = 2\mu \frac{\partial}{\partial n} + \lambda \hat{n} \, div + \mu (\hat{n} \times Curl) \qquad (2.5)$$

$T^{(n)}u(x)$ gives the intesity of stress in X on a surface element through X with normal $\hat{n}$. When

$$\alpha = \frac{\mu(\lambda+\mu)}{\lambda+3\mu} \quad , \quad \beta = \frac{(\lambda+\mu)(\lambda+2\mu)}{\lambda+3\mu} , \qquad (2.6)$$

the stress operator $P^{(n)}$ becomes Pseudo-stress operator denoted by $N^{(n)}$

$$N^{(n)} = \frac{2\mu(\lambda+2\mu)}{\lambda+3\mu} \frac{\partial}{\partial n} + \frac{(\lambda+\mu)(\lambda+2\mu)}{\lambda+3\mu} \hat{n} . div + \frac{\mu(\lambda+\mu)}{\lambda+3\mu} (\hat{n} \times Curl) \qquad (2.7)$$

3. Kelvin Somigliana and Kudpradze-Bashelishvili Tensor

Let Green's tensor of an finite elastic body be $G_i^k (\hat{x} , \hat{y})$ The vector $G^k (\hat{x} , \hat{y})$ satisfies the equation

$$\Delta^* G^k (\hat{x} , \hat{y}) = - \delta (\hat{x} - \hat{y}) e^k \qquad (3.1)$$

where $\delta (x - y)$ is Dirac Delta function concentrated at the point $\hat{y}$. On differentiation with respect to $\hat{X}$ the components G_j^k are given by

$$G_j^k (\hat{x},\hat{y}) = \frac{1}{8\pi\mu(\lambda+2\mu)} \left\{ (\lambda+3\mu) \frac{\delta_{kj}}{\rho(\hat{x},\hat{y})} + (\lambda+\mu) \frac{(x_k-y_k)(x_j-y_j)}{\rho^3(\hat{x},\hat{y})} \right\} \qquad (3.2)$$

where $\rho(\hat{x},\hat{y}) = \left\{ (x_1-y_1)^2 + (x_2-y_2)^2 + (x_3-y_3)^2 \right\} \qquad (3.3)$

and δkj is Kronecker delta.

Let the solution of homogeneous elastostatics equation (f_i=0) is given by displacement field u . Taking G(y) equal to $G^k(x,y)$ from (2.4) following Kudpradze [15] we get,

$$d(x) u_k(\hat{Y}) = \int_{d\Omega} \left[G^k (\hat{x},\hat{y}) \cdot \left\{ P^{n(y)} \hat{u}(y) \right\} - \hat{u}(y) \cdot \left\{ P^{n(y)} G^k (x,y) \right\} \right] dS_y \qquad (3.4)$$

where

$$d(\hat{x}) = \begin{cases} 1 , & x \in \Omega \\ \frac{1}{2} , & x \in d\Omega \\ 0 , & x \in \Omega' \text{ exterior to } \Omega . \end{cases} \qquad (3.5)$$

This fundamental relation (3.4) when $\alpha = \mu$ and $\beta = \lambda$ gives the basic relation of the boundary integral equation method (Cruse [18]).

Here the term $P^{n(y)} G^k(x , y)$ is singular for points $\hat{X}$ on $d\Omega$. This singularity is due to normal derivative of ρ^{-1}. Therefore for $d = \frac{1}{2}$ the integral (2.4) is to be understood in the sense of principal value.

Kudpradze-Bashelishvili [15] tensor is defined by

$$\Gamma_j^k (\hat{x},\hat{y},\hat{n}(\hat{y})) = 2 P^{n(y)} G^j (x,y) e^k \qquad (j,k = 1,2,3) \qquad (3.6)$$

constants α , β are chosen in such a way that Γ_j^K is proportional to normal derivative of ρ^{-1}. The value of α , β in this case are given by (2.6). Hence the components of tensor Γ_j^K are given by

$$\Gamma_j^K(\hat{x},\hat{y},\hat{n}(\hat{y})) = \frac{1}{2\pi}\frac{1}{(\lambda+3\mu)}\left\{2\mu\delta_{jK}+3(\lambda+\mu)(x_j-y_j)(x_K-y_K)\rho^{-2}\right\}\frac{\partial}{\partial n_y}(1/\rho) \quad (3.7)$$

Consider the plane P, normal to $\hat{n}(y)$ and containing the point y . Then the vector $\Gamma^K(\hat{x},y,\hat{n}(y))$ satisfies the homogeneous elastostatics equation outside the plane P. It can be shown that

$$\Gamma^K(\hat{x}^{\pm},\hat{y},\hat{n}(y)) = \pm\,\delta_p(\hat{x}-\hat{y})\,e^K \quad (3.8)$$

where $\delta_p(X-Y)$ is two-dimensional Dirac delta function on P concentrated at the point Y, with sign + or - according as the point X belongs to the positive or negative side of the plane P. The property of (3.8) will be used to describe the jump in the displacement field across the crack.

4- Single layer and double layer potential.

For any continuous vector density $\psi_k(s)$ the single layer potential is defined as

$$S_i(x) = 2\int_{d\Omega} G_i^K(\hat{x},z)\,\psi_K(z)\,dS_z \ , \quad (4.1)$$

satisfies the homogeneous elastostatic equation in Ω or Ω'. It is continuous across the surface $d\Omega$. Applying operator $T^{n(x)}$ to both sides of (4.1) and taking limit within Ω or Ω' when $\hat{X}\to\hat{Y}^-$ or $\hat{X}\to\hat{Y}^+$ the normal $\hat{n}(x)$ tending to the outward normal to Ω at the point $\hat{Y}$, we get

$$T^{\hat{n}(\hat{y})}S(Y\mp) = \mp\psi(Y) + 2\int_{d\Omega}^{(P)} T^{n(\hat{y})}G^K(\hat{Y},z)\,\psi_K(z)\,dS_z \quad (4.2)$$

Here (P) before the integral sign means integral is understood as a principal value. The stress vector is continuous at any point where the density vanishes. It may be noted that, if density is continuous it is continuous throughout.

In double layer potentials we need kernal depending on normal derivative of $1/\rho$. Kossecka [16] made use of T^n and defined

$$H_k(\hat{x}) = \int_{d\Omega}\Phi(z)\,T^{n(z)}G^K(\hat{x},z)\,dS_z \ . \quad (4.3)$$

We made use of the operator P to Kelvin-Somaglina tensor with values α,β given by (2.6) and introduce the potential

$$W_i(\hat{x}) = \int_{d\Omega}\Gamma_i^K(\hat{x},z,\hat{n}(z))\,\phi_K(z)\,dS_z \ . \quad (4.4)$$

Denoting by y^+ and y^- the point on $d\Omega^+$ and $d\Omega^-$ which have same co-ordinates as $\hat{y}$, we get

$$W_i(y^+) - W_i(y^-) = 2\,\phi_i(\hat{y}) \ . \quad (4.5)$$

and

$$W_i(y^-) = -\phi_i(y) + \int_{d\Omega}^{(P)}\Gamma_i^K(y,z,n(z))\,\phi_K(z)\,dS_z \quad (4.6)$$

When $d\Omega$ is a plane, the equation (4.6) takes a very simple form. The principal value of integral in (4.6) takes a very simple case and density $\phi_i(y)$ is simply equal to the displacement on the upper face P^+ , while $-\phi_i(y)$ is the displacement on the lower face P^- . The stress vector at any point X within Ω is easily calculated by appropriate differentiation of (4.4) using

the operator (2.5) . Because of strong singularity in the kernal there is some difficulty in deriving the stress vector in P^- .

5- Equation for the crack opening discontinuities

Let S be a plane crack in an infinite elastic body. The crack is subjected to equal and opposite tractions $\pm T_i$ on its faces. Let x - axis be normal to the plane of the crack. Equation (2.5) suggests that the density is interpreted as the half crack displacement discontinuity. $\phi_i = 0$ outside crack edge and at surface. The displacement field in infinite body is expressed in term of two elastic potentials :

$$U_i(Y) = W_i(Y) + S_i(Y) \tag{5.1}$$

The stress field generated by (5.1) vanishes at infity. The densities ϕ_i and ψ_i are now chosen in such a way that the boundary conditions are satisfied on crack faces. Since three conditions have to be satisfied we have three arbitrary choices for the densities.

In order to derive these conditions, one could determine components of potentials W_i and S_i on P^- . The stress components of the single layer are given by (4.2) :

$$\left.\begin{aligned}
\sigma_{\alpha 3}(Y) &= \psi_\alpha(Y) + \frac{\mu}{2\pi(\lambda+2\mu)} \int_S^{(P)} \psi_3(Z) \frac{\partial}{\partial y_\alpha}\left(\frac{1}{\rho(Y,Z)}\right) dS_Z \,, (\alpha = 1,2) \\
\sigma_{33}(Y) &= \psi_3(Y) - \frac{\mu}{2\pi(\lambda+2\mu)} \int_S^{(P)} \psi_\beta(Z) \frac{\partial}{\partial y_\beta}\left(\frac{1}{\rho(Y,Z)}\right) dS_Z \,, (\beta = 1,2)
\end{aligned}\right\} \tag{5.2}$$

The stress components on P^- of the double-layer potentials are given by

$$\left.\begin{aligned}
\sigma_{\alpha 3}(Y) &= \frac{\mu}{2\pi} \int_S^{(P)} \frac{\partial}{\partial y_\beta}\left(\frac{1}{\rho(Y,Z)}\right) \frac{\partial \phi_\alpha}{\partial z_\beta} dS_Z - \frac{2\mu^2}{\lambda+3\mu} \frac{\partial \phi_3}{\partial y_\alpha} \\
&\quad + \frac{\mu(\lambda+\mu)}{2\pi(\lambda+3\mu)} \int_S^{(P)} \left(\frac{\partial \phi_1}{\partial z_1} + \frac{\partial \phi_2}{\partial z_2}\right) \frac{\partial}{\partial y_\alpha}(1/\rho)\, dS_Z \,. \\
\sigma_{33}(Y) &= \frac{2\mu^2}{\lambda+3\mu}\left(\frac{\partial \phi_1}{\partial y_1} + \frac{\partial \phi_2}{\partial y_2}\right) + \frac{\mu(\lambda+2\mu)}{\pi(\lambda+3\mu)} \int_S^{(P)} \frac{\partial \phi_3}{\partial z_\alpha} \frac{\partial}{\partial y_\alpha}(1/\rho)\, dS_Z \,.
\end{aligned}\right\} \tag{5.3}$$

We take densities ψ_i as follows :

$$\left.\begin{aligned}
\psi_\alpha(Y) &= \frac{2\mu^2}{\lambda+3\mu} \frac{\partial \phi_3}{\partial y_\alpha} \quad , (\alpha = 1,2) \\
\psi_3(Y) &= -\frac{2\mu^2}{\lambda+3\mu}\left(\frac{\partial \phi_1}{\partial y_1} + \frac{\partial \phi_2}{\partial y_2}\right)
\end{aligned}\right\} \tag{5.4}$$

From boundary conditions and taking account of (5.2), (5.3) and (5.4) we obtain the basic equations for crack opening displacement discontinuities.

$$T_1(y) = \frac{\lambda\mu}{2\pi(\lambda+2\mu)} \int_S^{(P)} \left(\frac{\partial \phi_1}{\partial z_1} + \frac{\partial \phi_2}{\partial z_2}\right) \frac{\partial}{\partial y_1}\left(\frac{1}{\rho(Y,Z)}\right) dS_Z + \frac{\mu}{2\pi} \int_S^{(P)} \frac{\partial \phi_1}{\partial z_\alpha} \frac{\partial}{\partial y_\alpha}\left(\frac{1}{\rho}\right) dS_Z \,, \tag{5.5}$$

$$T_2(y) = \frac{\lambda\mu}{2\pi(\lambda+2\mu)} \int_S^{(P)} \left(\frac{\partial \phi_1}{\partial z_1} + \frac{\partial \phi_2}{\partial z_2}\right) \frac{\partial}{\partial y_2}\left(\frac{1}{\rho(Y,z)}\right) dS_Z + \frac{\mu}{2\pi} \int_S^{(P)} \frac{\partial \phi_2}{\partial z_\alpha} \frac{\partial}{\partial y_\alpha}\left(\frac{1}{\rho}\right) dS_Z \,, \tag{5.6}$$

$$T_3(y) = \frac{\mu(\lambda+\mu)}{\pi(\lambda+2\mu)} \int_S^{(P)} \frac{\partial}{\partial y_\alpha}\left(\frac{1}{\rho(Y,Z)}\right) \frac{\partial \phi_3}{\partial z_\alpha} dS_Z \,. \tag{5.7}$$

Equation (4.7) gives crack opening made under normal pressure and agrees with the result given by Kossecka [16] . All integrals are taken over crack surface S. This has advantage for numerical analysis. It is only the crack surface that has to be divided into elements. (3.4) applied to this present problem is extended to entire plane. The stress intensity factor may be determined by studying the behaviour of the discontinuity in the displacement of the crack edge.

Let us now consider an infinite crack, extending over $-\infty < x_2 < \infty$, $-a < x_1 < a$. Assume that the load T_i and densities are independent of the variable y_2.

On integration by parts (5.5) to (5.7)

$$T_1(y_1) = \frac{2\mu(\lambda+\mu)}{\pi(\lambda+2\mu)} \int_{-a}^{a} \phi_1'(t) \frac{dt}{t-y_1} \quad , \tag{5.8a}$$

$$T_2(y_1) = \frac{\mu}{\pi} \int_{-a}^{a} \phi_2'(t) \frac{dt}{t-y_1} \quad , \tag{5.8b}$$

$$T_3(y_1) = \frac{2\mu}{\pi} \frac{(\lambda+\mu)}{(\lambda+2\mu)} \int_{-a}^{a} \phi_3'(t) \frac{dt}{t-y_1} \quad . \tag{5.8c}$$

(prime denotes differentiation).

(5.8a) and (5.8c) corresponds to a plane strain case and (5.8b) corresponds to anti-plane strain loading.

6- Stress concentration factors

Let us consider the tangent $\hat{t}$ and the outward binormal $\hat{n}$ to ds at the point $\hat{z}$ on the crack edge. Let θ be the angle between s' and $\hat{n}$.

The stress concentration factor are determined by singling out asymptotic behaviour of the stress components $\sigma_{33}(y)$, $\sigma_{3m}(y)$, $\sigma_{3t}(y)$ with respect to local co-ordinates z_m, z_t, z_n :

$$K_1(z) = \lim_{\rho \to 0} \left\{ \sigma_{33}(y)\, \rho^{1/2}(y,z)\, (2\pi)^{1/2} \right\} \quad , \tag{6.1a}$$

$$K_2(z) = \lim_{\rho \to 0} \left\{ \sigma_{3m}(y)\, \rho^{1/2}(y,z)\, (2\pi)^{1/2} \right\} \quad , \tag{6.1b}$$

$$K_3(z) = \lim_{\rho \to 0} \left\{ \sigma_{3t}(y)\, \rho^{1/2}(y,z)\, (2\pi)^{1/2} \right\} \quad , \tag{6.1c}$$

The point y belongs to the plane P, outside the crack S. The stress components σ_{33}, σ_{31}, σ_{32} with respect to the x - axis are respectively given by the left sides of (5.5), (5.6) and (5.7).

Assuming the discontinuity $\phi_i(y)$ near the point z to be given by the asymptotic expression

$$\phi_i(y) = S_i(z) \left(\frac{d}{2\pi}\right)^{1/2} \quad , \tag{6.2}$$

where d is the distance of y to the tangent zt, the point y belonging to the crack surface. Now the limit (6.1a) is given by

$$K_1(z) = \frac{\mu(\lambda+\mu)}{\lambda+2\mu} S_3(z) \quad . \tag{6.3}$$

Hence the normal discontinuity $2\phi_3$ near the crack edge has the behaviour

$$[u_3] = u_3^+ - u_3^- = 2\phi_3 = K_1(z) \frac{2(\lambda+2\mu)}{\mu(\lambda+\mu)} \left(\frac{d}{2\pi}\right)^{1/2} \tag{6.4}$$

This is a well known result in case of a plane strain. Sih and Liebowitz [17] pointed out this remarkable property by studying the local behaviour of the solution of the homogeneous boundary conditions ($T_i = 0$) on the crack. Here we derive it from integral equation (5.5). The discontinuity in u_m near the crack edge is expressed by

$$[u_m] = 2\phi_1 \cos\theta + 2\phi_2 \sin\theta = K_2(z) \frac{2(\lambda+2\mu)}{\mu(\lambda+\mu)} \left(\frac{d}{2\pi}\right)^{1/2} \tag{6.5}$$

The discontinuity in u_t is expressed as in anti-plane strain case by

$$[u_t] = -2\phi_1 \sin\theta + 2\phi_2 \cos\theta = K_3(z) \frac{2}{\mu} \left(\frac{d}{2\pi}\right)^{1/2} \tag{6.6}$$

So when density ϕ_i is known (6.4), (6.5) and (6.6) can therefore be used to get stress concentration factors.

7- Observations

Let the problem of the elastic body without the crack is solved either by finite element method or by boundary integral method. The stress vector T_i on the area occupied by the crack is then known. Consider now the second problem for the same body subject to the traction $- T_i$ on crack surface S^- and $+ T_2$ on S^+ and the nullified boundary conditions elsewhere. This problem has been studied here where we approximate the body as an infinite elastic body. The stress concentration factor for the first problem are the same as those for the second.

The problem of crack opening under remote traction at infinity, for an infinite body may be solved in the same way.

Question arises whether this analysis for isotropic body can be extended for anistropic materials. Theoretically this can be done. This is based on Green's tensor in anistropic case, taken as the kernal of the single layer elastic potential, while the double layer potential can be obtained by mapping the physical stress operator on the tensor G. The use of this potential has been suggested by Kosecca [16] in her theory of defects of crystals. But since tensor G is known only indirectly from its Fourier Transform it is not easy to derive explicit equations for the crack problem in a form simple enough for practical use.

REFERENCES

1 C.E. Inglish, Stresses in a plate due to the presence of cracks and sharp corners, Trans.Inst. Nav. Arch. (Lond), 55 219-230 (1913).

2 G.I. Barenblatt, On the equilibrium cracks in flat plates, Prikld. mat. mech. 23 , 706-721 (in Russian) (1959).

3 I.N. Sneddon, Fourier Transforms (Mc-Graw Hill), (1951).

4 J.L. Sanders, Journal of Applied Mechanics 33 , 561 - 570 (1966).

5 A.E. Green and I.N. Sneddon, Cambridge Phil. Soc. 46 , 159 - 168 (1950).

6 S.M. Sharfuddin, Journ. Engg. Math 2 , No.4, 403 - 415 (1968).

7 S.M. Sharfuddin, ZAMM 55 , 731 - 737 (1975).

8 S.M. Sharfuddin, Journ. Engg. Math. 9 , No.3 , 177 - 187 (1975).

9 W.T. Koiter, An Infinite Row of Collinear Cracks in an Infinite Elastic Sheet, Ingenieur Arch, 28 , 168 - 172 (1959).

10 H.M. Westergaard, Bearing pressures and cracks, J. Appl. Mech 6 , No.2A 45 - 53 (1939).

11 N.I. Muskhelishvili, Some basic problems of mathematical theory of elasticity, English Edition, Groningen, Netherlands, P. Noordhoff Ltd. (1963).

12 N.I. Muskhelishvili, Singular integral equations, English Editions, Groningen, Netherlands, P. Noordhoff Ltd. (1963).

13 A.H. Cotrell, Fracture (The Bakerian Lecture, 1963), Proc. Roy. Soc (London) A 276 1-8 (1963).

14 I.N. Sneddon, Mixed Boundary Value Problems in Potential Theory, North Holland Publishing Co. Amsterdam. (1966).

15 V.D. Kudpradze, Progress in Solid Mechanics, (Edited by I.N. Sneddon and R. Hill) Vol. III Dynamical Problems in Elasticity, North Holland, Amsterdam (1963).

16 E. Kossecka, Theory of Defects in Crystals, Arch. Mech. 23 , 481-503 (1971).

17 G.C. Sih and H. Liebowitz, Fracture, An Advanced Treatise (Edited by H. Liebowitz) Vol. II (Mathematical Fundamentals) Academic Press New York, 67 - 190 (1968).

18 T.A. Cruse, Int. J. Solid Structure 5 , 1259 - 1272 (1969).

19 H.F. Bueckner, Mechanics of Fracture (Edited by G.C. Sih) Vol.I. Methods of Analysis and Solution of Crack Problems, Noordhoff Lynden 239 - 314 (1973).

20 I.N. Sneddon and M. Lowengrub, Crack Problems in Mathematical Theory of Elasticity, John Willey and Sons, New York (1969).

ACKNOWLEDGEMENT

This work is undertaken during author's stay as a visiting Professor in the Department of Mathematics, Al-Mustansiriyah.University, Baghdad, Iraq. A part of it was produced in a joint seminar of mathematicians of Universities of Baghdad and of Al-Mustansiriyah. Author expresses his deep gratitude to Dr. Sabri Radeef Al Daoud, Dean of College of Science and to Dr. Harith Gaylani Chairman, Department of Mathematics Al-Mustansiriyah University for all the facilities made available.

A WEAK INTERACTION MODEL FOR BARYONS AND MESONS

A. K. Bassiouny* and B. M. Al-Shalchy*

A B S T R A C T

A method of introducing weak interactions of baryons with leptons in the strong interaction Lagrangian for baryon fields coupled to meson fields is given. The weak currents of baryons are deduced depending on their strong coupling constants with mesons and the weak coupling constants of mesons with leptons.

I N T R O D U C T I O N

The PCAC hypothese has been suggested in order to prove the Goldberger-Treiman relation. It is assumed that the divergence of the axial vector current has the form:

$$\partial_\mu A^\mu = m_\pi^2 f_\pi \Pi \qquad (1)$$

where Π is the field operator of Π^+ mesons, and f_π is the coupling constant between mesons and leptons.

Some models yielding axial vector currents, which satisfy the PCAC hypothese, are constructed by many authors [1,2]. However, the nature of the axial vector current in these models is not clear. Here we construct a model based on the addition of weak interactions of mesons with leptons to the free field equations of mesons, which for Pions have the form:

* Department of Physics, College of Science, Al-Mustansiriyah University, Baghdad, Iraq.

Al-Mustansiriyah Journal of Science, Vol. 3 (1978).

$$\partial^\mu \Pi_{\mu 5} = m_\pi \Pi \qquad (2)$$

$$\partial_\mu \Pi = -m_\pi \Pi_{\mu 5} \qquad (3)$$

The analogue between equation (2) and the PCAC hypothese shows that there should be a close correspondence between $\Pi_{\mu 5}$ and the axial vector current A_μ. The relation between $\Pi_{\mu 5}$ and A_μ is discussed. Consequently, we dudce the ratio of the coupling constants of K and Π mesons with leptons, namely:

$$\frac{g_k}{g_\pi} = \frac{m_\pi}{m_k}$$

Furthermore, we give a rule to include weak interactions of baryons with leptons in the strong interaction Lagrangian, and hence derive the corresponding weak currents.

FIELD EQUATIONS OF FREE MESONS

The field equations of free mesons $M^{lm}_{\alpha\beta}$, coveriant under SU(3) x L_4 can be written in the form [3] :

$$\tfrac{1}{2}\left\{(\gamma P)_{\alpha\alpha'} M^{lm}_{\alpha'\beta} - (\gamma P)_{\beta\beta'} M^{lm}_{\alpha\beta'}\right\} = \mu M^{lm}_{\alpha\beta} \qquad (4)$$

where $\alpha, \beta = 0, 1, 2, 3$ and $l, m = 1, 2, 3$ and $\gamma P = i\gamma^\mu \partial\mu$

Using the completeness of Dirac algebra, $M^{lm}_{\alpha\beta}$ can be expressed in the form [4] ,

$$M^{lm}_{\alpha\beta} = \left\{\Phi^{lm}_o + i\gamma_5 \Phi^{lm}_5 + \gamma^\mu \gamma_5 \Phi^{lm}_{\mu 5} + \gamma^\mu \Phi^{lm}_\mu + \tfrac{1}{2}\sigma^{\mu\nu}\Phi^{lm}_{\mu\nu}\right\}\alpha\beta \qquad (5)$$

Where $\gamma^\circ = \gamma^{\circ +}$, $\underline{\gamma} = -\underline{\gamma}^+$ and $\gamma_5 = \gamma_5^+$

Substituting (5) in (4), we obtain:

$$\partial^\mu \Phi^{lm}_{\mu 5} = \mu \Phi^{lm}_5 \quad ; \quad \partial_\mu \Phi^{lm}_5 = -\mu \Phi^{lm}_{\mu 5} \qquad (6)$$

$$\partial^{\nu}\Phi^{lm}_{\mu\nu} = \mu\Phi^{lm}_{\mu} \quad ; \quad \mu\Phi^{lm}_{\mu\nu} = \partial_{\mu}\Phi^{lm}_{\nu} - \partial_{\nu}\Phi^{lm}_{\mu} \tag{7}$$

Equations (6) are the free field equations of the pseudoscalar mesons, which are classified by:

$$\Phi^{lm}_{5} = \begin{bmatrix} \frac{\eta}{\sqrt{6}} + \frac{\pi^{\circ}}{\sqrt{2}} & \pi^{+} & K^{+} \\ \pi^{-} & \frac{\eta}{\sqrt{6}} - \frac{\pi^{\circ}}{\sqrt{2}} & K^{\circ} \\ K^{-} & \bar{K}^{\circ} & \frac{-2\eta}{\sqrt{6}} \end{bmatrix} \tag{8}$$

Equations (7) are the free field equations of vector mesons, which are classified by:

$$\Phi^{lm}_{\mu} = \begin{bmatrix} \frac{\omega + \rho^{\circ}}{\sqrt{2}} & \rho^{+} & K^{*+} \\ \rho^{-} & \frac{\omega - \rho^{\circ}}{\sqrt{2}} & K^{*\circ} \\ K^{*-} & \bar{K}^{*\circ} & \Phi \end{bmatrix} \tag{9}$$

After switching on the strong interactions, SU (3) symmetry is broken, leading to the mass splitting of mesons. As we shall restrict outselves to weak interactions, we shall consider the masses in the free field equations to be the physical masses of

DECAY OF $\pi^{\pm}$ MESONS INTO LEPTONS

If weak interactions are added to the free Lagrangian for pions, then the Lagrangian can be written in the form:

$$L = (\partial_{\mu}\pi^{+}\partial^{\mu}\pi^{-} - m_{\pi}^{2}\pi^{+}\pi^{-}) + \tfrac{1}{2}(\partial_{\mu}\pi^{\circ}\partial^{\mu}\pi^{\circ} - m_{\pi}^{2}\pi^{\circ 2}) - \frac{g_{\pi}m_{\pi}}{\mu}\left\{\bar{\psi}^{i}\gamma_{\mu}(1+\gamma_{5})\tau_{-}\psi^{i}\partial^{\mu}\pi^{+} + \bar{\psi}^{i}\gamma_{\mu}(1+\gamma_{5})\tau_{+}\psi^{i}\partial_{\mu}\pi^{-}\right\} \tag{10}$$

where $\psi^{1} = \begin{pmatrix} e \\ \nu_{e} \end{pmatrix}$; $\psi^{2} = \begin{pmatrix} \mu \\ \nu_{\mu} \end{pmatrix}$; $\tau_{+} = \begin{bmatrix} 0 & 1 \\ 0 & 0 \end{bmatrix}$, $\tau_{-} = \begin{bmatrix} 0 & 0 \\ 1 & 0 \end{bmatrix}$

g_{π} is the coupling constant, μ is a parameter having the dimension of mass, which can be taken as a mean mass of mesons in the octet. $g_{\pi}m_{\pi}$ is dimensionless.

The assumption that the Lagrangian (10) is inveriant under the guage transformations

$$\pi^{+} \to \pi^{+} + a\Lambda(x) \quad ; \quad \pi^{-} \to \pi^{-} + a\Lambda^{*}(x) \tag{11}$$

yields the current

$$J_{\pi\mu} = \frac{\delta L}{\delta \Lambda^{i\mu}} = a\partial_{\mu}\pi^{-} - a\frac{g_{\pi}m_{\pi}}{\mu}\bar{\psi}^{i}\gamma_{\mu}(1+\gamma_{5})\tau_{-}\psi^{i} \tag{12}$$

where $\partial^{\mu}J_{\pi\mu} = \frac{\delta L}{\delta \Lambda} = -m_{\pi}^{2}a\pi^{-}$

Taking $a = -f_{\pi}$, where $g_{\pi} = f_{\pi}G^{v}_{\beta}$, then the PCAC hypothese is fulfilled. Actually, the current $J_{\pi\mu}$ is not an axial vector, but the vector term in $J_{\pi\mu}$ is divergenceless. Lagrangian (10) yields the fields equation:

$$(\Box + m_{\pi}^{2})\pi^{-} = \frac{g_{\pi}m_{\pi}}{\mu}\partial_{\mu}\bar{\psi}^{i}\partial^{\mu}(1+\gamma_{5})\tau_{-}\psi \tag{13}$$

which can be written in the form:

$$\partial^{\mu}\tilde{\pi}^{-}_{\mu 5} = m_{\pi}\pi^{-} \tag{14}$$

$$\text{where } -m_{\pi}\tilde{\pi}^{-}_{\mu 5} = \partial_{\mu}\pi^{-} - \frac{g_{\pi}m_{\pi}}{\mu}\bar{\psi}^{i}\gamma_{\mu}(1+\gamma_{5})\tau_{-}\psi^{i} \tag{15}$$

The comparison of equations (12) and (13) gives:

$$\tilde{\pi}^{-}_{\mu 5} = \frac{1}{m_{\pi}f_{\pi}}J_{\pi\mu} \tag{16}$$

DECAY OF $K^{\pm}$ MESONS INTO LEPTONS

The Lagrangian for $K^{\pm}$ mesons can be similarly written in the form: $-= \partial_\mu K^+ \partial^\mu K^- - m_k^2 K^+ K^- - \frac{g_\pi m_\pi}{\mu}\left\{\bar{\psi}^i \gamma_\mu (1+\gamma_5)\tau \psi^i \gamma_\mu K^+ + \bar{\psi}^i \gamma_\mu (1+\gamma_5)\tau_+ \psi^i \gamma_\mu K^-\right\}$

The inveriance under the guage transformations

$K^+ \to K^+ - f_k \Lambda \quad ; \quad K^- \to K^- - f_k \Lambda^*$

Gives the current:

$J_{k\mu} = -f_k\left\{\partial_\mu K^- - g_k \bar{\psi}^i \gamma_\mu (1+\gamma_5)\tau \psi^i\right\}$

where $\partial^\mu J_{k\mu} = m_k^2 f_k K^- \quad ; \quad g_k = f_k G_\beta^V$

The field equations are:

$$-m_k \tilde{K}^-_{\mu 5} = \partial_\mu K^- - \frac{g_k m_k}{\mu} \bar{\psi}^i \gamma_\mu (1+\gamma_5)\tau \psi^i \qquad (17)$$

$$\partial^\mu \tilde{K}^-_{\mu 5} = m_k K^- \qquad (18)$$

Therefore $\tilde{K}^-_{\mu 5} = \frac{1}{m_k f_k} J_{k\mu} \qquad (19)$

RELATION BETWEEN THE COUPLING CONSTANTS g_π, g_k

The total current of charged mesons in the octet is determined by :

$$J_\mu = J_{\pi\mu} + J_{k\mu}$$

where $\partial^\mu J_\mu = m_\pi^2 f_\pi \pi^- + m_k^2 f_k K^-$

Correspondingly, we can define the field operator $\Phi_{\mu 5}$ by the relation:

$$\Phi_{\mu 5} = \tilde{\pi}^-_{\mu 5} + \tilde{K}^-_{\mu 5}$$

Therefore $\partial^\mu \Phi_{\mu 5} = m_\pi \pi^- + m_k K^-$

It is obvious that one can interprete $\tilde{\pi}_{\mu 5}$, $\tilde{K}_{\mu 5}$ as the currents, if the total current J_μ is also proportional to $\Phi_{\mu 5}$ Letting $\Phi_{\mu 5} = \alpha J_\mu$ where α has the dimension of $1/m^2$ we obtain :

$$\frac{f_k}{f_\pi} = \frac{g_k}{g_\pi} = \frac{m_\pi}{m_k} \qquad (20)$$

DECAY OF VECTOR MESONS INTO LEPTIONS

The Lagrangian for $\rho^{\pm}$ mesons interacting with leptons is

$L = \partial_\mu \rho_\nu^+ \partial^\mu \rho^{-\nu} - m_\rho^2 \rho_\mu^+ \rho^{-\mu} - g_\rho\left\{\bar{\psi}^i \gamma_\mu (1+\gamma_5)\tau \psi^i \rho^{+\mu} + \bar{\psi}^i \gamma_\mu (1+\gamma_5)\tau_+ \psi^i \rho^{-\mu}\right\}$

The guage transformations

$\rho_\mu^+ \to \rho_\mu^+ + C\Lambda_{,\mu} \quad (2) \qquad , \quad \Lambda_{,\mu} = \frac{\partial \Lambda}{\partial x^\mu}$

yield the current

$$J_{\rho\mu} = -m_\rho^2 C \rho_\mu^- - C g_\rho \bar{\psi}^i \gamma_\mu (1+\gamma_5)\tau \psi^i \qquad (21)$$

which is divergenceless, since $\partial^\mu J_{\rho\mu} = \frac{\delta L}{\delta \Lambda} \qquad (22)$

The field equation is given by :

$(\Box + m_\rho^2)\rho_m^- = -g_\rho \bar{\psi}^i \gamma_\mu (1+\gamma_5)\tau \psi^i$

Denoting $m_\rho \rho_{\mu\nu}^- = \partial_\mu \rho_\nu^- - \partial_\nu \rho_\mu^-$ therefore

$\partial^\nu \rho_{\mu\nu}^- = m_\rho \tilde{\rho}_\mu^-$ where

$$\tilde{\rho}_\mu^- = \rho_\mu^- + g_\rho / m_\rho^2 \, \bar{\Psi}^i \gamma_\mu (1+\gamma_5) \tau^- \Psi^i = \frac{-1}{m_\rho^2 C} J_{\rho\mu} \qquad (23)$$

Similar to the ρ^- mesons, the equations of K^{*-} mesons can be written in the form :

$$\begin{aligned} m_{K^*} K^{*-}_{\mu\nu} &= \partial_\mu K^{*-}_\nu - \partial_\nu K^{*-}_\mu \\ \partial^\nu K^{*-}_\nu &= m_{K^*} \tilde{K}^{*-} \\ \tilde{K}^{*-}_\mu &= K^{*-}_\mu + \frac{g_{K^*}}{m^2_{K^*}} \bar{\Psi}^i \gamma_\mu (1+\gamma_5) \tau^- \Psi^i \end{aligned} \qquad (24)$$

β - DECAY OF BARYONS

The above analysis shows that one can introduce weak interactions of baryons with leptons in the strong interaction Lagrangian L_s, if we make the following replacements :

$$\begin{aligned} \pi^\pm_{\mu 5} \to \tilde{\pi}^\pm_{\mu 5} &= \frac{1}{m_\pi} \left\{ \partial_\mu \pi^\pm - \frac{g_\pi m_\pi}{\mu} \bar{\Psi}^i \gamma_\mu (1+\gamma_5) \tau_\pm \Psi^i \right\} \\ K^\pm_{\mu 5} \to \tilde{K}^\pm_{\mu 5} &= \frac{1}{m_K} \left\{ \partial_\mu K^\pm - \frac{g_K m_K}{\mu} \bar{\Psi}^i \gamma_\mu (1+\gamma_5) \tau_\pm \Psi^i \right\} \\ \rho^\pm_\mu \to \tilde{\rho}^\pm_\mu &= \rho^\pm_\mu + \frac{g_\rho}{m_\rho} \bar{\Psi}^i \gamma_\mu (1+\gamma_5) \tau_\pm \Psi^i \\ K^{*\pm}_\mu \to \tilde{K}^{*\pm}_\mu &= K^{*\pm}_\mu + g_{K^*} / m^2_{K^*} \bar{\Psi}^i \gamma_\mu (1+\gamma_5) \tau_\pm \Psi^i \end{aligned} \qquad (25)$$

The Lagrangian L_s, which is inveriant under the group SU (3) x L_4, is given by [5] ;

$$\begin{aligned} L_s = g N^{-lmn}_\alpha \Big\{ & 3 M^{nn'}_{\alpha\beta} N^{lmn'}_\beta + M^{ll'}_{\alpha\beta} N^{nlm}_\beta + M^{mm'}_{\alpha\beta} N^{m'nl}_\beta - M^{ll'}_{\alpha\beta} N^{mnl}_\beta \\ & - M^{mm'}_{\alpha\beta} N^{nlm'}_\beta + 2 \Phi^{ll'}_\mu \gamma^\mu_{\alpha\beta} N^{l'mn}_\beta + 2 \Phi^{mm'}_\mu \gamma^\mu_{\alpha\beta} N^{lm'n}_\beta \\ & - 2 \Phi^{ll'}_\mu \gamma^\mu_{\alpha\beta} N^{nl'm}_\beta - 2 \Phi^{mm'}_\mu \gamma^\mu_{\alpha\beta} N^{m'nl}_\beta \Big\} \end{aligned} \qquad (26)$$

where the baryons are classified by ;

$$N^{121} = P, \; N^{122} = n, \; N^{123} = -\frac{2}{\sqrt{6}} \Lambda, \; N^{311} = \Sigma^+, \; N^{232} = \Sigma^-$$
$$N^{312} = -\frac{\Sigma^\circ}{\sqrt{2}} + \frac{\Lambda}{\sqrt{6}}, \; N^{221} = \frac{\Sigma^\circ}{\sqrt{2}} + \frac{\Lambda}{\sqrt{6}}, \; N^{313} = \Xi^\circ, \; N^{233} = \Xi^- \qquad (27)$$

N^{lmn}_α satisfy the relations $N^{lmn}_\alpha = -N^{mln}_\alpha$

$$N^{lmn}_\alpha + N^{mnl}_\alpha + N^{nlm}_\alpha = 0$$

M has the decomposition

$$M^{lm}_{\alpha\beta} = Z_1 (i\gamma_5 \Phi^{lm}_5 + \gamma^\mu \gamma_5 \Phi^{lm}_{\mu 5}) + Z_2 (\gamma^\mu \Phi^{lm}_\mu + \tfrac{1}{2} \sigma^{\mu\nu} \Phi^{lm}_{\mu\nu}) \alpha\beta \qquad (28)$$

where mesons are classified by (8), (9), and Z_1, Z_2 are normalisation constants. Using (26), (27) and (28) ;

The strong Lagrangian including only charged mesons is given by ;

$$\begin{aligned} L_S = f_{N\pi N} \Big\{ & \sqrt{2}\, \bar{P} (i\gamma_5 \pi^- + \gamma^\mu \gamma_5 \pi^-_{\mu 5}) n + \tfrac{1}{5} \bar{P} (i\gamma_5 K^+ + \gamma^\mu \gamma_5 K^+_{\mu 5}) \Sigma^\circ \\ & - \frac{3\sqrt{3}}{5} \bar{P} (i\gamma_5 K^+ + \gamma^\mu \gamma_5 K^+_{\mu 5}) \Lambda + \frac{\sqrt{3}}{5} \bar{n} (i\gamma_5 K^+ + \gamma^\mu \gamma_5 K^+_{\mu 5}) \Sigma^- \\ & + \frac{\sqrt{2}}{5} \Xi^- (i\gamma_5 \pi^- + \gamma^\mu \gamma_5 \pi^-_{\mu 5}) \Xi^\circ + \sqrt{2}\, \bar{\Xi} (i\gamma_5 K^- + \gamma^\mu \gamma_5 K^-_{\mu 5}) \Sigma^\circ \\ & + \frac{\sqrt{3}}{5} \bar{\Xi}^- (i\gamma_5 K^- + \gamma^\mu \gamma_5 K^-_{\mu 5}) \Lambda + \sqrt{2}\, \bar{\Xi}^\circ (i\gamma_5 K^- + \gamma^\mu \gamma_5 K^-_{\mu 5}) \Sigma^+ \\ & - \frac{4}{5} \bar{\Sigma}^+ (i\gamma_5 \pi^+ + \gamma^\mu \gamma_5 \pi^+_{\mu 5}) \Sigma^\circ + \frac{2\sqrt{3}}{5} \bar{\Sigma}^+ (i\gamma_5 \pi^+ + \gamma^\mu \gamma_5 \pi^+_{\mu 5}) \Lambda \\ & + \frac{4}{5} \bar{\Sigma}^- (i\gamma_5 \pi^- + \gamma^\mu \gamma_5 \pi^-_{\mu 5}) \Sigma^\circ + \frac{2\sqrt{3}}{5} \bar{\Sigma}^- (i\gamma_5 \pi^- + \gamma^\mu \gamma_5 \pi^-_{\mu 5}) \Lambda \Big\} \\ & + f_{N\rho N} \Big\{ \sqrt{2}\, \bar{P} \gamma^\mu \rho^+_\mu n - \bar{P} \gamma^\mu K^{*+}_\mu \Sigma^\circ - \sqrt{3}\, \bar{P} \gamma^\mu K^{*+}_\mu \Lambda - \sqrt{2}\, \bar{n} \gamma^\mu K^{*+}_\mu \Sigma^- \\ & - \sqrt{2}\, \bar{\Xi}^- \gamma^\mu \rho^-_\mu \Xi^\circ + \sqrt{3}\, \bar{\Xi}^- \gamma^\mu K^{*-}_\mu \Lambda + \sqrt{2}\, \bar{\Xi}^- \gamma^\mu K^{*-}_\mu \Sigma^\circ + \sqrt{2}\, \bar{\Xi}^\circ \gamma^\mu K^{*-}_\mu \Sigma^+ \\ & - 2 \bar{\Sigma}^+ \gamma^\mu \rho^+_\mu \Sigma^\circ + 2 \bar{\Sigma}^- \gamma^\mu \rho^-_\mu \Sigma^\circ \Big\} + \text{herm. conj.} \end{aligned}$$

where $f_{N\pi N} = 10\, g\, z_1$, is the coupling constant of nucleons with π mesons, and $f_{N\rho N} = 6\, g\, z_2$ is the coupling constant

Making the replacements (25) in L , we get the Lagrangian

$$L = L_s + L_w$$

where L_w can be written in the form :

$$L_w = \frac{G}{\sqrt{2}} \left(J_\mu J^+_{l\mu} + J^+_\mu J_{l\mu} \right)$$

$J_{l\mu} = \bar{\psi}^i \gamma_\mu (1+\gamma_5) \tau \psi^i$ in the lepton current, and J is the baryon current.

In the following table we give the resulting baryon currents corresponding to the possible decay processes.

Process	$G J_\mu$
$n \to P + \bar{\nu} + e$	$\bar{n}\gamma_\mu (G^V_\beta + G^A_\beta \gamma_5) P$
$\Sigma^- \to n + \bar{\nu} + e$	$\bar{\Sigma}^- \gamma_\mu (-G'_V + \frac{1}{5} G'_A \gamma_5) n$
$\Sigma^- \to \Sigma^+ + \bar{\nu} + e$	$\sqrt{2}\,\bar{\Sigma}^- \gamma_\mu (G^V_\beta + \frac{2}{5} G^A_\beta \gamma_5) \Sigma^\circ$
$\Xi^- \to \Xi^\circ + \bar{\nu} + e$	$\bar{\Xi}^- \gamma_\mu (-G^V_\beta + \frac{1}{5} G^A_\beta \gamma_5) \Xi^\circ$
$\Xi^- \to \Lambda + \bar{\nu} + e$	$\bar{\Xi}^- \gamma_\mu (\sqrt{\frac{3}{2}} G'_V + \frac{1}{5}\sqrt{\frac{3}{2}} G'_A \gamma_5) \Lambda$
$\Xi^\circ \to \Sigma^+ + \bar{\nu} + e$	$\bar{\Xi}^\circ \gamma_\mu (G'_V + G'_A \gamma_5) \Sigma^+$
$\Lambda \to \Sigma^+ + \bar{\nu} + e$	$\sqrt{\frac{6}{5}}\, G^A_\beta \bar{\Lambda} \gamma_\mu \gamma_5 \Sigma^+$
$\Lambda \to P + \bar{\nu} + e$	$-\bar{\Lambda} \gamma_\mu (\sqrt{\frac{3}{2}} + \frac{3}{5}\sqrt{\frac{3}{2}} \gamma_5) P$

where $G^V_\beta = \frac{2 f_{\pi_N} g_\rho}{m_\rho^2}$; $G^A_\beta = \frac{2 f_{N\pi N} g_\pi}{\mu}$

$G'_V = \frac{2 f_{\pi_N} g_{K^*}}{m^2_{K^*}}$; $G'_A = \frac{2 f_{N\pi N} g_K}{\mu}$

As $g_\pi = f_\pi G^V_\beta$, and $f_{N\pi N} = \frac{m_\pi}{2M_p} g_{N\pi N}$

therefore $\frac{G^A_\beta}{G^V_\beta} = -\frac{m_\pi f_\pi g_{N\pi N}}{\mu M_p}$

If we take $\mu = m_\pi$, then $G^A_\beta / G^V_\beta = f_\pi g_{N\pi N} / M_p$ which is the Goldberger-Treiman relation.

We notice that the obtained baryon currents are expressed in terms of the strong coupling constants $g_{N\pi N}$, $g_{N\rho N}$ of nucleons with mesons and weak coupling constants of mesong with leptons [6] . These currents can be also expressed in terms of Cabbibo's angle and the ratio G^A_β / G^V_β [7].

Denoting $\frac{g_K}{g_\pi} = \frac{m_\pi}{m_K} = \tan\theta$, $G^V_\beta = G_V \cos\theta$, $G^A_\beta / G^V_\beta = X$ then

$G^A_\beta = G_V X \cos\theta$, $G'_A = 2 f_{N\pi N} g_K / \mu = G_V X \sin\theta$

Assuming that $G^{V_2}_\beta + G'^2_V = G_V^2$, therefore $G'_V = G^V_\beta \sin\theta$

Our results are then expressed in terms of the two parameters x, θ The currents obtained in this form agree with the results based on Cabbibo's theory for an F/D of 3/2.

REFERENCES

1) Schwinger, J. Phys. Letters 24 B, 473. (1967).

2) M. Gell-Mann, M. Levy, Nuovo Cimento 16, 705, (1960).

3) B. Bergman Wigner Proc. Nat. Acad. Sci. 34, 211, (1948).

4) A. Salam, Proc. Roy. Soc., 284, 145, (1965).

5) A. K. Bassiouny, D. F. Kurdgelaidze, Sov. J. Nucl. Phys. 8, 145, 1968, Nucl. Phys. 2, 432, (1969).

6) A. K. Bassiouny, Beta-Decay of Nucleons. Proceedings of the Mathematical and Physical Society of Egypt. 38, (1974).

7) N. Cabbibo. Proceedings of the 1966 Berkely Conference on High Energy Physics.

CONSTRUCTION OF SILICON SURFACE BARRIER DETECTORS FOR SLOW NEUTRON DETECTION

A.A. al-Saeed , R.A. Al-Kital and M.A. Al-Jeboori*

ABSTRACT

A new technique have been developed for preparing a self support radiator which can replace the direct evaporation method on the detector surface. The self converter foil is changeable so many kind of material can be used. This converter foil made of highly compressed LiF powder enriched with Li^6 isotope to 95%. The results obtained show superiority over those previously prepared by evaporation method. The detector energy resolution for tritons of energy 2.73 Mev and alphas of energy 2.04 Mev is found to be 200 kev, compared with the results of sandwich detector of energy resolution of 300 kev.

INTRODUCTION

Many investigators have shown marked interest in improving surface barrier detectors in order to achieve more reliable means for measuring slow neutrons. The technique used was by coating the sensitive surface of the detector by neutron-charged particle converting film. However, this technique lead to the deterioration of the detector characteristics because of the high temperature needed to evaporate the film material.

* Now at the Department of Physics, College of Science, Al-Mustansiriyah University, Baghdad, Iraq.

Al-Mustansiriyah Journal of Science, Vol.3 (1978).

The present work was aimed to develope a new technique for preparing a self support radiator which can replace the evaporation technique. The effect of different types of neutron - charged particle radiators have been investigated. It has been demonstrated that, it is possible to use foils made of highly compressed powder as a neutron converter. The converter foils have been made from LiF powder enriched with Li^6 isotope to 95%. The LiF self supporting radiator foils showed superiority over those previously prepared by the evaporation method.

EXPERIMENTAL

Silicon surface barrier detectors are mainly used as charged particle detectors. However, when using semiconductors for neutron detection several problems are involved. [1]

1) Because the neutrons are uncharged particles, they cannot be detected directly. They have to interact with some reactive element to produce charged particles through some nuclear reactions.

2) Neutrons are commonly accompanied with gamma rays of comparable or greater energy, so a suitable detector should be either insensitive to gamma radiation or capable of separating the two components.

3) Multiple scattering of fast neutrons causes rapid degradation in their energies which differs from the initial neutron energy.

4) Most of the useful reactive elements have much higher cross sections for thermal neutrons than for fast neutrons.

The most sensitive thermal neutron detectors commonly used are the BF_3 gas-filled proportional counter. The behavior of this counter is severely affected by the change in the electron space charge at the central wire which

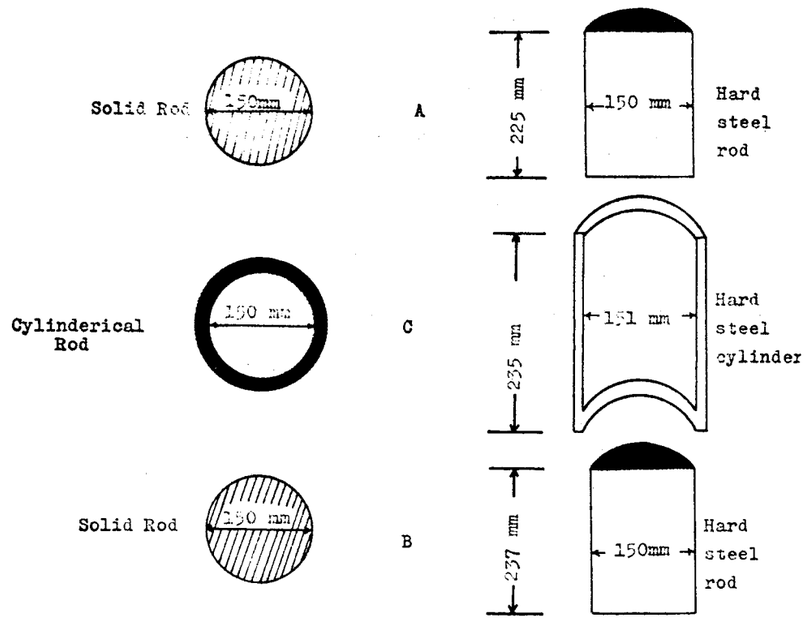

Fig. 1. Foil mold assembly.
a- Longtudenal section (side view).
b- Cross section (top view).

results from high neutron flux. In 1961, E. Sakai [2] prepared silicon surface barrier detector for thermal neutron detection by evaporating B^{10} isotope on the sensitive surface of the detector, and in the same year, T.A. Love et al. [3] prepared sandwich detector by evaporating LiF on the surface of one of the detectors. The low efficiencies of these detectors limit their use to problems which involve high neutron intensities.

In 1968 [4], a silicon surface barrier detector was prepared with gadolinium and Gd^{157} isotope foils or a convertor foil which will produce conversion electron by the prompt neutron capture gamma rays in the foil. A detection efficiency exceeding 40 % was obtained. Martin et al.[5] in 1974 prepared a solution enriched with LiF onto an aluminium backing and drying it under infra red lamp, but they were not able to explain the spectrum obtained from the interaction of thermal neutron with Li^6 isotope.

The present work was aimed to adapt the surface barrier detector to a neutron detector by construction of a neutron convertor material as an adapter. The behavior of these detectors for neutron detections were studied by the use of C_f^{252} fission fragment neutron source with paraffin as a moderating medium.

Preparation technique

The process of construction of surface barrier detectors with better than 12 k e v linewidth at room temperature was an outgrowth of previously used methods followed in this laboratory [6,7]. Conversion foils were prepared using a press method as in the following description. Mold was machined from a particular hard steel as shown in Figure 1. Li^6 isotope were supplied by A.E.R.E. Harwell England as LiF compound powder whose enrichment with Li^6 isotope is 95%. The mold assembly and the powder were pressed under

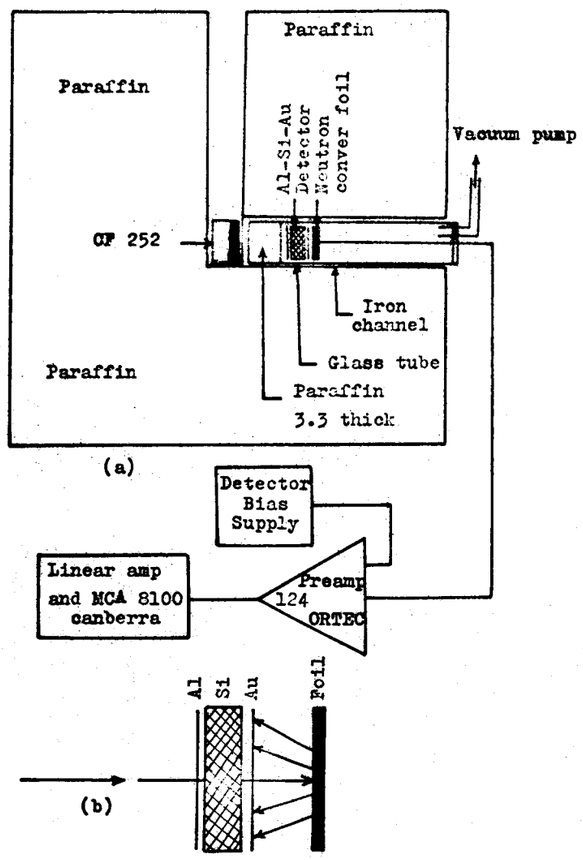

Fig. 2. a- CF-252 Neutron detection assembly.
b- The neutron source, detector and foil arrangement.

a disc of standard tensile machine to a pressure of about 5×10^4 kgm/cm^2. The uniformity and the thickness of the foils were measured by means of a travelling microscope.

The foil was then mounted between two thin tephlone rings. The rings were thin enough to make the convertor foil as near as possible to the detector surface. Mounting Araldite was used, and then cured under infra red lamp for 24 hours. Tephlone and Araldite materials are hydrogeneous, and since are highly pure and thermally insulated they will be inactive during irradiation with thermal neutrons, in addition the ring is not seen by the sensitive face of the detector.

Detector response to neutron

Californium 252 neutron source was used for testing the detector response to neutron. This neutron source is spontaneous fission fragment neutron source, with the following specifications ;

Activity = 27 mci generated by 50 μgm of C_f^{252},

yield = 1.15×10^8 n/sec., sealed source,

average neutron energy = 2.3 Mev, three neutron per fission, half life = 2.65 years for alpha particles, mode of decay is 96.9 % alpha and 3.1 % spontaneous fission. Figure .a shows the arrangement used for studying the detector response to neutrons. The neutron converting foils were made from LiF as described before. In the channel of irradiations paraffin of 3.3 cm thick as a neutron bulk moderator was put in order to obtain slow neutrons. The neutron beam so obtained has fast neutrons component together with the slowed down by the moderator. The multichannel analyser (MCA) of 512 channels was calibrated using Ra^{226} alpha particle source. The arrangement of Figure 2.a was then used for determination of neutron detection spectrum. Convertor foils of

optimum thicknesses were used and arranged in 2π geometry as shown in Figure 2.b. The holder carrying the neutron converter foil and the detector were fixed inside an opaque glass tube. The tube was then evacuated and fixed inside the moderator at a distance of 3.3 cm from the neutron source. The spectrum with and without converter foil was taken and printed out by a telytype printer as shown in Figure 3. The spectrum without converter foil was always taken as a background, however, a low yield background was obtained. The passage of fast neutron through matter may result in (n, charged particle) reactions and recoil nuclei is approximately negligible. Thus the geometry shown in Figure 2.b had been chosen to be the irradiation arrangement in order to decrease the fast neutron counting effect on the detector.

RESULTS AND DISCUSSION

The thermal neutron flux after passing a certain thickness of a moderator was calculated according to the following equation [8] .

$$\frac{E}{Eo} = \frac{A^2 + 1 + 2A\cos\phi}{(A+1)^2}$$

where Eo is the incident neutron energy, E is the scattered neutron energy, A is the mass number of the moderator atom, and ϕ is the neutron scattering angle in the centre of mass system. By using this relation, and from the specifications of the neutron source used, such as its initial yield, date of use, half life, average energy, the thermal neutron flux after passing a thickness 3.3 cm of paraffin was calculated to be 2.96 n/cm^2. sec. The efficiency for detecting neutrons of energy E by a detector of thickness x , containing N atoms per cm^3 of neutron absorber for which the absorption cross

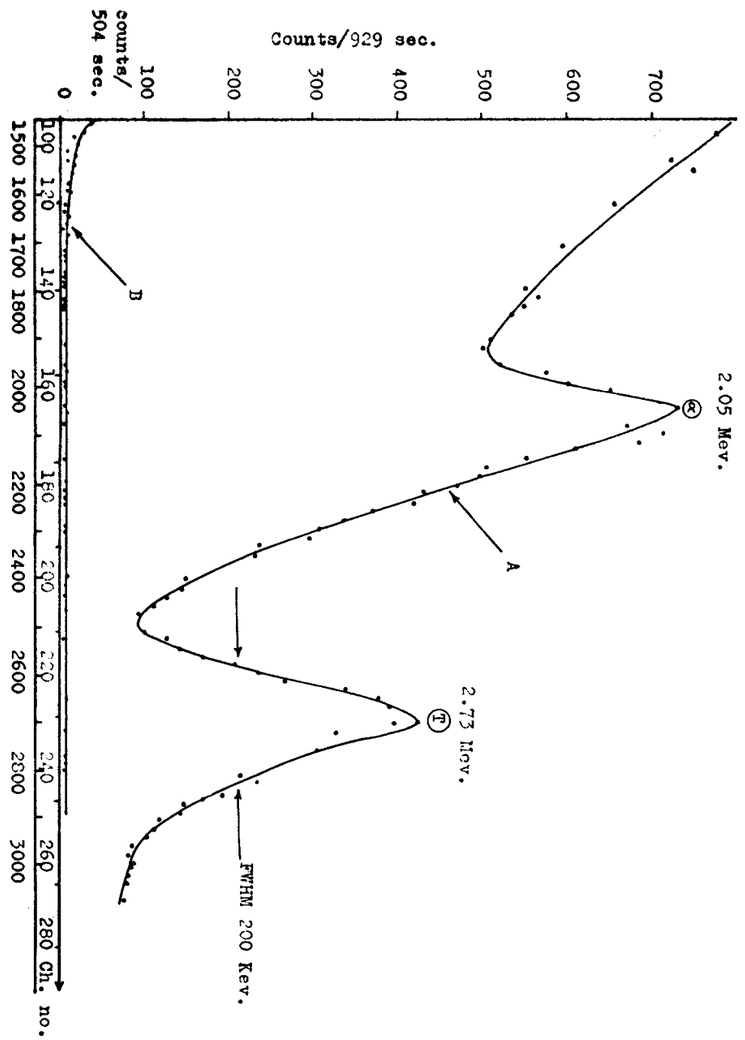

Fig. 3. LiF foil of 0.2 mm thick spectrum.

section is σ_a at a given neutron energy may be related by [9]

$$\text{Efficiency} = \left(1 - e^{-N\sigma_a x}\right)\epsilon$$

The term $\left(1 - e^{-N\sigma_a x}\right)$ gives the fraction of the incident neutrons which are absorbed in the detector, and the factor ϵ is the fraction of these neutrons which result in an output pulse from the detector, and it depends on the range of charged particles in a material. The detector efficiency for neutron detection is found to be 0.016 for tritons at E = 2.73 Mev due to the reaction of $Li^6(n,\alpha)T^3$ in LiF foil. The thickness of the LiF converter foil used in such geometry as shown in Figure 2.a was 0.2 mm. The spectrum obtained from slow neutron interaction with LiF due to $Li^6(n,\alpha)T^3$ reaction is shown in Figure 3. This reaction is exoergic reaction. The released energy Q is shared between the product particles and were calculated as 2.05 Mev alpha and 2.73 Mev tritons. The cross section of this reaction for neutrons of 0.025 ev is 945 barns. The high count rate which appear in the lower channel of Figure 3.a are believed to be caused by gamma radiation from the neutron source and gamma radiation from the neutron interaction with iron channel, paraffin, and surroundings. Because of the high cross section and high Li^6 enrichment - 95 % , such discrete spectrum was obtained. The two peaks are the triton at 2.73 Mev and alpha at 2.05 Mev. The energy resolution of the detector with LiF converter foil full width half maximum at 2.73 Mev tritons is 200 kev which is better than the energy resolution obtained by sandwich detector[3]. The detection efficiency for LiF foil of thickness 0.2 mm, atomic density 0.533×10^{33} atoms/cm^3, and absorption cross section 880 barns, was 0.016 while the detection efficiency of sandwich detector was 0.003, for the same neutron energy.

CONCLUSIONS

1- A new technique have been developed for preparing a self support radiator which can replace the direct evaporation method on the detector surface. The self support converter foil is changeable, so many kind of material can be used.

2- The results obtained show superiority over those previously prepared by evaporation method.

REFERENCES

1. J. Sharpe, Nucl. Eng. 3, 251, June (1958).
2. E. Sakai, IAEA Nuclear electronics, Vol. 1, 551, (1961).
3. T.A. Love R.B. Murray, J.J. Manning, and H.A. Todd, IAEA Nuclear electronics, Vol. 1, 415, (1961).
4. B. Feigl, and H. Rauch, Nucl. Inst. and Methods, 61, 349, (1968).
5. L.P. Birstein, A. Martinez, and F. Filevich. Nucl. Inst. and Methods, 116, 615 (1974).
6. M.G. Mosh , R.A. Al-Kital, and M.A. Al- Jeboori. Bull. Coll. Sci. Vol. 18, No. 1, 271 (1977).
7. T.M. Al-Adawi, A.A. Abdulla, and M.A. Al-Jeboori. Al-Mustansiriyah Journal of Science, Vol. 2, 5, (1977).
8. K.H. Beckurts, and K. Wirtz. Neutron physics, Springerverlag, Berlin (1964).
9. S.J. Cooking, F.J. Webb, and B.A. Egelstaff. Thermal neutron scattering, Academic Press (1965).

ACKNOWLEDGEMENT

Thanks are due to the University of Baghdad for their financial support and also for I.A.E.C, Twitha and staff for assisting in taking the data with the neutron detection geometry and other electronic systems.

مجلة علوم المستنصرية

كانون الأول ١٩٧٨

رقم الايداع في المكتبة الوطنية ببغداد (٢٧٨) لسنة ١٩٧٨